UNIVERSITY OF EMBU

ROBIN SIMIYU

MSc

2025

QUANTIFICATION OF *Escherichia coli* BACTERIA IN MUNICIPAL WASTEWATER TREATMENT PLANT AND THEIR DEGRADATION USING ADVANCED OXIDATION PROCESSES

ROBIN SIMIYU

A THESIS SUBMITTED IN PARTIAL FULFILMENT OF THE REQUIREMENTS FOR THE AWARD OF A MASTER OF SCIENCE IN CHEMISTRY DEGREE OF THE UNIVERSITY OF EMBU

SEPTEMBER, 2025

DECLARATION

This thesis is my original work and has not been presented elsewhere for a degree or any other award.

Signature…… Date…….....

Robin Simiyu

Department of Physical Sciences

B523/1466/2021

This thesis has been submitted for examination with our approval as the University supervisors.

Signature…… Date…….

Dr. Seth Apollo

Department of Pure and Applied Chemistry

Masinde Muliro University of Science and Technology

Signature……. Date…….

Dr. Genson Murithi

Department of Physical Sciences

University of Embu

TABLE OF CONTENTS

LIST OF TABLES

LIST OF FIGURES

LIST OF ABBREVIATIONS

AOPs	Advanced oxidation processes
CFU	Colony Forming Units
EDX	Energy dispersive X-ray Fluorescence
FTIR	Fourier Transform Infra-Red
MPN	Most probable number
SEM	Scanning electron microscope
UV	Ultra-violet light
XRD	X-ray diffractometer
WHO	World Health Organization

ABSTRACT

Pathogenic microorganisms in wastewater present a major global public health concern, underscoring the critical necessity for effective wastewater treatment and advanced distribution infrastructure. While chlorination remains a common disinfection method, it presents notable drawbacks, including the necessity for high dosages and the potential formation of toxic trihalomethanes, which are detrimental to human health. This research sought to assess the efficacy of advanced oxidation processes (AOPs) for disinfecting municipal wastewater obtained from the Embu sewage treatment plant. AOPs are chemical oxidation methods that generate highly reactive oxygen species (ROS), such as hydroxyl radicals, which rapidly disinfect water by attacking impurities. The study investigated individual AOP systems, specifically UV photolysis and H_2O_2 disinfection, alongside various hybrid AOP configurations: UV/H_2O_2, UV/TiO_2, and UV/TiO_2/H_2O_2. The findings indicated that UV photolysis alone achieved 81% *E. coli* removal, while H_2O_2 disinfection yielded an 86% efficiency. However, it was observed that excessive H_2O_2 concentrations could scavenge the generated hydroxyl radicals, thereby impeding *E. coli* inactivation. Significantly, the UV/H_2O_2, UV/TiO_2, and UV/TiO_2/H_2O_2 hybrid systems consistently demonstrated higher disinfection percentages compared to their single-process counterparts. The UV/H_2O_2 system achieved 89% *E. coli* removal within 60 minutes using a 1.4 mM H_2O_2 concentration. The UV/TiO_2 system showed a slightly greater inactivation rate, reaching 91%. The UV/TiO_2/H_2O_2 hybrid system proved most effective, achieving 100% *E. coli* inactivation within 50 minutes. This inactivation grew due to the combined effect that was caused by hydroxyl radical formation when UV, H_2O_2, and TiO_2 were applied collectively. The successful destruction of E. coli was also facilitated by the application of zeolite, a highly effective adsorbent whose surface area was 22.44 m^2/g and therefore enhanced immensely the adsorption process. There was also no reactivation of *E. coli* observed after being treated, confirming for certain the complete destruction of bacterial cells. This was also confirmed by protein analysis, whose result showed protein content reduction in treated solutions. Catalyst characterization also showed that the used TiO_2 had 95.6% anatase phase. Based on these findings, it is recommended that hybrid UV/H_2O_2/TiO_2 be applied for disinfection at the Embu wastewater treatment plant to prevent discharging poorly treated wastewater to the environment. In this study, the zeolite used was clinoptilolite, which acted as both an adsorbent and a support for TiO_2. The photocatalyst applied in hybrid systems was therefore TiO_2–clinoptilolite, not TiO_2 alone, and this composite material enhanced both adsorption and photocatalytic activity during disinfection.

CHAPTER ONE

INTRODUCTION

1.1 Background of the study

Accelerated population expansion, city growth, and socio-economic progress have led to the production of billions of tons of waste and wastewater (Yasir, 2021). About 80% of the wastewater is directly released to the global ecosystem untreated (Tulchinsky et al., 2018). This exposes close to 1.8 billion people to the risk of contracting water-borne infections such as cholera due to pathogenic material of the wastewater (Tulchinsky et al., 2018). Besides the presence of the pathogens, the wastewater contains heavy metals, organic, and other inorganic compounds (Claverie et al., 2019).

Organic and inorganic impurities found in effluent are eliminated during various primary and secondary treatment processes that are classified as biological, physico-chemical, and chemical methods. Usually, disinfection using various techniques are employed as the last treatment step to remove micro-organisms (Saravanan et al., 2021). Choosing a suitable disinfection technique depends on aspects such as cost-effectiveness, environmental implications, and the nature of micro-organisms, among other parameters (Latif et al., 2022) for example, wastewater contains different types of bacteria with varying degrees of impact on humans. They comprise *Campylobacter jejuni, E. coli, Salmonella spp, Shigella spp, Klebsiella spp, Leptospira spp, Aeromonas hydrophila, Vibrio cholera,* and *Yersinia spp* (Chahal et al., 2016). Enteric bacterial microorganisms such as *E.coli* are known to trigger gastrointestinal diseases such as gastroenteritis, dysentery, and diarrhea (Fairbrother & Nadeau, 2006).

Chlorination was historically employed as the premier technique for disinfection; its flaws, such as having to be applied in large volumes and having a penchant to create unwanted byproducts, caused various alternative technologies to be examined, consisting of AOPs (Mazhar et al., 2020). AOPs owe their action to creating high quantities of hydroxyl radicals to destroy organic pollutants efficiently by oxidation and to destroy microbial cell membranes (Deng & Zhao, 2015). A couple of such processes are photocatalytic oxidation (photocatalysis), employing

ultraviolet, visible, or solar radiation with a semiconductor catalyst, and hydrogen peroxide or ozone oxidation processes (Liu et al., 2020). The produced hydroxyl radicals acts as strong oxidation agents with 2.8 eV oxidation potential (Wang & Zhang, 2018). Amongst photocatalytic semiconductors, titanium dioxide (TiO_2) is favored because it possesses high photocatalytic capacity, high stability, environmental friendliness, and accessibility (Fernandes et al., 2020). To boost TiO_2 effectiveness, it can be combined with relevant adsorbents like zeolite, carbon, or chitosan, leading to a collective boost of adsorption and catalysis by virtue of a synergistic effect. TiO_2-supported zeolite catalysts, for instance, exhibited higher photodegradation effectiveness for various organic pollutants (Apollo et al., 2014a). Zeolite, by virtue of its adsorptive capacity, supports TiO_2 performance by boosting a collective adsorptive and catalytic oxidation process within such composite catalysts.

Advanced Oxidation Processes (AOPs) demonstrate significant prospects for practical implementation within hybrid systems that are capable of accelerating the degradation process and facilitating rapid disinfection. Hybrid configurations of different types have been applied to wastewater treatment, such as UV/TiO_2 hybrids, UV/H_2O_2 hybrids, UV/ozone hybrids, UV/H_2O_2/ozone hybrids, UV/H_2O_2/TiO_2 hybrids, and UV/H_2O_2/TiO_2-supporting zeolite catalyst hybrids. The present research considered the capacity of a hybrid system, in the form of various AOPs, to disinfect and disintegrate *E. coli*. Additionally, the study aims to investigate the capacity of AOPs to elevate the quality of the processed wastewater from the Embu municipal wastewater treatment facility.

1.2 Statement of the problem

Access to water has grown scarce today, particularly in developing countries. Approximately 660 million people live without access to safe drinking water globally. Therefore, most people rely on untreated water sources such as rivers and dams. Disposal of inadequately treated wastewater also pollutes the available water sources, leading to increased water stress and environmental concerns, such as an increase in waterborne diseases. After biological treatment of municipal wastewater, the effluent often still contains fecal bacteria contaminants; therefore, there is a need

to employ a highly promising disinfection technology for wastewater treatment. Other disinfection methods like chlorination and ozone have been used, but the great concern is the by-products produced by these techniques. In order to minimize the fecal bacteria in municipal wastewater treatment effluent, AOPs can be utilized to kill the pathogenic microorganisms present, such as *E. coli* bacteria, completely into CO_2 and H_2O, stopping the bacteria's replication and reproduction. AOPs can be combined in different methods to create hybrid systems, which shorten disinfection time and increase degradation efficiency. The semiconductor (TiO_2) can also be modified to accelerate its photocatalytic activity during wastewater disinfection. In this work, the efficacy of a hybrid system of artificial UV light, H_2O_2, and a modified TiO_2-supported zeolite catalyst is examined in *E. coli* removal from Embu sewage wastewater. Since the effluent from Embu municipal wastewater enters the river Rupingazi without disinfection after biological treatment, this study will help employ disinfection techniques that are more efficient and mitigate the danger of water-related diseases among the locals. Also, the majority of the municipal wastewater treatment works within Kenya have poor usage of disinfection methods. Thus, this research work will help the country to reach the best-operational disinfection systems to effectively address wastewater so that it is safe to utilize.

1.3 Justification of the Study

The majority of Kenya's municipal wastewater treatment works have inadequate disinfection practices, with grave health and environmental implications. Embu municipal wastewater treatment works effluent, for instance, is directly discharged into River Rupingazi following biological treatment with no disinfection treatment. Such untreated effluent increases the prevalence of waterborne diseases among the catchment population at the detriment of public health and environmental integrity. This work is thus timely since its focus is on the identification and application of disinfection methods to municipal wastewater treatment works. By removing deficiencies of the current procedures, the research will prevent the spread of waterborne infections, ensuring the safety and welfare of the communities utilizing River Rupingazi to fetch water.

Furthermore, this research's findings will assist in developing efficient and sustainable disinfection systems tailored to Kenya's conditions. By determining best practices and raising the standards of wastewater treatment, the research contributes to the overall aim of making waters safer, protecting the environment, and public health within the region. In this sense, this research is a step toward integrating improved wastewater management infrastructure and encouraging the safe use of water within Kenya.

1.4 Hypothesis

1. TiO_2 does not have good adherence to the zeolite surface therefore not improving the photodegradtion.
2. The amount of *E.coli* in Embu Sewage wastewater treatment plant is above the recommended NEMA limits.
3. The hybrid UV/TiO_2/H_2O_2 system does not improve bacterial disinfection efficiency compared to UV, H_2O_2 single processes.
4. There will be no regrowth of *E.coli* bacteria in the municipal wastewater after AOPs treatment.

1.5 Objectives

1.5.1 General objectives

To quantify *E.coli* bacteria in municipal wastewater and evaluate their degradation using artificial UV light on hybrid oxidation processes consisting of H_2O_2 and TiO_2-supported zeolite catalyst.

1.5.2 Specific objectives

1. To synthesize and characterize TiO_2 zeolite-supported catalyst.
2. To quantify the *E.coli* concentration in the Embu sewage wastewater treatment plant.
3. To determine the efficiency of UV/TiO_2 zeolite-supported catalyst/H_2O_2 hybrid system compared to UV, H_2O_2, UV/H_2O_2 and UV/TiO_2 in bacterial degradation.
4. To asses *E.coli* photo-reactivation (regrowth) after disinfection using AOPs.

1.6 Scope and limitation

The study investigated whether the hybrid system consisting of artificial UV light, H_2O_2, and TiO_2-supported zeolite catalyst will inactivated fecal Coliform and *E.coli* bacteria present in Embu municipal wastewater (real

wastewater). This research study only covered on *E.coli* bacteria inactivation and not any other bacterial type.

CHAPTER TWO

LITERATURE REVIEW

2.1 Municipal wastewater

Water pollution is a global problem with increasing usage of freshwater to undertake domestic, industrial, and agricultural activities (Kokkinos et al., 2020). Current stringent water quality protection management is an effort to control the impacts of hazardous waters on the ecosystem. In that sense, tough legislations regulate the effluent treatment of treated municipal waters that are discharged into natural waters such as rivers (Gomes et al., 2019). The exponentially growing population, speeding cityscapes, and increasing human interventions have brought about rapidly damaging effects on watersheds, leading to water depletion and deterioration (Wang et al., 2019). Even in highly sanitized industrialized countries, waterborne diseases dominate. These issues have brought forth additional research on higher-level wastewater treatment and water reclamation (Paździor et al., 2019). Water reclamation concepts have evolved to address the world's scarce and often decreasing freshwater availability. Reclamation concepts enable treated wastewater reuse industrially and also for irrigation (Frasson et al., 2019).

The organisms that create pathogenic conditions within waters have also been successfully studied since the prevalence of waterborne diseases has been documented both within developing and developed countries (Kokkinos et al., 2011). Microorganisms in wastewater are: viruses, protozoa, and bacteria that are principally produced through contamination caused by animal and human wastes. These organisms can bring about various waterborne pathogens (Jacangelo & Trussell, 2002). AOPs are a viable technique for pathogen inactivation during tertiary wastewater treatment (Feitz, 2005). AOPs are a successful technological measure due to their environmental friendliness, rapid oxidation kinetics, and superiority over classic disinfection processes such as chlorination (Sgroi et al., 2021).

Advanced Oxidation Processes (AOPs) operate by in *situ* production of ROS, which are highly powerful and highly active oxidants (Ma et al., 2021). The ROS consists of different types, i.e., hydroxyl radicals, superoxide radicals, sulfate

radicals, and hydrogen peroxide (Ma et al., 2021). Several types of AOPs were found to be very effective, for example, ozonation, electrochemical oxidation, UV light-based procedures, photocatalytic oxidation, Fenton and Fenton-like oxidation, and oxidation by sulfate radicals.

2.2 The Recent trends and performance of different AOPs

2.2.1 Ozonation

Ozone (O_3) stands as a highly reactive molecule, characterized by a 2.07 eV oxidation potential (Ikehata & Li, 2018). Ozone, with 2.8 eV more potential, is capable of generating subsequent oxidants like hydroxyl radicals. With 2.87 eV of potential, they are the sole constituent to stand as a runner-up to that of fluorine in the reactivity series (Ma et al., 2021). Ozone, with these attributes, through reaction, can react with numerous microbial structures of cells, including the cell wall and deoxyribonucleic acid (DNA) structures (Singh et al., 2020). The results of available literature studies of ozone application for real wastewater disinfection are listed in Table 2.1. The table demonstrates that the ozone dosage that is to be applied depends on both microbial load and species of wastewater.

Table 2.1: Required Transferred and Injected Ozone Doses for Effective Pathogen Disinfection

Water Source	**Water Source Water Characteristics**	**Microbial Inactivation**	**Ozone dose**	**Reference**
Secondary municipal wastewater effluent	Initial *E. coli* concentration: 1.8 x 10^3 CFU/mL Total Suspended Solids (TSS): 4.5-6 mg/L Chemical Oxygen Demand (COD): 42-49 mg/L	Complete removal of *Escherichia coli*	0.3mg/L (Transferred dose)	(Michael-Kordatou et al., 2017)
Secondary municipal wastewater effluent	*Escherichia coli* (initial): 2.7-4.3 log *Clostridium* (initial): 3.0-5.5 log COD: 30-71 mg/L TSS: 2.3-18 mg/L	*Clostridium* was the hardest to treat pathogen. It forms highly resistant endospores, and it is highly resistant to antibiotics.	2-15 mg/L (Transferred dose depending on water quality)	(P. Xu et al., 2002)
Real secondary urban wastewater effluents	Initial COD: 25-50 mg/L TSS: 5.2 mg/L Initial Fungi: 2.0 log Initial Bacteria: 3.0 log	3-4 log reduction for bacteria, 3.9 log reduction for fungi	225mg/L Injected dose	(Sousa et al., 2017)

Low ozone (O_3) breakdown efficiency often results in poor hydroxyl radical production and hence limited sustained capacities for disinfection (Wang et al., 2017). Ozone-based AOPs have therefore been used to support ROS generation

during disinfection processes (Fu et al., 2019). Kim and Yousef *et al*. showed 5–6 log reductions in bacterial counts (including *E. coli, Pseudomonas fluorescens*, and *Leuconostoc mesenteroides*) when treated with 2.5 mg/L O_3 for 40 seconds (Kim & Yousef, 2000). Experiments carried out with *Bacillus cereus* bacteria further showed rate constants for deactivation of 0.3482, 0.3579, and 0.3761 for ozone dosages of 1 mg/L, 2 mg/L, and 3 mg/L, respectively, and hence showed that higher O_3 dosages are necessary to obtain enhanced deactivation efficiency (Ding et al., 2019). Jamil *et al*. appraised ozonation-based disinfection for *E. coli* and *Salmonella* in clean drinking water and demonstrated that 2 mg/L O_3 produced successful 5–6 log destruction of *Salmonella* within 45–60 seconds. However, they also demonstrated that their findings indicate that *Salmonella* was more resistant to ozonation relative to *E. coli* during ozonation-based disinfection (Jamil et al., 2017).

Research was carried out by Maniakova *et al.* to assess H_2O_2/UV, solar photo-Fenton, and O_3 for deactivating some microbial targets (*E. coli, Salmonella spp.*, and *Enterococcus spp*.) found within actual secondary-treated municipal wastewater (Maniakova et al., 2021). The O_3 concentration was 83 mg/L, and complete inactivation was achieved with 45 minutes of treatment. This particular treatment yielded the top inactivation rate across all the microorganisms studied. The deactivation processes observed with sunlight/H_2O_2 (at 50 mg/L) and solar photo-Fenton (employing 0.1 mM Fe^{2+} and 50 mg/L H_2O_2) demonstrated comparable effectiveness. Notably, *Salmonella* and *Escherichia coli* exhibited lower resistance to solar-driven disinfection methods than *Enterococcus* species. Furthermore, the presence of carbonates influenced the efficiency of both the UV light/H_2O_2 and solar photo-Fenton techniques.

Table 2.2: The Summary of Results from Studies on Pathogen Inactivation Mechanisms by Ozonation

Name of the microorganism	**Working condition**	**Deactivation efficiency**	**The deactivation mechanisms**	**Reference**
Bacillus cereus	Ozone (O_3) 3 mg/L	Reduction to 3-log	Ozonation successfully disinfected chlorine-resistant spores by destroying both microbial cell structures and genetic makeup.	(Ding et al., 2019)
Salmonella enteritidis, *Escherichia coli*	Ozone (O_3), 20 mg/L of H_2O_2	Bacteria reduction to 5-log	Ozonation proceeded via the progressive oxidation of vital cellular parts, extending to complete destruction of cell function.	(Nahim-Granados et al., 2020)
Escherichia coli, *Pseudomonas spp*	20 mg/L of total dissolved carbon, 1 mg/L Fe^{2+}	There was 3.3-log reduction	A significant reduction in adenosine triphosphate (ATP) was observed.	(Malvestiti et al., 2019)

2.2.2 Demerits of ozonation

The efficiency of ozonation in practical sewage wastewater decreases compared to that in model effluent due to dissolved organics in water (Hodges et al., 2018). The dissolved organics are able to prevent some oxidant species at a given concentration and subsequently decrease their availability to microbial cell degradation (Sousa et

al., 2017). Ozone thus makes disinfection less efficient for real effluents, irrespective of modeled wastewater having a higher COD concentration compared to real effluents. The decreased efficiency in practical secondary wastewater can also be attributed to some competing oxides, such as total suspended matter, cationic, and ionic species.

2.3 The electrochemical oxidation

Oxidation occurring at the surface of an electrolytic cell's anode is called electrochemical oxidation (Körbahti & Tanyolaç, 2003). The technique is applied to remove wastewater pollutants efficiently (Un et al., 2008). Desired pollutants are oxidized by accepting electrons that are passed by the anode or through intermediates like radicals of hydroxyl that are generated by the anode (Martínez-Huitle & Brillas, 2009). Historically, researchers have explored this process for both wastewater disinfection and surface water disinfection (Schaefer et al., 2015). The reason that research was applied to such processes is that it is a more economical procedure when compared to disinfection procedures such as ozonation, ultraviolet irradiation, and photocatalytic oxidation. The reason for that is that it is a technology with low initial investment, is easy to install, does not need to utilize catalysts at all, and is capable of carrying out various processes with only one installation (Anglada et al., 2009).

Cho *et al*. employed electrochemical oxidation for disinfection of household effluent, with0.8-7.8 x 10^5 CFU/100mL coliform load. The multiple metal-doped titanium anode technique and 2.09mA/cm^2 current density resulted in complete disinfection in 3 hours (Cho et al., 2014). The 3 hours recorded complete disinfection. Lacasa *et al*. revealed that operation with a boron-doped diamond (BDD) anode having 25.5 mA/cm^2 current density, combined with 18.3 g/L chlorine concentration, resulted in a stunning 6-log *E. coli* reduction of synthetically prepared ballast wastewater in 3 minutes. Their investigation further indicated that the addition of chlorine to the electrolyte had the effect of enhancing microbial inactivation efficiency (Lacasa et al., 2013).

Rajab *et al*. achieved 6-log inactivation of *Pseudomonas* within 15 minutes by employing a boron-doped diamond (BDD) anode with 167 mA/cm^3 applied current density, with no chlorine addition. Their test proved that such effective disinfection was a result of sufficient hydroxyl radical production (Rajab et al., 2015).

2.4 UV Light disinfection

The most widely used technique in the world for disinfecting water is this one, which uses ultraviolet (UV) light (Matos et al., 2019). Either artificial UV lighting or light from the sun is this UV source. Since photons in the 200–300 nm spectrum have a germicidal effect through DNA molecule absorption within the cells, UV light can be used to disinfect. As a result, many microorganisms, comprising bacteria, viruses, and protozoa, become inactive and distracted(Green et al., 2004). Among other things, the type of pathogenic microbe to be targeted determines how successful artificial UV lighting is at disinfecting (Gomes et al., 2019).

Hamilton *et al*. indicated that bacterial spores and viruses exhibit the highest resistance to inactivation by artificial UV light. They are followed in resistance by intestinal protozoa, such as *Giardia* and *Cryptosporidium*, with intestinal bacteria being the least resistant (Hijnen et al., 2006). Nevertheless, certain microbial cells, including *Deinococcus radiodurans* (Makarova et al., 2001), demonstrate resilience to low UV irradiation doses, necessitating higher doses for complete inactivation (Sun et al., 2019). Despite artificial UV disinfection typically inactivating microbial cells by disrupting their cell walls and damaging their DNA (Rodriguez et al., 2014) and (Sousa et al., 2017), Some microbes possess the ability to repair their genetic material through photo-reactivation, potentially leading to the re-contamination of water by previously inactivated pathogens. Furthermore, certain viruses like polyomaviruses and human adenoviruses, which contain dsDNA genomes, can leverage their host cells' machinery for repair during replication (Calgua et al., 2014), thereby overcoming UV-induced DNA damage (Shin et al., 2009).

Guo *et al*. revealed that a UV dose of 1.2 mJ/cm^2 efficiently deactivated *E. coli* O157:H7, achieving a 2-log to 6-log reduction (Guo et al., 2017). Traditionally, water disinfection has extensively employed both medium and low-pressure UV lamps

(Guo et al., 2009). Medium-pressure lamps typically emit UV light across a broader wavelength spectrum, approximately 200–400 nm. More recently, LEDs were found to be a fitting replacement for disinfection purposes (Chen et al., 2017). Sholtes *et al*. took into consideration the evaluation of a comparative analysis of UV-LEDs and low-pressure mercury-arc lamps for wastewater treatment purposes. They recorded that there was an insignificant contrast in inactivation capacity for *coliphage MS-2* and *Escherichia coli B* bacteria. Specifically, 4-log inactivation for *E. coli B* required a 6.5 mJ/cm^2 dosage by a low-pressure UV light treatment, and *coliphage MS-2* required a 59.3 mJ/cm^2 effective dose to achieve successful disinfection. UV-LEDs, however, inactivated *E. coli* with 6.2 mJ/cm^2 and *coliphage MS-2* with 58 mJ/cm^2 (Sholtes et al., 2016).

2.5 Photocatalytic oxidation

This process involves a semiconductor catalyst that is activated by an appropriate radiation wavelength (Liu et al., 2020). The probable radiation sources include environmental, sunlight, or simulated UV radiation. Irradiation of water-wetted photocatalyst forms highly active hydroxyl radicals. The widely employed photocatalyst is TiO_2, due to its strong photocatalytic ability, high chemical stability, reduced toxicity, and inexpensive production (Regmi et al., 2018). The large band gap of TiO_2 can, however, lead to its lowered efficiency through swift recombination of photoelectron-hole pairs and poor usage of light (Luo et al., 2017). The photocatalytic efficacy of semiconductors is fundamentally regulated by their surface properties (morphology) as well as energy band gap structures (Chen et al., 2021).

2.5.1 Principle of photocatalytic oxidation.

A semiconductor features a band gap that divides the valence band (VB) and the conduction band (CB) (Haq et al., 2021). The photocatalyst helps its electrons move from the valence band (VB) to the conduction band (CB) in response to UV light with the right energy level. These result in the formation of a negatively charged electron (e^-) at the conduction band (CB) and a positive hole (h^+) at the valence band (VB). Redox reactions with the adsorbed chemicals at the catalyst take place when holes (h^+) and electrons (e^-) are produced and move to the surface of a semiconductor photocatalyst without undergoing recombination (Ma et al., 2021). However, some

electrons (e^-) produced within the semiconductor may recombine with holes (h^+) during their transfer, consequently diminishing the reaction's quantum efficiency (Ilinoiu et al., 2013). Pollutants are degraded either directly through oxidation by the valence band holes (h^+) or indirectly via their reaction with water to yield highly potent hydroxyl radicals. Concurrently, the conduction band electrons (e^-) participate in the elimination of oxygen species adsorbed onto the photocatalyst. The interaction with moisture and oxygen (O_2) during the photocatalytic process also leads to the production of superoxide radicals and other reactive species. Fundamentally, photocatalysis is underpinned by reduction and oxidation reactions. The key reactions involved in photocatalytic processes are as follows;

$$TiO_2 + hv \rightarrow TiO_2(e_{CB} + h^+_{VB}) \quad (1)$$

$$TiO_2(h^+_{VB}) + H_2O \rightarrow TiO_2 + H^+ + HO^{\cdot} \quad (2)$$

$$TiO_2(h^+_{VB}) + OH^- \rightarrow TiO_2 + HO^{\cdot} \quad (3)$$

$$TiO_2(e_{CB}) + O_2 \rightarrow TiO_2 + O_2^- \quad (4)$$

$$O_2^- + H^+ \rightarrow HO_2^{\cdot} \quad (5)$$

$$HO_2^{\cdot} + HO_2^{\cdot} \rightarrow H_2O_2 + O_2 \quad (6)$$

$$TiO_2(e_{CB}) + H_2O_2 \rightarrow HO^{\cdot} + OH^- \quad (7)$$

$$H_2O_2 + O_2 \rightarrow HO^{\cdot} + OH^- + O_2 \quad (8)$$

2.5.2 Methods of enhancing photocatalytic activity

For enhanced photocatalytic performances, there are various alterations that are used, for example, using the heterojunction technique. The method involves two semiconducting materials that are of close crystalline structures that are directly joined together (Ren et al., 2019). Recent discoveries indicate that TiO_2 heterojunction structures with incorporated $Ni(OH)_2$, $NiTiO_2$, and various nickel compounds exhibit higher photocatalytic efficiency and performance (Huo et al., 2015).

Titanium dioxide (TiO_2) alteration tends to involve elemental doping that is categorized as cationic and anionic techniques (Abdullah et al., 2017). Upon doping TiO_2 with some metal ions, a new energy band emerges in the vicinity of its valence band and renders it activated when it is exposed to irradiation by visible light (Roy et

al., 2013). TiO_2 alteration also employed noble metal doping (Q. Zhang et al., 2016). The technique comprises incorporating a limited quantity of noble metal, for instance, silver, to a compound and modifying its characteristics. Noble metals are extremely prized due to their preferred electric properties. In addition to that, surface plasmon resonance contributes to higher photocatalytic efficiency: when photons excite them with a frequency that coincides with their natural vibration rate of surface free electrons, free electrons within noble metals resonate with incoming electrons (Hou & Cronin, 2013).

In addition, morphological control was applied to enhance semiconductors' activities (TiO_2). The creation of a surface of a semiconductor with controllable surface flaws is among the methods applied to enhance TiO_2 photocatalytic activity. As a result, photogenerated electron-hole pairs can segregate more efficiently (Ruan et al., 2019). It influences the photocatalyst surface area and porosity, which in turn impacts the TiO_2 efficiency (Li et al., 2014).

2.5.3 Mechanism of photocatalytic in disinfection

Photocatalysis generates highly reactive and inherently potent oxidizing agents, including superoxide radicals and hydroxyl radicals. The formation of hydroxyl radicals during photocatalysis is improved under UV irradiation when an additional oxidant, like H_2O_2 or O_3, is introduced (Apollo et al., 2014a). For instance, an H_2O_2 molecule splits into two $^{\cdot}OH$ when it is exposed to UV radiation (Foster et al., 2011). Additionally, when the wavelength falls below 242 nm, OH^- are produced via photolysis of H_2O. Semiconductors yield various reactive oxygen species, comprising O_2^-, $HO^{\cdot}$ and H_2O_2 during photocatalytic treatment. These abundant ROS can induce adverse stress responses in microbial cells, causing impairment of essential components, including the peptidoglycan layer, genetic information (DNA and RNA), and ribosomes (Chen et al., 2021). By targeting specific regions of the pathogenic cells' semi-permeable membrane, ROS can alter the permeability of those cells and compromise their integrity (Ray et al., 2017). Therefore, the cytoplasm contents are freed (Huang et al., 2017). The harms that ROS microbes cause to an organism start on the exterior side of the body in relation to the semi-permeable membrane. The consequence of this is the disruption of the metabolic process and

destruction to the genetic structure (Gomes et al., 2019). Moreover, the generated species suppress some protein functions which are essential to the physiological activities of the cell (Padmavathy & Vijayaraghavan, 2011).

According to the cellular cell wall composition and structure, bacteria are classified into two groups. The cell wall of gram-positive pathogens is composed of phosphoric acid and a thick, dense peptidoglycan containing cell wall. Gram-negative pathogens have a multilayered structure that includes peptidoglycan, phospholipid/lipoprotein, and lipopolysaccharide, and moderately thin cells (Rtimi et al., 2019). The protein and phospholipid bilayer create a semi-permeable membrane and physical barrier that prevents the extracellular materials being transferred into the cell. The bacterial cell envelope, comprising lipopolysaccharide, peptidoglycan, and phospholipid bilayers, is the perfect target of ROS produced in AOPs. The nanoparticles are in diameter 2 nm, and they can traverse a cell through the porous nature of the peptidoglycan layer. ROS can move freely due to this this event (Maness et al., 1999). Kühn *et al.* conducted an investigation into the deactivation of *E. coli*, *Staphylococcus aureus*, *Pseudomonas aeruginosa*, and *Enterococcus faecalis* using TiO_2 under mild ultraviolet (UV) irradiation. They have found that disinfection efficiency decreased with an increase of both the peptidoglycan layer's thickness and the complexity of the overall structure of the microbial cell (Kühn et al., 2003).

Both the phospholipid and lipopolysaccharide bilayer are primarily targets of attack by reactive oxygen species composed of fatty acids highly prone to peroxidation (Dutta et al., 2019). ROS triggers the oxidation of unsaturated fatty acids, which also entails the generation of lipid-peroxyl radicals (Chen et al., 2021). The newly developed radicals have the ability to cause a chain reaction by removing hydrogen atoms on different diallyl methylene groups (Chen et al., 2021), and ultimately resulting in the creation of ketone groups (Xiao et al., 2019). Also, it has been shown that reactive oxygen species have a significant influence on protein effective functioning. During the cellular deactivation process, proteins within the cell undergo structural alterations and aggregation. Such changes can consequently impair cellular metabolism, lead to a loss of function, hinder DNA replication, and induce mutations (Bosshard et al., 2010).

The semi-permeable bacterial membrane, which is made up of a phospholipid bilayer, lipopolysaccharide, and peptidoglycan, is preferentially associated with ROS. ROS can move freely due to the porous nature of peptidoglycan, which allows them to enter the microorganism's cell. Kühn *et al*. Conducted research on TiO_2 efficiency on *Staphylococcus aureus, Pseudomonas aeruginosa, Enterococcus faecalis* and *E.coli* (Kühn et al., 2003). The study found that disinfection efficiency decreased with increasing cellular structure complexity and peptidoglycan layer depth. Highly oxidizing potential ROS produced by AOPs react with DNA to cleave a phosphodiester bond between bases in a DNA molecule's double-strand structure (Muller et al., 1997). Pathogen regulators also manage ROS imbalances and cellular enzyme autoxidation. Co-enzyme A (CoA), glutathione reductase (GR), hydroperoxidases (HPI), and catalase (CAT) are among the enzymes (Hoerter et al., 2005). An essential enzyme for cellular respiration in cells is CoA. By taking an electron from CoA, the ROS produced directly contributes to CoA oxidation, restricting bacterial cell respiration and initiating pathogen death (Wang et al., 2017).

Much attention has been paid to disinfection by means of photocatalysis following effective killing of *Lactobacillus acidophilus*, *E. coli* and *Saccharomyces cerevisiae* by a TiO_2 -Pt supported catalyst (Matsunaga et al., 1985) and (Laxma Reddy et al., 2017). Specifically, the photocatalytic deactivation of *Escherichia coli* reports numerous scientific articles (Gomes et al., 2019). Rincón & Pulgarin *et al*. looked at deactivation of coliforms and *E. coli* in sunlight by the use of TiO_2 and noted that there was faster disinfection of *E. coli* than other coliforms such as *Enterococcus species* (Rincón & Pulgarin, 2004). Bogdan *et al*. presented a comprehensive susceptibility classification of various pathogens to modified semiconductors for photocatalytic treatment: viruses > prions > Gram-negative bacteria > Gram-positive bacteria > yeasts > molds (Bogdan et al., 2015). Gomes *et al*. revealed that the semiconductor TiO_2 doped and modified with noble metals showed a great effect on the total removal of *E.coli* from water within a dilution factor range of 10^3-10^4 CFU/ml. Notably, their findings indicated that catalysts such as Ag-TiO_2 and Pd-TiO_2 (TiO_2 doped with Pd) facilitated complete *E. coli* deactivation without requiring

UV radiation. This implies that noble metals would be quite appropriate to use in them, as they do not require much or any energy at all (Gomes et al., 2018).

To adjust the optimal disinfection time, which is necessary to achieve the complete and sustained deactivation of microorganisms, so that the latter would not regrow after a photocatalytic disinfection, it is important to ascertain the effective disinfection time (Rincón & Pulgarin, 2004). This effective disinfection period indicates the length of disinfection essential to kill or inactivate the pathogen, after which no recovery follows, especially after the treated samples stay within the dark phase during 48 hours of phototreatment. The major advantage of the use of photocatalytic disinfection is its long-lasting disinfection power. Effects of residual disinfection, which are observed due to a drop in the bacterial level under dark conditions, is still carried out after the photocatalytic process is terminated (Rincón & Pulgarin, 2005). Xiong & Hu *et al*. also documented this residual disinfection effect following photocatalytic oxidation, suggesting it may stem from the *in situ* production of H_2O_2 during the process, which subsequently produces additional ROS to sustain the photocatalytic reaction (Xiong & Hu, 2013). Dunlop *et al*. investigated on the effectiveness of UV-irradiated TiO_2 Degussa (P25) in deactivating *E. coli* was investigated. According to the study, the elimination of antibiotic resistance genes (ARGs) in pathogens was lower in real wastewater than on laboratory-created (synthetic) wastewater (Dunlop et al., 2015). This inconsistency was explained by the occurrence of both the organic and inorganic substances in real wastewater which can form scavengers to ROS.

2.6 Fenton oxidation reaction and Fenton-like processes

Fenton-oxidation is a modified oxidation system that relies on a catalytic chain reaction between ferrous ions (Fe^{2+}) and H_2O_2 to produce highly reactive species. The addition of H_2O_2 to a Fe^{2+} solution in acidic conditions itself triggers the Fenton reaction(Biton Seror et al., 2022). This is the main form of reaction that usually occurs in three phases (Chen et al., 2021).

Chain initiation stage:

$$Fe^{2+} + H_2O_2 \rightarrow Fe^{2+} + OH^- + HO^{\cdot} \quad (9)$$

$$Fe^{3+} + H_2O_2 \rightarrow Fe^{2+} + H^+ + HOO^{\cdot} \quad (10)$$

$$HOO^{\cdot} \rightarrow H^{+} + O_2 \quad (11)$$

Chain propagation stage:

$$H_2O_2 + HO^{\cdot} \rightarrow H_2O + HOO^{-} \quad (12)$$

$$H_2O_2 + HOO^{\cdot} \rightarrow O_2 + H_2O + HO^{\cdot} \quad (13)$$

$$H_2O_2 + O_2^{-} \rightarrow O_2 + HO^{\cdot} + OH^{-} \quad (14)$$

Chain termination stage:

$$Fe^{3+} + HOO^{\cdot} \rightarrow Fe^{2+} + O_2 + H^{+} \quad (15)$$

$$Fe^{2+} + HOO^{\cdot} \rightarrow Fe^{3+} + OH^{-} \quad (16)$$

$$HO^{\cdot} + HO^{\cdot} \rightarrow H_2O_2 \quad (17)$$

$$2HO^{\cdot} + 2HO^{\cdot} \rightarrow O_2 + 2H_2O \quad (18)$$

$$HOO^{\cdot} + HOO^{\cdot} \rightarrow O_2 + H_2O_2 \quad (19)$$

$$HOO^{\cdot} + HO^{\cdot} \rightarrow O_2 + H_2O \quad (20)$$

The low rate of Fenton systems is associated with the fact that they are specific with their use limited to acidic conditions, i.e., the pH of 3 and produce large amounts of iron-based sludge that increases the operating expenses (Hodges et al., 2018). As a set of solutions to these drawbacks, there are combined methods like photo-Fenton process in which the UV light is incorporated in standard Fenton technique and electro-Fenton process and others. These methods aim to enhance Fenton and Fenton-like reactions, leading to a greater production of hydroxyl radicals $HO^{\cdot}$ (Wang et al., 2016).

As presented in Table 2.3, Fenton or Fenton-like reaction helps in breaking down the H_2O_2 to produce highly oxidative hydroxyl radicals that can destroy microorganisms. Depending on the concentrations of Fe^{2+} and H_2O_2 used at the deactivation phases, the effects of the Fenton system on the microbial cells are directly proportional (Uhl et al., 2015). Diao *et al.* specifically examined the mechanism by which Fenton reagents inactivate *E. coli*. They found that exposure to such reagents resulted in leakage of intracellular material and cell surface deformation. This deformation can consequently decrease the rupture of the cells, their permeability and swelling (Diao et al., 2004).

Table 2.3. Effectiveness and deactivation mechanism of Fenton and Fenton-like processes.

Microorganism	Experimental Conditions	System Inactivation Efficacy	Deactivation mechanisms	References
Escherichia coli	H_2O_2, Fe^{2+} in a ratio of 1:10. UVA-VL lamp of 200W, For 120 minutes	Complete inactivation (100%) of *E.coli*.	Low irradiation, which was dependent on intracellular photo-Fenton reaction, was boosted by H_2O_2 concentration and Fe^{2+}.	(Mosteo et al., 2020)
E.coli	H_2O_2, Fe^{2+} in a ratio of 1:10 VL lamp of 200W, For 120 minutes	100% inactivation of *E. coli* bacteria.	Irradiation was dependent on H_2O_2 activities. H_2O_2 and Fe^{2+} extracellular photo-Fenton	(Mosteo et al., 2020)
E.coli	H_2O_2 50mg, FeOx, 6762.W/m^2 irradiance	Bacterial removal to 5-log	Fe^{3+} and HO• destroyed the microbial cell	(de la Obra Jiménez et al., 2020)
E.coli, S. aureus	2mg of $FeSO_2$, 32ml H_2O_2 and MoS_2	99.96% 100%	Hydroxyl radicals were crucial for *E.coli* deactivation in the MoS_2 co-catalytic system	(Liu et al., 2018)
Microcystis aeruginosa	Fe^{2+} concentration of 1 mg/L and H_2O_2 concentration of 1 mg/L, 20 kHz, 0.42 W/ml	Removal from 4.19 x 10^6 to 0.45 x 10^6 CFU/ml	20 kHz sonication generated holes in the bacterial cell wall via cavitation and acoustic streaming.	(Wu et al., 2019)

Microcystis aeruginosa	Fe^{2+} concentration of 1 mg/L and H_2O_2 concentration of 1 mg/L, 800 kHz, 0.07 W/ml	Removal from 4.19 x 10^6 to 2.33 x 10^6 CFU/ml	Low light intensity of 800kHz sonication induced H_2O_2 inside the cell via endocytosis process	(Wu et al., 2019)
Escherichia coli	H_2O_2 concentration of 8.5 mg/L, Fe^{2+} concentration of 0.85 mg/L, at a pH=4, for 10 minutes	99.4%	Formation of hydroxyl radicals led to serious destruction and rupturing of the cells cell walls resulting in extensive cell lysis	(Diao et al., 2004)
Escherichia coli	H_2O_2 concentration of 8.5 mg/L, Fe^{2+} concentration of 0.85 mg/L, at a pH=4, for 30 minutes	99.8% inactivation.	Generation of hydroxyl radicals caused significant destruction and rupturing of the cell's walls, resulting in widespread cell lysis.	(Diao et al., 2004)
Escherichia coli	pH 3.5-9.5; H_2O_2; Magnetic Fe_2O_3 deposited flower-like MoS_2.	100% inactivation	Hydroxyl radical production resulted in severe distortion of the cell membrane and cell walls.	(Tong et al., 2020)

2.7 Sulfate radical-based advanced oxidation processes.

The effectiveness of the AOPs relying on Sulfate radicals is much more operational across an extended pH interval than that of Fenton reactions (Xiao et al., 2018). Sulfate radicals(SO_4^-) have received a considerable amount of focus owing to their

high redox oxidation potential (2.5 -3.1 eV) and their stability and versatility over a range of pH values (Duan et al., 2020). Wastewater bacteria can be disinfected with the help of sulfate radicals either alone or by mixing with the hydroxyl radicals through advanced oxidation techniques. Sulfate radicals are produced when peroxydisulfate (PDS) or peroxymonosulfate (PMS) is activated (Yang et al., 2020). PDS and PMS are inactive unless assisted with external energy (Song et al., 2020). PMS and PDS have been activated using a variety of techniques, including thermal treatment, non-metallic and metallic catalysis, UV-vis light, ultrasonic, microwave, and photocatalytic activation (Giannakis et al., 2021). The electrocatalytic and photocatalytic activation of the metal and the electrode have been applied in transferring electrons between the photogenerated electrons. Homogeneous catalysts have been selected instead of non-homogeneous or heterogeneous ones because they are good during the activation process (Xiao et al., 2020). Also, other triggers of activation such as UV light and ultrasound, incorporate their own energies to switch on PMS and PDS. Activation of PMS and PDS proceeds as follows;

$$HSO_5^- + e^- \rightarrow SO_4^- + OH^- \quad (21)$$

$$HSO_5^- + e^- \rightarrow SO_4^{2-} + HO^{\cdot} \quad (22)$$

$$S_2O_8^{2-} + e^- \rightarrow SO_4^- + H^+ \quad (23)$$

$$HSO_5^- + h^+ \rightarrow SO_5^- + H^+ \quad (24)$$

$$HO^{\cdot} + H^+ + e^- \rightarrow H_2O \quad (25)$$

$$SO_4^- + H^+ + e^- \rightarrow HSO_4^{\cdot} \quad (26)$$

$$SO_4^- + OH^- \rightarrow SO_4^{2-} + HO^{\cdot} \quad (27)$$

Table 2.4. The current performance of sulfate-based AOPs in pathogens deactivation.

Microorganism	Operational Conditions	Observed Inactivation	Mechanisms of Inactivation	Reference
E. coli	T=25^{O}C, (PS)=2mM, (MHC)=200 mg/L, ʎ=420nm And pH=6.0	8-log cell reduction in 40 minutes.	Generated sulfate radicals inflicted destruction to the cell membrane, followed by the destruction of genetic material (DNA)	(Wang et al., 2020)
E. coli	PS=0.5, ilmenite= 1 g/L	6-log cell reduction within 60 minutes	Produced reactive oxygen species (ROS) led to leakage and breakdown of *E.coli* intracellular components.	(Xia et al., 2018)

E. coli	PDS=2mM, Na_2SO_4=50mM, GAC = 10 g/L	4.6-log cell reduction in 10 minutes	ROS ($SO_4^{\cdot-}$ >$HO^{\cdot}$>H_2O_2) compromised the cell membrane's integrity and disrupted the microbe's cellular metabolism	(Ma et al., 2019)
E. coli	SDBC=0.5g/L, PDS = 6mM	93% inactivation within 90 minutes	Bacterial cell membranes were disrupted via an electron-transfer mechanism	(Ma et al., 2019)
E. coli K-12	PDS=1g/L, magnetic pyrrhotite	7-log reduction within 15 minutes	ROS ($SO_4^{\cdot-}$ >$HO^{\cdot}$>H_2O_2) caused damage to the bacterial cell membrane and cell wall, followed by protein degradation, and subsequent breakdown of genetic material	(Xia et al., 2017)

2.7 Advanced oxidation processes (AOPs) hybrid systems

In response to disadvantageous limitations of each individual AOPs in abundance of reactive oxygen species (ROS) production and operating conditions, the combination of two or more AOPs has been envisioned and studied. The combination of the AOP systems is expected to optimize the process of pathogenic contaminants oxidation at a high rate compared to the single treatment methods based on the synergy effect realized in such combined systems (Abdelhaleem & Chu, 2020). In addition, the hybrid AOP designs extend the possibility of a wide set of conditions in which each incorporated technology could be operating(Yi et al., 2021).

2.7.1 UV/ozone coupled process

Ozone (O3) may significantly be enhanced by its combination with other treatment systems, including hydrogen peroxide (H_2O_2) or persulfate (JunSik et al., 2014). Since H_2O_2 acts as a potent oxidant, its presence can notably boost the generation of hydroxyl radicals ($HO^{\cdot}$). Strong oxidant sulfate ion radicals are also produced by persulfate. The synergetic effect of ozonation and UV photolysis can be explained by the fact that radical generation is promoted in the course of this interaction (Moreira et al., 2016). Pathogen destruction can be enhanced by the usage of ultraviolet irradiation together with ozone technology (O_3/UV).

Jung *et al*. Investigated a study on the joint use of ultraviolet (UV) radiation and ozone (O3) in order to inactivate *Bacillus subtilis* spores (Jung et al., 2008). In their experiments, UV radiation was simultaneously introduced with a 2 mg/L ozone concentration into a reactor containing *B. subtilis* spores at a concentration of 2-4 × 10^6 CFU/ml. The combination of ozone and UV radiation led to an overall deactivation efficacy with exceeding 4.5 log reduction. Nevertheless, when studying the inactivation profile using ozone and UV as the independent killing factors, there was close resemblance between the two. The ozone CT value was used to assess the synergy of the combined ozone/UV process and the standalone ozone process, with the synergy characterized using the enhanced efficiency. Here, the increased presence of residual ozone was found in the standalone ozone process than in the combined process of O_3/UV.

Fang *et al.* studied and compared the deactivation of *Escherichia coli* and *bacteriophage MS2*, using UV photolysis, ozonation, and UV/O_3 combined process components of pH 7 and 22°C temperature (Fang et al., 2014). The deactivation kinetics of *Escherichia coli* were specifically investigated using UV, O_3, and UV/O_3, with an O_3 dosage of 0.05 mg/L. *Escherichia coli's* log inactivation showed a linear trend during UV photolysis until about a 3-log reduction, at which point the deactivation rate decreased. There was a 1.2-log deactivation following the 15 seconds of O_3 exposure. The ensuing inactivation stayed constant because of ozone depletion. Exposure to O_3/UV accelerated the inactivation of *E. coli*.

2.7.2 Photocatalysis coupled oxidation process

The treatment efficacy can be significantly improved by integrating photocatalytic processes with other AOP technologies, such as ozonation (O_3) and hydrogen peroxide (H_2O_2) (Mecha et al., 2016). This combination improves the production of hydroxyl radicals $HO^{\cdot}$ owing to a synergistic effect. Mecha *et al*. evaluated the synergistic effect and the possibility of the regrowth of bacteria during the photo-catalytic ozonation of municipal wastewater (Mecha et al., 2017). Their investigation targeted *Escherichia coli, Salmonella spp.*, *Shigella spp.*, and *Vibrio cholerae*. The study's conclusions demonstrated that photocatalytic ozonation surpassed the performance of independent, individual unit processes. In the case of synthetic wastewater, the whole (99.9%) inactivation of all target bacteria was obtained in all trials within 15 min by use of UV/O_3 process. Also, the recovery was not seen in bacteria after 48-hour post-treatment period. Table 5 is a literature review of the research findings that describe the reduction of pathogenic bacteria, antibiotic resistance genes (ARGs), from different sources of water through the photo-coupled oxidation process. Dunlop *et al*. explored the efficacy of TiO_2 (P25) under UVA light for *E. coli* inactivation (Dunlop et al., 2015). This was because the depletion of the antibiotic resistance genes was not as efficient in real wastewater and the reason behind this was the presence of reactive oxygen species (ROS) scavenging by the inorganic and organic entities in the effluent. Still, it was observed that in addition to the pathogen regrowth, there is a possible greater transfer of antibiotic resistance genes in case the disinfection is not carried out up to the moment it completely deactivates the pathogen before the discharge.

Table 2.5. Antibiotic resistance genes (ARGs) bacterial destruction from water through a photo-coupled oxidation process from different sources.

Hybrid systems	**Working conditions**	**Significant findings**	**Pathogens**	**References**
Photo-catalysis with natural sunlight. TiO_2/H_2O_2 Solar light/ H_2O_2	Urban wastewater effluent H_2O_2=20mg/ L TiO_2(P25) GO- TiO_2	TiO_2(P25)/ H_2O and solar light/ H_2O was the most efficient hybrid system for removal of ARGs	*Enterococci* and *Fecal coliforms*	(Moreira et al., 2018)

Photo-catalysis/UVC/H_2O_2	UV-C lamp (254nm, 300W,800W) TiO_2 thin film Fluence=0-120mJ/cm^2 H_2O_2=10-100mM Phosphate-buffered saline solution (pH = 7.4) Natural water from drinking water source(pH = 7.2)	Increasing H_2O_2 concentration enhanced photocatalysis efficiency	*Pseudomonas aeruginosa* *staphylococcus aureus*	(Guo et al., 2017)

Photo-catalysis/UVC/H_2O_2	UVC (254nm, 300W,800W) TiO_2 thin film Fluence=0-120mJ/cm^2 H_2O_2=10-100mmol/L Phosphate-buffered saline solution (pH = 7.4) Natural water from drinking water source(pH = 7.2)	There was no significant difference noted between natural water and phosphate-buffered saline solution in bacteria deactivation. 4.7 log ampC and 5.8 log mecA elimination were achieved in the presence of TiO_2 for both matrices	*Pseudomonas aeruginosa* ,*staphylococcus aureus*	(Guo et al., 2017)

2.7.3 Photo-Fenton coupled oxidation process

This variant of the Fenton oxidation process, known as photo-Fenton, employs a Fenton catalyst and is activated by exposure to UV light (Deemter et al., 2021). The photo-Fenton process combines the traditional Fenton reagents (H_2O_2 and Fe^{2+}) with UV-Vis-activation, which produces more hydroxyl radicals. Such increase in radical production is achieved through two auxiliary processes: photoreduction of Fe^{3+} to Fe

$^{2+}$ ions and photolysis of peroxide (Rahim Pouran et al., 2015). Compared to other Advanced Oxidation Processes (AOPs) like the UV/H_2O_2 system and the standard Fenton technique, photo-Fenton systems offer advantages such as a higher Fe^{2+} removal rate and more efficient H_2O_2 utilization (Ma et al., 2021). The effectiveness of the Fenton system in cell inactivation is contingent on the concentrations of Fe^{2+} and H_2O_2 employed in the treatment (Uhl et al., 2015). The best limitation of the Fenton process is that it may be less efficient in the decomposition of H_2O_2 and this can be associated with the slow kinetics of the Fe^{3+} /Fe^{2+} redox cycle. On the other hand, the UV/Fe^{2+}/H_2O_2 system could be a good treatment method of destruction of bacterial pollutants in wastewater because the use of UV light gives a considerable speed in Fe^{2+} regeneration in Fenton system.

Photo-Fenton has been demonstrated in many research to play a relevant part in the pathogenic inactivation of wastewater under the excitation of both UV and sun radiation. García-Fernández *et al*. examined the deactivation of bacteria and fungi, namely *Escherichia coli* and *Fusarium solani*, via the use of Fe^{3+}/sun light, H_2O_2/fulfilling sunlight and solar photo-Fenton methodologies within an environment that was nearly neutral (García-Fernández et al., 2012). Their findings revealed that highly efficient bacterial inactivation was achieved with a photo-Fenton treatment employing 5 mg/L of Fe^{3+} and 10 mg/L of H_2O_2, resulting in a 5-log pathogenic deactivation of *E. coli* within just 10 minutes. The reduction of *Fusarium solani* was further achieved with a coupling 2.5 mg/L of Fe^{3+} and 5 mg/L of H_2O_2, and a 3.4-log reduction was observed after 3 hours.

2.7.4 Enhancement of disinfection using natural adsorbents

The natural adsorbents have an ability to enhance the process of disinfection; conveniently removing the contaminants of the wastewater (Aryee et al., 2021). Some of these natural materials consist of activated carbon, silver nanoparticles, chitosan, natural zeolites, and many other adsorbents based on minerals. Results indicate that these materials show great promise with respect to their ability to adsorb various water pollutants, including pathogens (protozoa, bacteria and viruses), organic residues and heavy metals so as play a key role in improving water quality. Such adsorbents also increase the disinfection activity when combined with the

Advanced Oxidation Process (AOP) systems because of their advantageous adsorption site (Souza et al., 2011).

Unit crystalline microporous alumina-silicate solids are the zeolites that very usefully have been employed as adsorbents due to zeolites surface chemistry and morphology (Korkuna et al., 2006). Through increased residual contaminants, Zeolites improve disinfection by minimizing its inhibitors (Alonso-Vicario et al., 2010). Lately, the study has concentrated on enhancing the efficiency of AOPs systems using zeolites instead of activated carbons as well (Soon & Hameed, 2011). Natural zeolite, activated carbon, and clays are only a few of the materials that have been successfully embedded with transition metals, which led to outstanding catalytic performance in Advanced Oxidation Processes (AOPs) (Buthiyappan et al., 2016). When natural zeolites are used as carriers of TiO_2 a synergy effect is supposed to take place enhancing photocatalytic performance. It is possible by combining the natural zeolites adsorption ability and photocatalytic activity of TiO_2 (Castañeda-Juárez et al., 2019). Application of the combination of zeolites and TiO_2 has also been uniformly efficient in the process of enhancing the rate of disinfection of dangerous water pollutants. In enhancing this performance, it is because the by-product of the adsorption of the bacterial pollutants onto the surface of the zeolite compound raises the localized concentration of the bacterial pollutants near the TiO_2 semiconductor, thus boosting the rate of the decomposition of the pollutants (Diban et al., 2021).

Muleja *et al*. studied the removal of *Escherichia coli* utilizing cobalt-impregnated natural zeolite (Co-Nat/Zeolite) (Muleja et al., 2022). They concluded that their findings revealed that the Co-Nat/Zeolite activated the inactivation of the *E. coli* bacteria by way of its adsorption to the surface of the microorganism. The adsorption resulted in the oxidative stress that functionally inactivated *E. coli*. The study also found out that there was a filtration effect of the cobalt impregnated natural zeolite when the effluent was being treated.

CHAPTER THREE

Materials and Methods

3.1 Materials and Reagents

The reagents utilized in this research were purchased from Biocare Enterprises Limited, Nairobi, Kenya, and were of analytical grade. These included Eosin Methylene Blue Agar ES (EMB Agar), Lactose Broth (LB Agar), Nutrient agar (NA), anhydrous sodium sulfate, sulfuric acid, sodium hydroxide, boric acid, hydrochloric acid, ethanol, hydrogen peroxide (H_2O_2), and sodium hydroxide (NaOH). Sigma Aldrich supplied Titanium dioxide (TiO_2) powder (Technical grade, 99% purity), while natural zeolites were bought from Pratley Mining Company in South Africa. The tests were conducted in a UV reactor fitted with an 8 W UV-C lamp. The tests were conducted in a bench-scale UV reactor fitted with a low-pressure mercury UV-C lamp (8 W, emission peak at 254 nm) housed inside a quartz sleeve. The reactor was operated in batch mode with ~300 mL effective working volume. Based on the manufacturer's specifications, the average irradiance at the water surface was approximately 0.5 mW cm^{-2}, corresponding to fluence values of 0–1800 mJ cm^{-2} depending on exposure time. Mixing was maintained with a magnetic stirrer (300 rpm) to ensure uniform catalyst suspension, and the temperature was held at 25 ± 2 °C. A Scanning Electron Microscope (FEI NOVANANO SEM 230) was employed to assess the surface morphology of the TiO_2-Zeolite catalyst and the zeolite. An X-ray diffractometer (Bruker D8) was utilized to examine the crystalline structure of the TiO2 particles, applying nickel copper filtered Cu K (α) radiation (40 kV and 40 mA). Nitrogen physisorption measurements were performed using ASAP 2020 V3.00 H, Unit 1 Serial #: 590 physisorption analyzer built-in software, and the data were evaluated according to Brunauer, Emmett, Teller (BET).

3.2 Sampling and sample analysis

The samples were collected from the Embu sewage treatment plant located in Embu County. It lies at a latitude of 0.5504812˚S and a longitude of 37.4625973˚E.

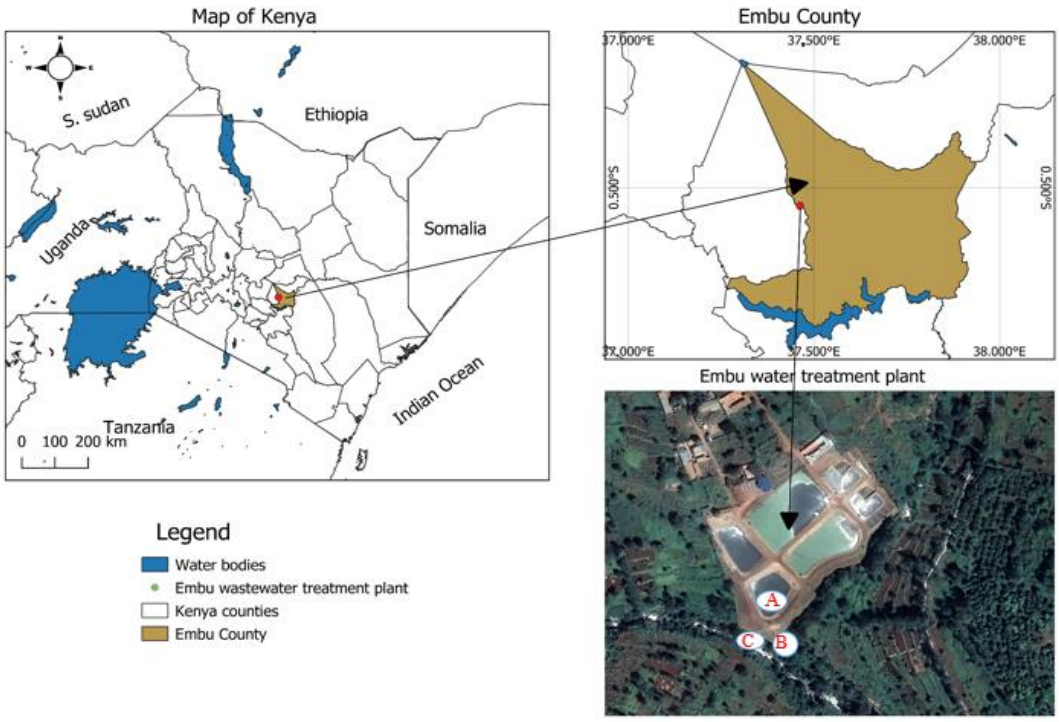

Figure *3*.1: Aerial view of Embu Waste Stabilization Pond system showing treatment sequence (anaerobic pond → facultative pond → maturation pond) and the three sampling sites: (A) WWTP outflow, (B) first dilution point (~100 m downstream), and (C) second dilution point (~500 m downstream).

The wastewater used in this study was obtained from the Embu Municipal Wastewater Treatment Plant (WWTP), Kenya, which is operated as a Waste Stabilization Pond (WSP) system. The facility has a hydraulic capacity of approximately 5,000 m^3/day and serves an estimated population equivalent of 20,000. The system comprises a series of ponds designed for sequential treatment, including an anaerobic pond, a facultative pond, and a maturation pond, before discharging treated effluent to a nearby river Rupingazi.

Sampling was conducted at three points along the treatment train: (A) the final pond outflow (WWTP effluent), (B) a point ~100 m downstream where effluent mixes with river water, and (C) a second dilution point further downstream (~500 m). Sampling followed a discrete grab sampling method, where mid-depth samples were collected in sterile containers and immediately transported on ice to the laboratory for analysis within 6 h. Each sample was taken at mid-depth (~30 cm) to avoid surface films and bottom sediment interference. Sampling was conducted on five consecutive dry-weather days, with no recorded rainfall and steady hydraulic operation of the ponds,

in order to minimize short-term variability and avoid stormflow effects. At each of the three sites, triplicate biological samples were collected, and each analysis was performed in technical triplicate, ensuring reproducibility and robust statistical treatment of the data.

We acknowledge that the dataset is limited to a short dry-weather period and does not capture seasonal variability or stormflow conditions, which may affect effluent quality and inactivation performance. These constraints are discussed as limitations of the study. An aerial photograph of the WWTP and surrounding catchment (Figure 3.1) illustrates the process flow from influent inlet to final outlet, with arrows indicating hydraulic direction and the three sampling sites.

3.3 Experimental set-up

The experiments were conducted in a UV (Ultraviolet) photoreactor. The reactor consisted of reactor outer body, UV sleeve and UV lamp. The lamp emitted UV-C radiation, which has a wavelength range between 200 and 280 nm. The wavelength range is highly effective at disrupting the genetic material of bacteria rendering it incapable of reproduction or growth. The details of the reactor is shown in Figure *3.2*.

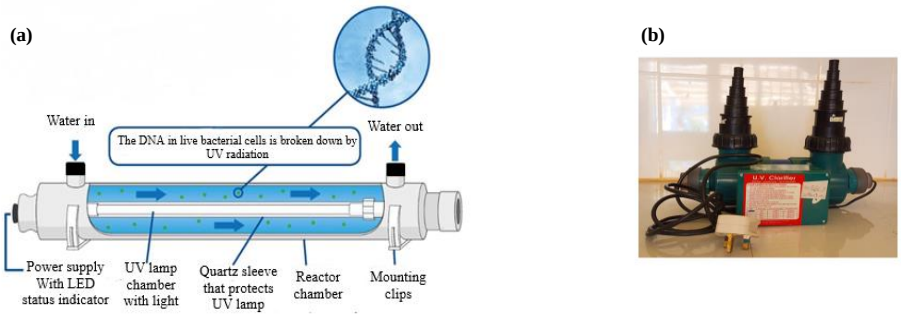

Figure *3.2*: The UV reactor details for (a) internal component and (b) external component

The UV lamp is housed within a protective quartz sleeve made of high-purity quartz to allow the UV-C light to pass through without interference while protecting the lamp from direct contact with the water. The UV is powered by electricity from the main socket. The reactor is fitted with a ballast which ensures a steady supply of electricity and protects against power surges. The reactor chamber is the enclosure of the UV lamp and quartz sleeve. Wastewater flows through the chamber, and the UV-C light emitted by the lamp irradiates the water, causing disinfection.

3.4 Synthesis of TiO_2/Zeolite catalyst

A zeolite-based photocatalyst was prepared via a solid-solid dispersion technique. Briefly, TiO_2 powder was added to natural zeolite and mixed in an agate pestle and mortar with ethanol (10 mL ethanol per gram of solid) for 20 minutes to ensure homogeneity. The resulting paste was evaporated at 60 °C for 2 h to remove residual solvent, then dried at 105 °C overnight in an oven. The dried material was subsequently calcined in air at 450 °C for 4 h using a heating ramp rate of 2 °C/min, followed by cooling to room temperature inside the furnace. Catalysts were prepared with TiO_2 loadings of 5, 10, 15, and 20 g/L on zeolite.

3.5 Photodegradation experiments

3.5.1 UV photolysis

The main aim of this study was to assess the effect of UV photolysis on bacterial disinfection under different pH conditions, i.e., at pH values of 3.0, 7.7, and 9.0. The 300 ml of wastewater was added to the UV reactor in every trial. The samples were taken every 10 minutes and over a total of 60 minutes. Thereafter, these samples were evaluated with the aid of a UV-Vis spectrophotometer.

3.5.2 H_2O_2 disinfection

In order to determine how the concentration of hydrogen peroxide (H_2O_2) affects the disinfection of bacteria, H_2O_2 was added to the wastewater to yield final concentrations of 0.7 mM, 1.4 mM, 2.1 mM, and 2.8 mM (Apollo et al., 2014a).

3.5.3 UV/H_2O_2 disinfection

The objective of this experiment was to determine how varying the dosage of the hydrogen peroxide (H_2O_2) affected the UV disinfection of *E. coli*. During the investigation, the concentrations tested were of H_2O_2, which included 0.7 mM, 1.4 mM, 2.1 mM, and 2.8 mM, which were tested in 300 ml wastewater samples in a UV reactor. There were 10-minute intervals in which the samples were taken with the overall duration being 60 minutes. The experiment was carried within a pH level of 7.7 since it was also the initial pH of the sample of wastewater collected in the sampling point.

3.5.4 Adsorption on zeolite

Zeolite is known to have a wide range of adsorption sites, and they can be useful in concentrating bacteria over its surface. The feature then makes catalytic disinfection easier with the variable very strain in which a photocatalyst is put on the zeolite support. To clarify the character of bacterial adsorption into zeolite, adsorption tests were thus carried out, since it may be of the ability to improve the working of hybrid zeolite-photocatalyst combinations utilized in the disinfection of bacteria. In particular, this experiment was set up to research how adsorption happened, *E. coli* on zeolite. The adsorption study was performed in a reactor without a UV lamp, utilizing zeolite dosages of 10.0 g, 18.0 g, and 30.0 g. For each experimental condition, sampling occurred at 10-minute intervals over a total period of 60 minutes.

3.5.5 UV/TiO_2-Zeolite disinfection

The performance of UV/TiO_2-Zeolite **s**ystem was investigated under pH of 7.7. A sample of 18.0g of the TiO_2-supported zeolite catalyst was weighed and then transferred into a 500 ml conical flask and 300 ml of wastewater sample was added to the flask with shaking for mixing. The prepared sample was transferred into a UV reactor. Sampling was done after every 10 minutes.

3.5.6 UV/TiO_2-Zeolite/H_2O_2 disinfection

The performance of UV/TiO_2-Zeolite/H_2O_2 system was also investigated under pH condition of 7.7 and 1.4mM hydrogen peroxide. The hydrogen peroxide dosage of 1.4mM was used because it was the best condition from the preliminary experiment that investigated the effect of peroxide on direct bacterial disinfection. A sample of 18.0g of TiO_2-supported zeolite catalyst was weighed and put in a 500ml conical flask. 300 ml of wastewater was added. The flask sample was transferred in the UV reactor with the addition of 1.4 mM hydrogen peroxide. Each disinfection experiment was repeated in triplicate (n = 3) under identical conditions. Results were reported as mean ± standard deviation (SD). Statistical significance between treatments was determined using one-way ANOVA with Tukey's post hoc test ($p < 0.05$). Pairwise comparisons were further analyzed using a two-tailed Student's t-test where applicable.

3.5.7 Physicochemical characterization of effluent

Wastewater samples were characterized for key physicochemical properties known to affect disinfection. Parameters measured included pH, electrical conductivity, turbidity (NTU), chemical oxygen demand (COD), total organic carbon (TOC), UV absorbance at 254 nm (UV254), specific UV absorbance (SUVA), alkalinity (as $CaCO_3$), and major anions (Cl^-, NO_3^-, HCO_3^-). COD was determined by the closed reflux method (APHA 5220D), TOC by a TOC analyzer (Shimadzu TOC-L), turbidity using a Hach 2100N turbidimeter, and UV254 with a spectrophotometer (1 cm path length). Ion concentrations were analyzed by ion chromatography (Dionex ICS-1100).

3.5.8 Residual H_2O_2 measurement and quenching

Immediately after treatment, aliquots were taken to quantify residual H_2O_2 and to quench it before microbiological plating. Residual H_2O_2 was measured colorimetrically using the titanium sulfate method (peroxytitanic acid complex; measurement at 405–410 nm; 1 cm cuvette). A 6-point calibration curve (e.g., 0, 0.05, 0.10, 0.25, 0.50, 1.00 mM) was prepared fresh with analytical-grade H_2O_2 in the same matrix. Concentrations were calculated from the linear fit ($C = (A - b)/m$; A = absorbance, m = slope, b = intercept).

To eliminate any carryover disinfection during plate incubation, samples were quenched as follows:

- Primary quencher: Catalase to a final activity of 200 U mL^{-1}, gentle mix for 2 min at room temperature.
- Verification: Re-test residual H_2O_2 with the titanium method; proceed only if below method LOD (see below).
- Alternative (verification required): Sodium thiosulfate at 10 mg L^{-1} final. Prior to use, confirm no toxicity to *E. coli* at this dose via control platings (Section 2.7).

Method performance: Instrument blank = reagent water; LOD (method) ~ 0.02 mM based on 3σ of blank; LOQ set at 0.05 mM from the calibration. All CFU samples were plated only after quenching reduced residual H_2O_2 below the method LOD.

Quality control: (i) Spike-recovery: add known H_2O_2 (e.g., 0.10 mM) to a quenched aliquot; acceptable recovery after quench <10% of spike, confirming effective

removal. (ii) Plate-viability control: expose untreated cells to the quencher alone to confirm no reduction in CFU relative to a no-quencher control.

3.5.9 Mechanistic controls for •OH involvement

Radical scavengers. To test the role of hydroxyl radicals (•OH), we repeated the UV/H_2O_2, UV/TiO_2–zeolite, and UV/TiO_2–zeolite/H_2O_2 experiments in the presence of selective •OH scavengers:

- tert-Butanol (t-BuOH): final concentration 50 mM (excess relative to expected radical levels).
- Sodium formate ($HCOO^-$): final concentration 20 mM.

Scavengers were added 2 min before treatment. Controls without scavenger were run in parallel under identical conditions. Inactivation rate constants (k_app) were re-estimated as in Section 2.8.

Inhibition metric. Scavenger inhibition of disinfection kinetics was calculated as:

$$\%\ inhibition = \frac{k_o - k_{scav}}{k_0} \times 100$$

where k_0 is the apparent rate constant without scavenger and k_{scav} is with scavenger.

3.5.10 Chemical probe for •OH (benzoate → salicylate fluorescence)

Probe dosing. Sodium benzoate was added at 1.0 mM immediately before treatment. Aliquots (1.0 mL) were withdrawn at 0, 5, 10, 20, 30, 40, and 60 min, filtered (0.22 μm), and analyzed by fluorescence. Fluorescence detection. Formation of salicylate (hydroxylated benzoate) was monitored on a fluorometer at λ_ex = 305 nm and λ_em = 410 nm using 1 cm quartz cuvettes. A 6-point external calibration (0–50 μM sodium salicylate) in matrix-matched effluent was used for quantification (linear regression $C=(A-b)/m$).

Controls.

(i) Light control (benzoate without UV).

(ii) Matrix control (UV without benzoate).

(iii) Scavenger control (benzoate + UV + 50 mM t-BuOH) to confirm fluorescence is •OH-dependent.

All tests were in triplicate (n = 3).

3.5.11 Regrowth and Photoreactivation Experiment

It has been recorded that *E.coli* can regain viability and regrow after the stress impacted by disinfection is removed [20]. To assess the potential for bacterial repair and regrowth, two post-treatment conditions were tested: dark repair and photoreactivation. Immediately after UV/AOP treatment, 10 mL aliquots of effluent were transferred into sterile Petri dishes. For dark repair, samples were wrapped in aluminum foil and incubated at 25 ± 2 °C for 24 h. For photoreactivation, samples were exposed to visible light (400–700 nm) using two cool-white fluorescent lamps positioned 30 cm above the samples, providing an average irradiance of ~6 W m^{-2} (measured with a lux meter equivalent to ~2000 lux) at room temperature for 24 h. After incubation, aliquots were plated on nutrient agar and colony-forming units (CFU) were enumerated. The extent of repair was expressed as [21];

$$\text{Percentage photoreactivation } (\%) = \frac{(N_P - N)}{(N_O - N)} \times 100\% \quad (2)$$

where N_P = is the *E.coli* cells in the photoreactivated sample (CFUs/ml), N = is the *E.coli* cells that survived after disinfection (CFUs/ml), and N_O = is the *E.coli* cells before disinfection (CFUs/ml).

3.6 Photo-reactivation experiment

3. 6.1 Disinfection capacity

This experiment was designed to assess the potential for bacterial regrowth or reactivation following each tertiary wastewater treatment process. Sewage wastewater samples underwent characterization to quantify cultivable *E. coli* microorganisms at three distinct time points: prior to tertiary treatment, immediately post-treatment, and after a three-day storage period. The disinfected wastewater samples were subsequently stored in cotton-plugged Erlenmeyer flasks under ambient light and temperature conditions (approximately 12 hours light/12 hours dark, 22°C) to evaluate the recovery of fecal coliforms and *E. coli* bacteria after tertiary treatment. Untreated wastewater samples were concurrently stored and analyzed alongside the treated samples for comparative purposes.

3.7 Sample analysis

3.7.1 Culture media preparation (Qualitative analysis)

This experiment was done to prepare the nutrients, a source of energy and environmental conditions in order for the *E. coli* bacteria to grow and reproduce for

enumeration. The Lactose broth (LB) medium was prepared in single (x1) and double-strength (x2) concentrations. Single strength medium (x1) means that the lactose broth medium was prepared at its standard concentration, as recommended by the manufacturer. Double-strength medium (x2) means that the lactose broth medium was prepared at twice the standard concentration of the ingredients. Double-strength medium was prepared to promote the growth of microorganisms that required more nutrients. Five tubes of double-strength LB medium and ten tubes of single-strength LB medium for each wastewater sample were prepared. The control medium was also prepared in each of the media concentrations. To sterilize the prepared media and eliminate any infectious bacteria, it was autoclaved at 121°C for 15 minutes. Subsequently, using a sterile pipette, 10ml of the wastewater sample was introduced into five tubes, each containing 10ml of double-strength (2x) medium. Similarly, 1 ml of the water sample was added to another five tubes, each holding 10ml of single-strength (1x) medium. The remaining five tubes, also containing 10ml of single-strength (1x) medium, received 0.1ml of the water sample. All these tubes were then incubated at 37.0°C for 24 hours to facilitate bacterial culturing.

3.7.2 Bacterial culture and isolation

This experiment was conducted in order to isolate and differentiate *E.coli* bacteria from other fecal coliform bacteria and monitor their growth. The streak technique was used to obtain a pure culture of *E.coli*. To perform the streak method on the EMB agar media, the following steps were followed: Each of the Petri dishes was labeled with the sample name and the name of the bacterial culture to be streaked. The inoculation loop was sterilized by flaming it until it turned red hot, then allowed to cool, making sure that all contaminants on the wire were incinerated. A small bacterial culture sample was obtained from the positive vial using the inoculation loop. The loop was touched to the surface of the agar, starting at the edge of the plate and moving in a straight line towards the center of the plate to achieve the isolation goal and microbe purity. Without lifting the loop, the Petri dish was turned 90 ^{O}C and streaked with the bacterial culture by moving the loop across the agar surface in a straight line perpendicular to the first streak in order to obtain isolated, well-distributed, and identifiable colonies. The above step was repeated 5 times, making sure that the second and third streaks overlap slightly with the previous streaks. The plates were incubated at 37 ^{O}C for 25 hours in order to isolate *E.coli* bacteria from

other fecal coliforms, quantify the bacteria and monitor their growth and colony morphology.

3.7.3 Enumeration of *E.coli* bacteria (Quantitative analysis)

This experiment was conducted in order to isolate and differentiate *E.coli* bacteria from other fecal coliform bacteria that might have recovered during re-culturing. This method was also applied during the quantification of *E.coli* bacteria. The quantified bacteria were then related to the absorbance of UV spectrophotometer at OD_{600} of the original sample before dilution which acted as a blank sample. *E.coli* bacteria were enumerated based on the serial dilution method.

For the determination of *E.coli* bacteria within the samples, serial dilution method was applied. It entailed diluting 10ml of the wastewater samples in a series of tubes with diluent sterilized solution. Each dilution was plated (0.1ml each) on EMB agar plates and incubated at 37.0 OC for 24 hours to allow the bacteria to proliferate. Viable cells within the initial wastewater samples were counted using the colony counter to enumerate. Only plates with colony numbers ranging within a range of 30 to 300 were counted to yield accurate results. Any value less than 30 colony numbers was recorded too few to count (TFTC) and more than 300 colony numbers too numerous to count (TNTC). The number of colony-forming units (CFUs) in the original bacterial wastewater samples was calculated using the following formula:

$$\text{Colony forming units per ml} = \frac{\text{Number of colonies} \times \text{dilution factor}}{\text{Volume of the culture plates}} \quad (28)$$

3.8 Protein analysis by the Kjeldahl method

The main aim of this study was to gain insights into the inactivation mechanism of *E. coli* bacteria in wastewater. Wastewater samples, both before and after *E. coli* inactivation via UV photolysis, UV/TiO_2-Zeolite, and UV/TiO_2-Zeolite/H_2O_2 treatments, underwent protein analysis using the Kjeldahl technique. During this process, amino nitrogen within a sample, along with any free ammonia, is quantitatively transformed to ammonium in the amidst of concentrated H_2SO_4, potassium sulfate (K_2SO_4), and cupric sulfate ($CuSO_4$) as catalysts. Following the addition of a base, the ammonia is distilled from the alkaline medium and subsequently absorbed into a boric acid solution. The quantity of ammonia is then determined by back titration with a standard mineral acid. The fundamental principle

of the Kjeldahl method is that nitrogen-containing samples, upon heating with concentrated H_2SO_4, are entirely converted to ammonium sulfate ($(NH_4)_2SO_4$). The resulting liquid is then treated with an excess base, and the liberated ammonia gas (NH_3) is absorbed by an excess of standard acid. The amount of ammonia is ascertained by quantifying the amount of acid neutralized during the back titration.

$$N\% = \frac{V_1 \times n_1 \times F_1 \times MWn}{Ws \times 10} \quad (29)$$

$$\text{Protein } \% = N\% \times \text{Factor} \times F_2 \quad (30)$$

Ws is the sample weight, V_1 is the volume of 0.1M hydrochloric acid, n_1 is the hydrochloric normality, Factor is the constant value, which is 6.25, F_1 is the acid factor, MWn is the molecular weight of Nitrogen, and F_2 is the dilution factor.

3.8.1 Digestion of the sample

Initially, 2 ml of the sample was precisely measured and transferred into a flask. Subsequently, 2 g each of $CuSO_4$ catalyst and K_2SO_4 were weighed and introduced into the wastewater sample within the flask. A volume of 20 ml of concentrated H_2SO_4 was then added to the flask via a pipette, followed by shaking to ensure thorough mixing. The sample was later placed on a digester rack and heated at 300 degrees Celsius within the amount of time 2 hours. The digestion process was complete as illustrated by the visualization of a clear green solution. Before distillation, the sample was digested then cooled down to room temperature and subsequently diluted using distilled water. The final step is filling the diluted digested sample in a 100ml volumetric flask and adding further distilled water to make it reach the final volume of 100ml.

3.8.2 Distillation of the sample

To start the distillation, 30 mL of 4% boric acid solution was measured and transferred into a conical flask. This flask was then positioned on the distillation unit, where it would collect the evolving distillate. Subsequently, 10 ml of the digested and diluted sample was introduced into the distillation flask. Following this, 50 ml of 40% sodium hydroxide was added to the distillation flask, along with an additional 50 ml of distilled water. The distillation unit was heated to 200°C, ensuring the water circulation pump of the condenser was operational. A total of 100 ml of the distillate was collected.

3.8.3 Titration of the sample

0.1M of standardized hydrochloric acid was put in a burette. A few drops of the methyl indicator were added to the conical flask containing the collected distillate changing from transparent color to yellow. The distillate was titrated with 0.1M HCl. The color changed from yellow to orange.

We quantified Total Kjeldahl Nitrogen (TKN) following the closed-reflux digestion and titration/colorimetric determination. Because Kjeldahl nitrogen includes ammonium and organic nitrogen from all dissolved/particulate matter, it is not specific to bacterial biomass. For reporting, we present TKN (mg N/L) and the derived "protein" only as a proxy for total organic nitrogen (conversion factor protein = 6.25 × organic-N), recognizing potential interference from dissolved organic matter (DOM) in the effluent.

Quality control. We analyzed matrix blanks (filtered effluent with no cells) and spike recoveries (glycine standard) to assess background and method performance. Where noted, "protein" results are blank-corrected by subtracting the matrix blank. To obtain a cell-specific signal, we additionally measured the Live/Dead fluorescence staining: SYTO 9/propidium iodide with epifluorescence microscopy or flow cytometry; percent intact cells reported.

3.9 Experimental analysis

A UV-Vis spectrophotometer was employed to monitor the *Escherichia coli* bacterial population at a wavelength of 600 nm. Additionally, UV-Vis scanning was performed to gain insights into the reduction profile of the bacterial wastewater under different experimental conditions. The surface morphology of the TiO2-Zeolite catalyst and the elemental composition of zeolite were investigated using a Scanning Electron Microscope (SEM), specifically the FEI NOVANANO SEM 230 model, which was equipped with Energy Dispersive X-ray spectrometry (EDX). To evaluate the crystalline structure of the TiO_2 particles, an X-ray diffractometer, model Bruker D8, was utilized, employing nickel-copper filtered Cu K (α) radiation at 40 kV and 40 mA. The adsorption characteristics of nitrogen gas on zeolite were precisely described using an adsorption isotherm. This isotherm graphically depicts the amount of nitrogen molecules (adsorbates) captured within the zeolite's porous structure

(adsorbent), correlating it to the partial pressure of the gas phase at a consistent temperature. Following this, the zeolite's surface area was established via a BET single-point approach. This calculation relied on the measured nitrogen uptake at liquid nitrogen temperature, as depicted in Figure 8. It's worth noting that both single-point and multipoint methods are valid for determining surface area.

3.10 Data Analysis

Data from disinfection experiments were analyzed statistically. Values are expressed as mean ± SD of three independent replicates (n = 3). The LOD was set at <1 CFU/100 mL, while the LOQ was defined as 30 – 300 range CFU/plate. Analysis of variance (ANOVA) was applied to determine significant differences among multiple treatments, with Tukey's HSD post hoc test for pairwise comparisons. In cases where only two treatments were compared, a two-tailed Student's t-test was used. A p-value <0.05 was considered statistically significant. Model fits. For mechanistic tests, differences in k_{app} and salicylate formation rates were evaluated by one-way ANOVA with Tukey's HSD ($p < 0.05$). Report values as mean ± SD (n = 3).

3.11 Energy consumption and cost estimation

The specific energy consumption (SEC) of the UV-based systems was calculated using:

$$SEC = \frac{P \times t}{V}$$

where P is the UV lamp power (8 W = 0.008 kW), t the treatment time (h), and V the treated volume (0.0003 m³ for 300 mL reactor). SEC was normalized to kWh/m³. Approximate operational cost was estimated by multiplying SEC with the average electricity tariff in Kenya (~0.15 USD/kWh). Values were then compared with literature reports for chlorination and ozonation.

3.12 Disinfection kinetics modeling

Inactivation kinetics of *E. coli* under UV and AOP treatments were modeled using three classical approaches:

Pseudo-first-order model

$$\ln(\frac{N}{N_O}) = -K_{app}t$$

Chick–Watson model

$$log\ (\frac{N}{N_O}) = -kC^n t$$

Hom model

$$ln\left(\frac{N}{N_O}\right) = -kt^n$$

where N_0 = initial bacterial concentration (CFU/100 mL), N = bacterial concentration at time t, C = oxidant concentration (H_2O_2 dose), k = rate constant, and n = reaction order. Model parameters were estimated by nonlinear regression (OriginPro 2022), and goodness-of-fit was assessed using the coefficient of determination (R^2) and the Akaike Information Criterion (AIC).

Table *3.1*: Operational conditions for UV, H_2O_2, UV/H_2O_2, UV/TiO_2–zeolite, and UV/TiO_2–zeolite/H_2O_2 experiments.

Parameter	**Value(s) used**	**Reference**
pH	3.0, 7.7, 9.0	Adjusted with HCl/NaOH
UV wavelength	254 nm (low-pressure Hg lamp)	Peak emission
UV fluence (dose)	0 – 1800 mJ cm^{-2}	Calculated as irradiance × time
H_2O_2 concentration	0.7, 1.4, 2.1, 2.8 mM	Analytical grade
TiO_2 loading	15 g/L (calcined TiO_2–zeolite composite)	Dried 105 °C, calcined 450 °C, 4 h
Catalyst dosage	3–5.4 g per 300 mL reactor volume	Equivalent to 10–18 g/L
Reactor volume	300 mL	Quartz sleeve, bench-scale
Mixing speed	300 rpm (magnetic stirrer)	Ensures suspension & uniform UV
Residence time	10–60 min	Sampled at intervals
Initial *E. coli*	~10^8 CFU/100 mL	Real WWTP effluent, Embu, Kenya
Temperature	25 ± 2 °C	Maintained with water bath

CHAPTER FOUR

RESULTS AND DISCUSSION

4.1 Catalyst characterization

The structural and morphological properties of the TiO_2–clinoptilolite catalyst were investigated to confirm its crystallinity, phase composition, and surface features, since these characteristics greatly influence photocatalytic activity. Techniques such as X-ray diffraction (XRD), energy-dispersive X-ray spectroscopy (EDX), scanning electron microscopy (SEM), and BET surface area analysis were employed. The results provide insight into the distribution of TiO_2 phases, elemental composition, and the adsorption capacity of clinoptilolite, all of which determine the overall efficiency of the hybrid disinfection system.

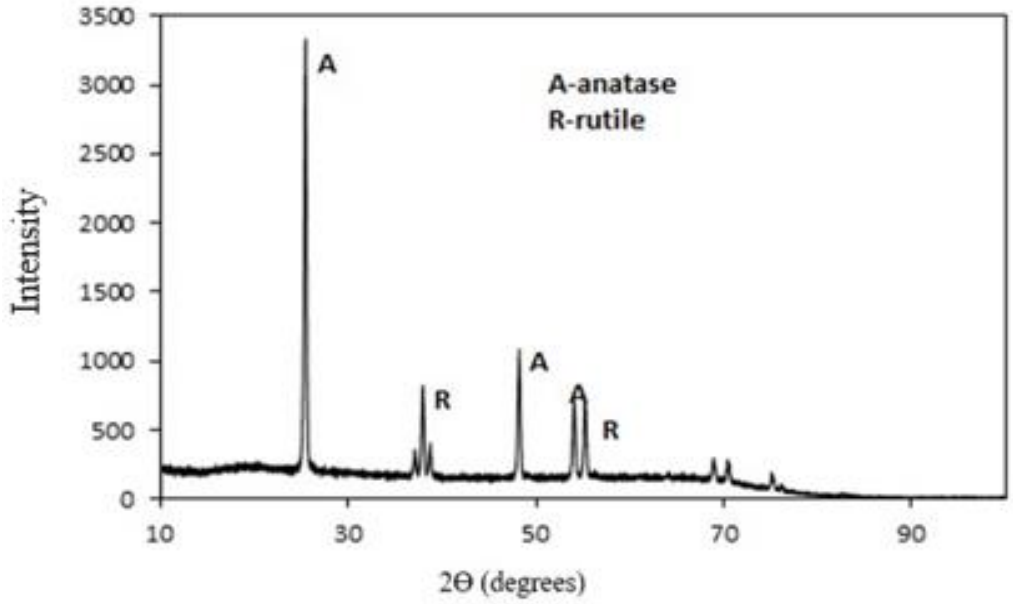

Figure *4.1*: XRD characterization of TiO_2 powder

The crystalline structure of the TiO_2 particles was assessed using X-ray power diffraction. The anatase's XRD peak characteristics were seen in Figure 4.1 at 2θ = 25.4. Other anatase-corresponding peaks also showed up at 2θ = 48.3 and 54.9 (Wang et al., 2008). The content of rutile in the sample was determined as (Xiao et al., 2008).

$$X_R = \frac{1}{\left(1+\frac{0.8I_A}{I_R}\right)}$$

(31)

Where X_R is the mass fraction of rutile, I_A and I_R are the intensities of anatase and rutile, respectively. The anatase phase of the TiO_2 was discovered to be 95.6%. Because of the nature of the surface hydroxyl groups, the anatase phase has much better photocatalytic activity than rutile. It also has a higher energy gap of 3.20 eV than rutile, which has an energy gap of 3.02 eV (Armaković et al., 2023).

EDX evaluation was done to ascertain the zeolite's elemental composition; the findings are shown in Figure 4.2 and Table 4.2. The findings showed that the structure of the clinoptilolite zeolite used has more silicates than aluminates. Since zeolites with a larger Si/Al ratio are negatively charged, it can be inferred that the zeolite has an overall negative charge on its surface (Montalvo et al., 2012). Positively charged pollutants are drawn to the negatively charged zeolite's surfaces and brought closer to the photocatalyst, improving the photocatalytic process.

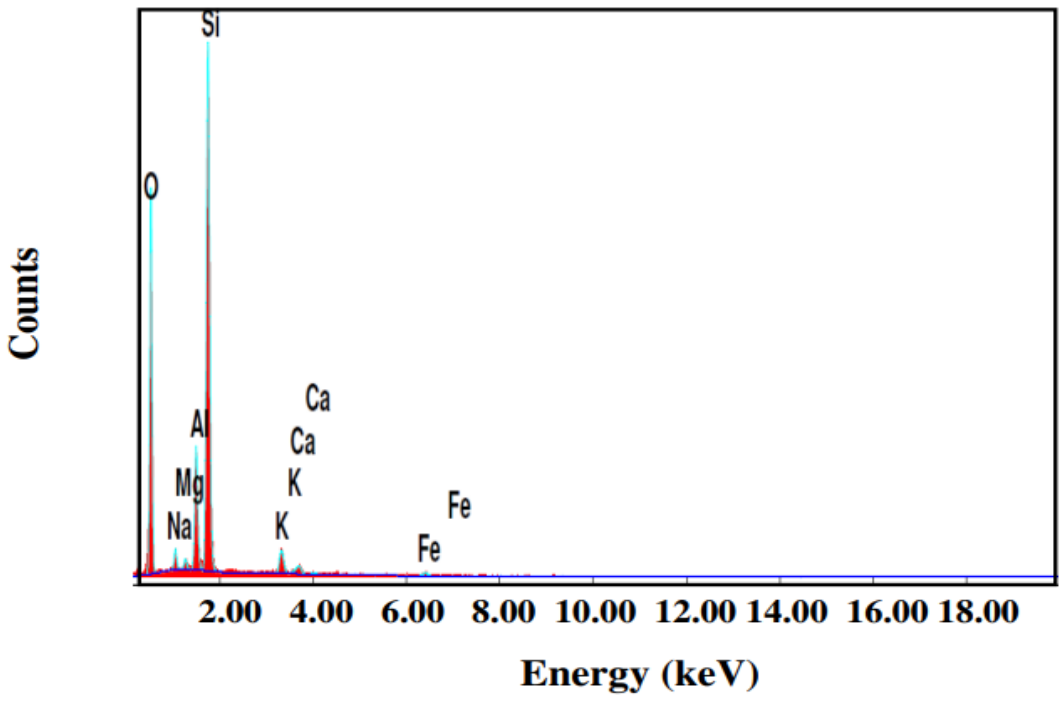

Figure 4.*2*: Results of EDX analysis of zeolite

Table 4.1: EDX data for elemental composition of natural zeolite.

Elements	Wt%
OK	57.41
NaK	1.52
MgK	0.63
AlK	6.5
SiK	30.63
KK	1.99
CaK	0.73
FeK	0.57
Total	100%

Figure *4*.3 presents the findings for SEM assessment for zeolite, TiO_2 and TiO_2-Zeolite supported catalyst before and after utilization. It is clear from a contrast of the SEM images in Figure 4.3(a) (zeolite only) and Figure 4.3(b) (TiO_2 affixed to zeolite) that the TiO_2 is firmly connected to the zeolite's surface. Additionally, TiO_2 was remained firmly connected to the zeolite even after deterioration (Fig. 4.3(c)), despite the fact that the density had decreased because some of the particles may have broken off as a result of attrition brought on by agitation throughout the reaction.

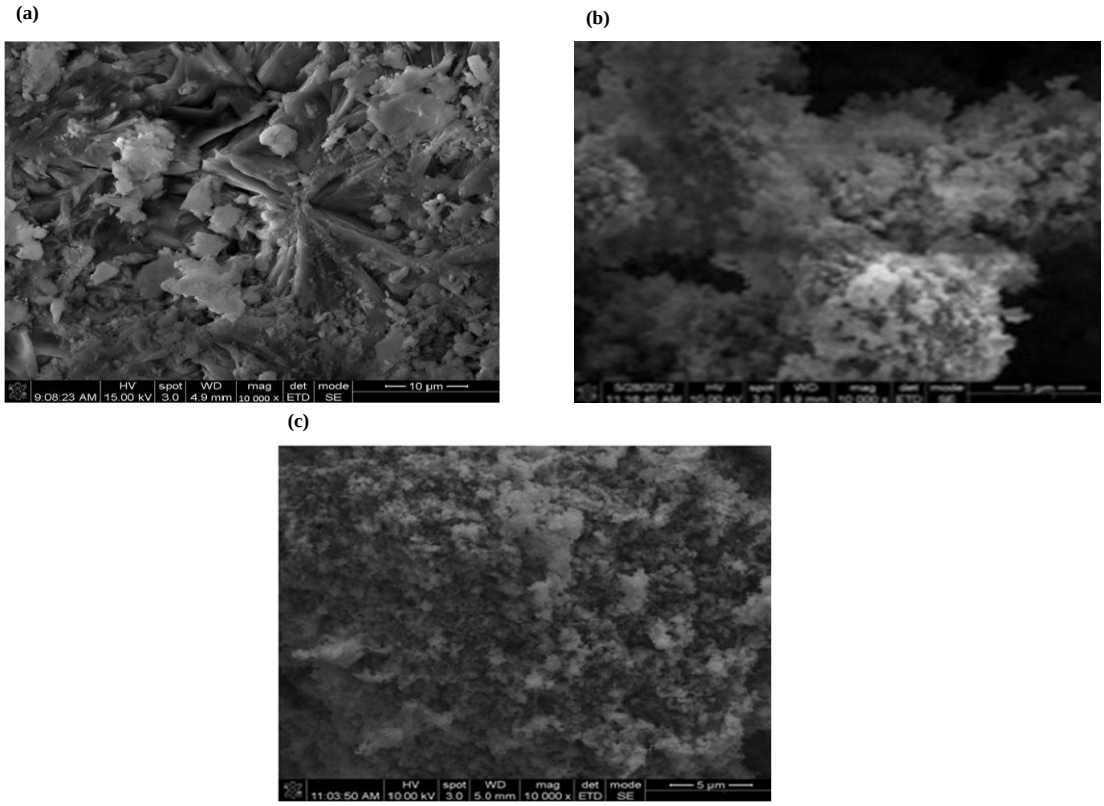

Figure *4*.3: SEM analysis for (a) Zeolite (b) TiO_2-Zeolite before disinfection and (c) TiO_2-Zeolite after disinfection

The specific surface area of zeolite, pore size and volume distribution were studied by BET. The linear plot of adsorption versus desorption isotherm of Zeolite was drawn as per the following equation (Ebadi et al., 2009).

$$\frac{1}{X\left[\left(\frac{P_O}{P}\right)-1\right]} = \frac{1}{X_m C} + \frac{C-1}{X_m C}\left(\frac{P}{P_O}\right) \quad (32)$$

X is the amount of N_2 gas adsorbed at a given relative pressure$\left(\frac{P}{P_O}\right)$, X_m is the monolayer capacity, which is the volume of the gas at STP and C is the BET constant. The plot of quantity adsorbed (cm^3/g STP) versus relative pressure$(\frac{P}{P_O})$, shows the adsorption and desorption behavior isotherm. Surface area, pore volume and pore-size distribution were obtained by measuring volume adsorbed at different $\frac{P}{P_O}$ values and by applying the Bruaner-Emmet-Teller (BET) method. In Figure 4.4, the BET surface area for the zeolite was determined to be 22.44 m^2/g, with its pore size falling within the mesoporous range (2-50 nm). This substantial surface area facilitated enhanced adsorption and loading of the target bacteria. The observed high surface area further indicated an increased number of active sites on the zeolite's surface. In mesoporous materials, the sorption behavior is governed by the strength of the fluid-

wall interface and the attractive interactions among fluid molecules. The mesoporous nature of the zeolite contributed to improved photocatalytic activities by promoting efficient *E. coli* mass transport to the zeolite surface and enhancing *E. coli* accessibility for the photocatalyst, thereby maximizing photocatalysis. Consistent with typical mesoporous materials, which often exhibit flat slits between two crystallographic planes, the zeolite displayed characteristic hysteresis loops. At the hysteresis point, the adsorption and desorption curves converged, forming a closed loop. Consequently, the isotherm presented two different characteristics: rapid adsorption near zero relative pressure and the onset of adsorption/desorption hysteresis at a relative pressure of 0.4. This phenomenon corresponds to multilayer adsorption and capillary condensation occurring within the mesopores (Ramesh et al., 2014).

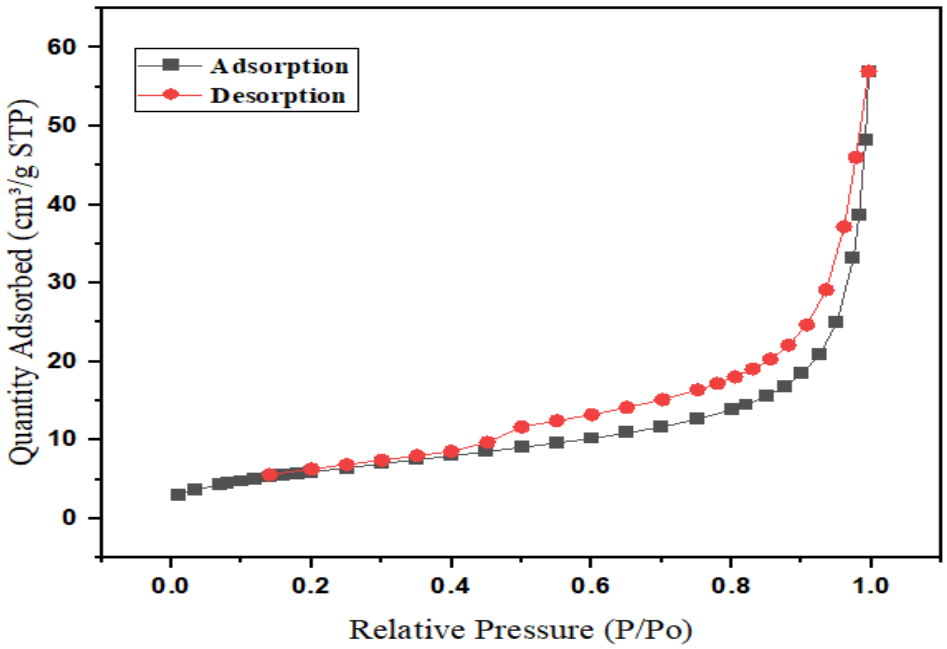

Figure *4.4*: BET adsorption isotherm analysis of natural zeolite.

4.2 Quantification of *E.coli* bacteria

Figure presents the concentration of *E. coli* (CFU/ml × 10^8) in wastewater discharged at the Embu sewage treatment plant, with samples collected from three locations (A, B, and C) over a five-day period. Location A corresponds to the wastewater effluent outflow, location B is the first dilution point (~100 m downstream), and location C is the second dilution point (~500 m downstream).

The results reveal clear spatial variation in *E. coli* counts across the three sites. Location A consistently recorded the highest bacterial concentrations, followed by locations B and C. Although slight fluctuations were observed across the five days, the relative ranking of the sites remained constant, indicating that dilution and natural die-off along the river are key contributors to reduced bacterial loads downstream. Location B showed moderately lower *E. coli* counts compared to site A, as the effluent mixed with river water, while location C, further downstream, showed the lowest concentrations due to additional dilution. Importantly, *E. coli* levels at all sites exceeded the National Environment Management Authority (NEMA) discharge standards of Nil/100 ml, highlighting the potential health risks associated with the current wastewater management practices.

To statistically verify these observed differences, a one-way ANOVA test was performed. The analysis showed a highly significant difference in *E. coli* counts between the three locations ($F = 10{,}283.36$, $p < 0.001$). This confirms that the variation in bacterial concentrations was not due to random chance but represents true site-to-site differences. A post hoc Tukey HSD test was then applied to determine which groups differed significantly. The results demonstrated that site A had significantly higher *E. coli* counts compared to both sites B and C ($p < 0.001$). Additionally, site B exhibited significantly higher counts than site C ($p < 0.001$). These findings align with the expected dilution effects along the river, where bacterial concentrations decrease progressively downstream.

Overall, the results demonstrate that the Embu wastewater treatment plant effluent introduces high *E. coli* loads into the receiving river, which are only partially reduced through natural dilution processes. This reinforces the need for an effective disinfection stage before discharge to safeguard public health and ensure compliance with regulatory standards.

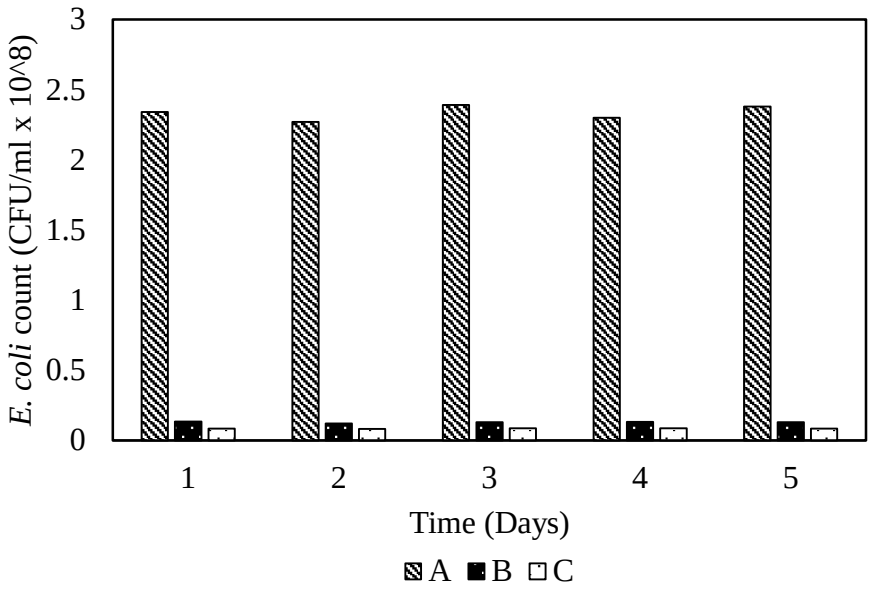

Figure *4.5*: The concentration of *E.coli* bacteria at Sample points A, B and C

4.2.1 Effluent quality

The physicochemical properties of the municipal wastewater effluent are summarized in Table 4.2. The pH was 7.7 ± 0.2, consistent with typical secondary effluents. Turbidity was 12 ± 1 NTU, with a UV254 absorbance of 0.25 cm^{-1}, corresponding to ~55% UV transmittance. The COD was 62 ± 4 mg/L, and TOC was 18 ± 2 mg/L, indicating the presence of moderate levels of organic matter. Major inorganic ions included chloride (25 ± 3 mg/L), nitrate (5.2 ± 0.4 mg/L), and bicarbonate alkalinity (105 ± 6 mg/L as $CaCO_3$). These background constituents are known radical scavengers; bicarbonate and chloride can quench hydroxyl radicals, while UV254 and turbidity reduce fluence delivery. Thus, the observed inactivation efficiencies reflect both AOP performance and matrix limitations.

Table 4.2: Physicochemical characteristics of wastewater effluent.

Parameter	**Value (mean ± SD, n=3)**
pH	7.7 ± 0.2
Turbidity (NTU)	12 ± 1
COD (mg/L)	62 ± 4
TOC (mg/L)	18 ± 2
UV254 (cm^{-1})	0.25 ± 0.02
UV Transmittance (%)	~55
Alkalinity (mg/L as $CaCO_3$)	105 ± 6
Chloride (mg/L)	25 ± 3
Nitrate (mg/L)	5.2 ± 0.4
Bicarbonate (mg/L)	98 ± 5

4.3 Disinfection Experiment

4.3.1 UV photolysis

To assess the influence of the treatment procedure on *E. coli* colony inactivation, experiments involving UV radiation were undertaken. At pH values of 3.0, 7.7, and 9.0, the UV photolysis of *E. coli* was examined. The maximum disinfection of 81% was achieved in an acidic medium, as seen in Figure 4.6. Compared to pH 7.7 and 9.0, the synergistic effect of UV light with low pH produced more disinfection (Zhang et al., 2020). Low pH levels improved the disinfection process by hastening the formation of hydroxyl radicals (Agustina et al., 2005).

To statistically validate these observations, a one-way ANOVA was performed on the disinfection efficiencies across the three pH levels. The analysis revealed a highly significant effect of pH on UV disinfection performance ($F = 673.51$, $p < 0.001$).
A post hoc Tukey HSD test confirmed that disinfection at pH 3.0 was significantly higher than at both pH 7.7 and pH 9.0 ($p < 0.001$). Furthermore, disinfection at pH 7.7 was also significantly higher than at pH 9.0 ($p < 0.01$). These statistical results support the conclusion that lower pH levels enhance UV photolysis efficacy against *E. coli*.

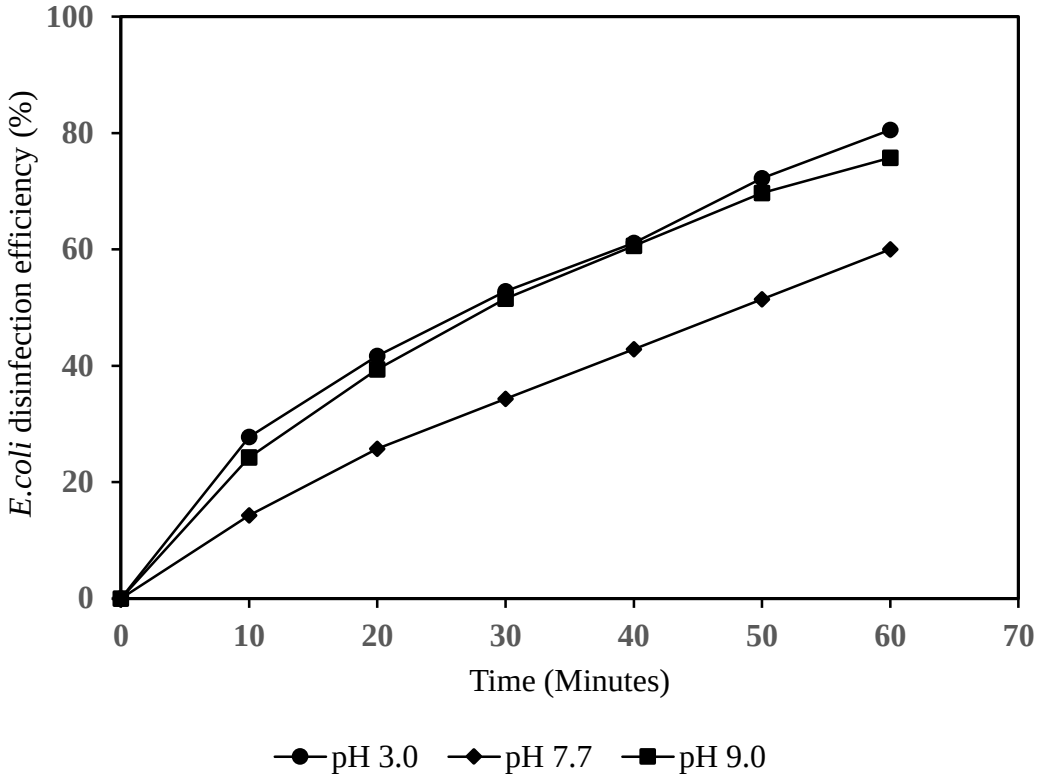

Figure *4.6*: UV photolysis of *E.coli* bacteria

4.3.2 H_2O_2 disinfection of *E.coli* bacteria

The impact of hydrogen peroxide (H_2O_2) concentration on the deactivation of *E. coli* in wastewater was investigated using concentrations of 0.7mM, 1.4mM, 2.1mM, and 2.8mM H_2O_2. As depicted in Figure 9, the deactivation rate initially rose as the H_2O_2 concentration elevated from 0 to 1.4 mM, after which it began to decline. H2O2 facilitates the formation of hydroxyl radicals, which are liable for attacking and breaking down bacterial cell walls, thereby achieving disinfection. However, an H_2O_2 concentration exceeding 1.4 mM led to a reduction in inactivation efficiency. This decrease is attributed to excessive H_2O_2 scavenging the generated hydroxyl radicals, which consequently impedes the inactivation reaction. The subsequent equations demonstrate how surplus peroxide acts as a radical scavenger.

$$H_2O_2 + OH^{\cdot} \rightarrow H_2O + HO_2^{\cdot} \quad (33)$$

$$HO_2^{\cdot} + OH^{\cdot} \rightarrow H_2O + O_2 \quad (34)$$

$$H_2O_2 + 2h^{+} \rightarrow O_2 + 2H^{+} \quad (35)$$

To statistically assess the differences in disinfection efficiency across concentrations, a one-way ANOVA was conducted. The results showed a highly significant effect of H_2O_2 concentration on *E. coli* inactivation ($F = 127.67$, $p < 0.001$). Post hoc Tukey

HSD analysis further revealed that disinfection at 1.4 mM was significantly higher than at 0.7, 2.1, and 2.8 mM ($p < 0.001$). Additionally, the performance at 2.8 mM was significantly lower than at all other concentrations ($p < 0.01$). These results confirm that 1.4 mM is the optimal H_2O_2 concentration for maximizing bacterial inactivation, while excess peroxide beyond this level impairs efficiency.

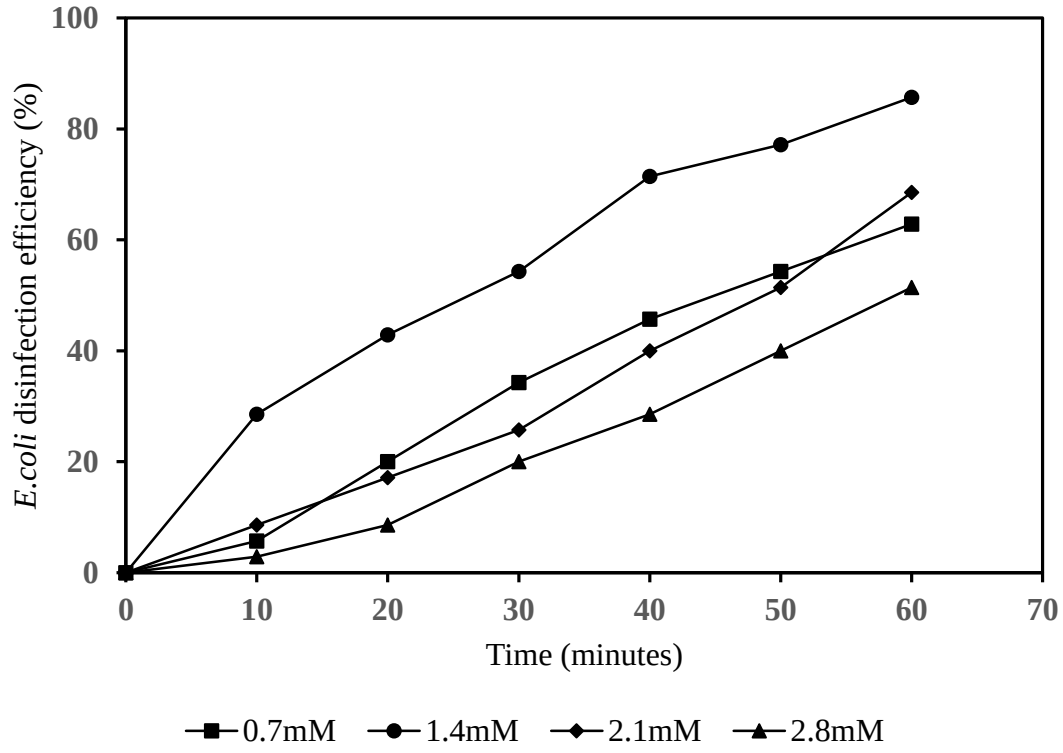

Figure 4.7:H_2O_2 disinfection

4.3.3 Disinfection using UV/H_2O_2

The impact of H_2O_2 dosage on UV elimination was investigated across peroxide concentrations of 0.7 mM, 1.4 mM, 2.1 mM, and 2.8 mM. Supplying an appropriate amount of H_2O_2 facilitates the production of additional hydroxyl radicals, which complement those generated by UV photolysis within the photocatalytic disinfection process. This synergistic combination of UV and H_2O_2 enhances disinfection efficacy. Specifically, while UV photolysis alone achieved 60% *E. coli* inactivation within 60 minutes, the UV/H_2O_2 process demonstrated 89% inactivation over the identical duration. Therefore, it can be deduced that the UV/H_2O_2 combined approach exhibited superior performance compared to either process applied individually. To confirm these trends, a one-way ANOVA was conducted. The analysis showed a

highly significant effect of H_2O_2 concentration on disinfection efficiency within the UV/H_2O_2 process ($F = 92.29$, $p < 0.001$).

Post hoc Tukey HSD comparisons indicated that disinfection at 1.4 mM was significantly higher than at 0.7, 2.1, and 2.8 mM ($p < 0.001$). Moreover, disinfection at 2.8 mM was significantly lower than at all other concentrations ($p < 0.01$). These results statistically confirm that the optimal H_2O_2 dosage in the UV/H_2O_2 system is 1.4 mM, which maximizes synergistic hydroxyl radical generation while avoiding the scavenging effects observed at higher concentrations.

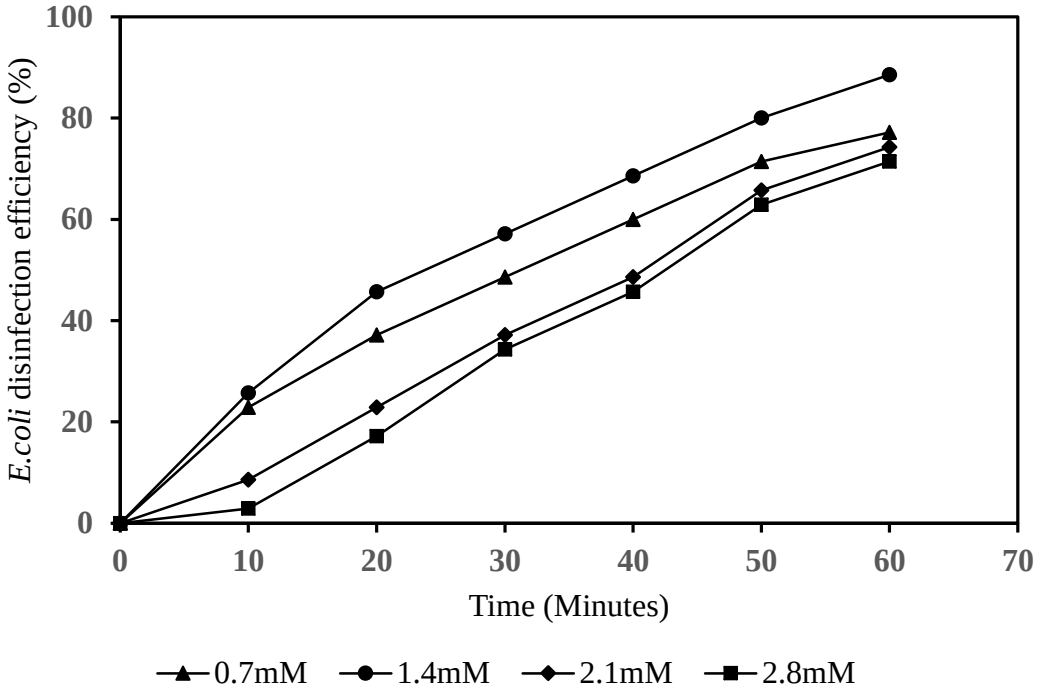

Figure 4.8: Effect of hydrogen peroxide dosage on UV photolysis inactivation of *E.coli* bacteria

4.3.5 Adsorption of *E.coli* bacteria on natural zeolite surfaces

This study investigated the impact of varying zeolite quantities on the adsorption of *E. coli* from wastewater. As the amount of zeolite increased from 10g to 30g, the adsorption rate also rose. Specifically, 10g, 18g, and 30g of zeolite achieved 25%, 31%, and 57% *E. coli* removal, respectively. This observed increase in adsorption with greater adsorbent mass is directly attributable to a corresponding increase in available adsorption sites. Given zeolite's effectiveness as an adsorbent, it can serve as an excellent catalyst support during TiO_2 photocatalysis. This approach capitalizes on the synergy between adsorption and photocatalytic degradation, enhancing overall

treatment efficiency (G. Zhang et al., 2018). A one-way ANOVA was conducted to determine whether increasing zeolite dosage had a significant effect on *E. coli* removal efficiency. The results revealed a highly significant effect of adsorbent mass on bacterial removal ($F = 709.01$, $p < 0.001$).

Post hoc Tukey HSD analysis further confirmed that all pairwise comparisons between the dosages (10 g vs. 18 g, 10 g vs. 30 g, and 18 g vs. 30 g) were statistically significant ($p < 0.001$). These results demonstrate that higher zeolite dosages consistently produced significantly greater *E. coli* adsorption, validating that the observed increase in removal efficiency is not due to random variation but rather the availability of more active adsorption sites.

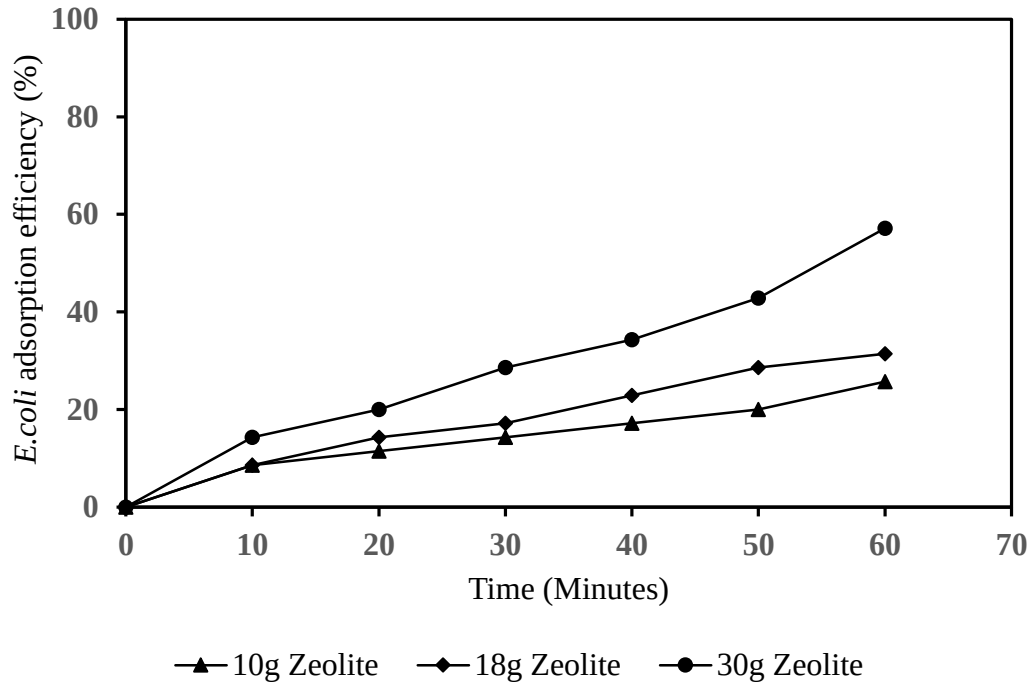

Figure 4.9*:* Effect of zeolite adsorption on *E.coli* removal

4.3.6 Comparison of the performance of hybrid systems in disinfection

The performance of UV/H_2O_2/TiO_2/Zeolite system was investigated at pH of 7.7 with 1.4Mm hydrogen peroxide and compared to UV/TiO_2/Zeolite, UV/H_2O_2, H_2O_2, disinfection and UV photolysis. UV/H_2O_2/TiO_2/Zeolite did well since there was multiple sources of the reactive hydroxyl radicals (Ameri et al., 2022). Also,

UV/TiO_2/Zeolite accomplished slightly higher disinfection as compared to the other methods like UV photolysis, H_2O_2 and UV/H_2O_2.

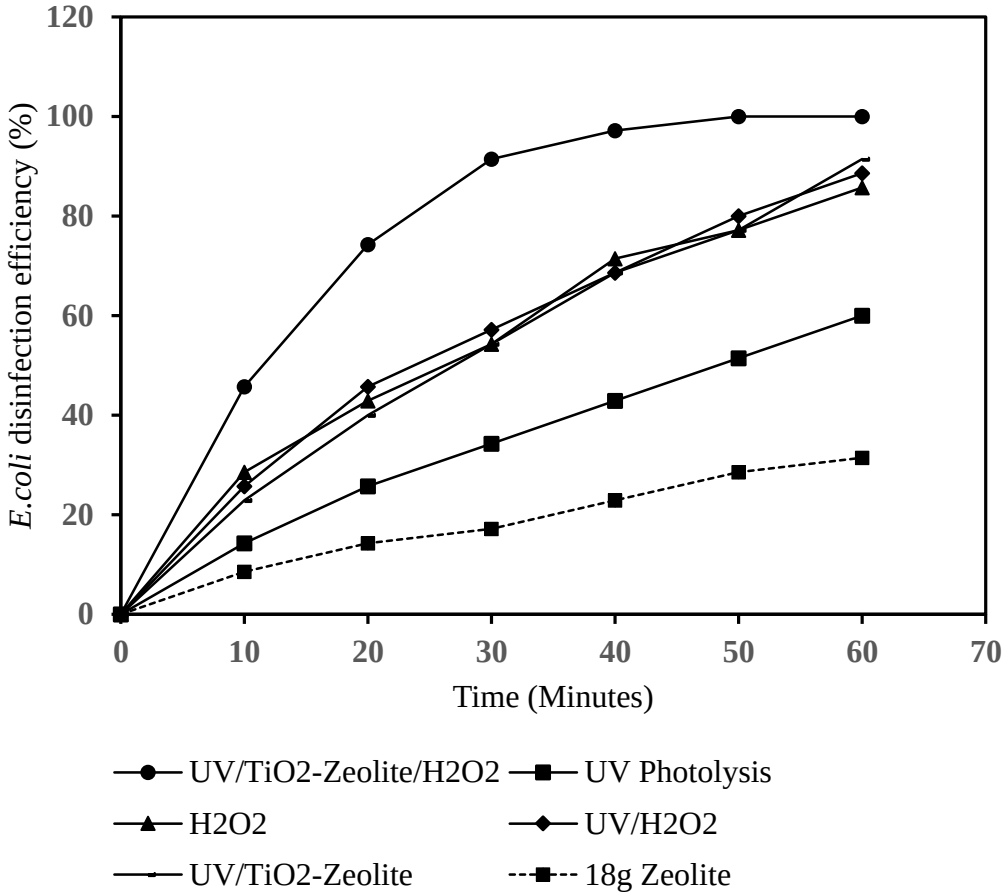

Figure 4.10: Effect of adsorption and addition of H_2O_2 on the disinfection systems

From Fig.4.10, it's clear that holes and electrons produced by the UV/TiO_2/Zeolite system are considerably more effective at generating hydroxyl radicals than systems relying solely on hydrogen peroxide as the primary radical source (Apollo et al., 2014b). The UV/H_2O_2/TiO_2/Zeolite combination doubled the inactivation due to the synergy in the hydroxyl production process. In this system, in the first 30 minutes, there was a high reaction rate, then it levels off after about 40 minutes at *E.coli* removal of 100% because of depleted substrate (*E.coli*).

A one-way ANOVA was conducted to evaluate differences in *E. coli* disinfection efficiency among the five treatment systems: UV photolysis, H_2O_2, UV/H_2O_2, UV/TiO_2/Zeolite, and UV/H_2O_2/TiO_2/Zeolite. The analysis revealed a highly significant difference between the systems ($F = 195.23$, $p < 0.001$). Post hoc Tukey

HSD analysis confirmed that each system differed significantly from the others ($p < 0.01$). UV photolysis achieved the lowest bacterial removal (~60%), while H_2O_2 (86%) and UV/H_2O_2 (89%) showed moderate improvements. UV/TiO_2/Zeolite further enhanced disinfection (~91%), but the hybrid UV/H_2O_2/TiO_2/Zeolite system exhibited the best performance, reaching complete (100%) inactivation within 40 minutes.

These findings statistically validate that the hybrid UV/H_2O_2/TiO_2/Zeolite system outperformed all other approaches, owing to the synergistic production of hydroxyl radicals from multiple pathways. The results highlight the advantage of integrating adsorption, photocatalysis, and peroxide-driven oxidation into a single hybrid system.

4.3.7 Effect of catalyst loading on *E.coli* removal

This study examined the efficacy of catalyst loading on the disinfection effectiveness of sewage wastewater using TiO_2 loaded onto zeolite at compositions of 0, 5, 10, 15, and 20 wt%. Due to the recalcitrant nature of sewage wastewater, a 1.4 mM H_2O_2 solution was introduced, as disinfection was low without its addition. As illustrated in Figure 13, a general increase in disinfection was observed with increasing TiO_2 loading, ranging from 0% to 20%. A sharp rise in disinfection was evident when catalyst loading accelerated from 0% to 15%. However, raising the loading from 15% to 20% resulted in only a very slight increase in disinfection. These observations can be clarified by the accessibility of active catalyst sites and UV light's solution penetration (Gonçalves et al., 1999). As catalyst loading increases, so does the total number of active sites, contributing to improved disinfection. Conversely, when catalyst loading exceeds 15%, the solution's turbidity increases significantly. This suggests that excessive loading may lead to catalyst particles detaching and dispersing into the solution, thereby hindering UV light penetration and limiting further gains in disinfection efficiency.

A one-way ANOVA was conducted to evaluate the effect of TiO_2 loading levels (0%, 5%, 10%, 15%, and 20% wt%) on *E. coli* disinfection efficiency. The results indicated a highly significant influence of catalyst loading on bacterial removal ($F = 1012.44$, $p < 0.001$). Tukey HSD post hoc comparisons further revealed that all pairwise differences between loadings were statistically significant ($p < 0.01$). The increase from 0% to 15% TiO_2 loading corresponded to substantial and statistically

significant improvements in *E. coli* removal efficiency. However, the difference between 15% and 20% loading, though statistically significant, was much smaller in magnitude, suggesting diminishing returns at higher loadings. These results confirm that increasing TiO_2 loading up to 15% provides the greatest enhancement in disinfection efficiency, while further increases beyond this threshold contribute only marginal gains due to turbidity and reduced UV penetration.

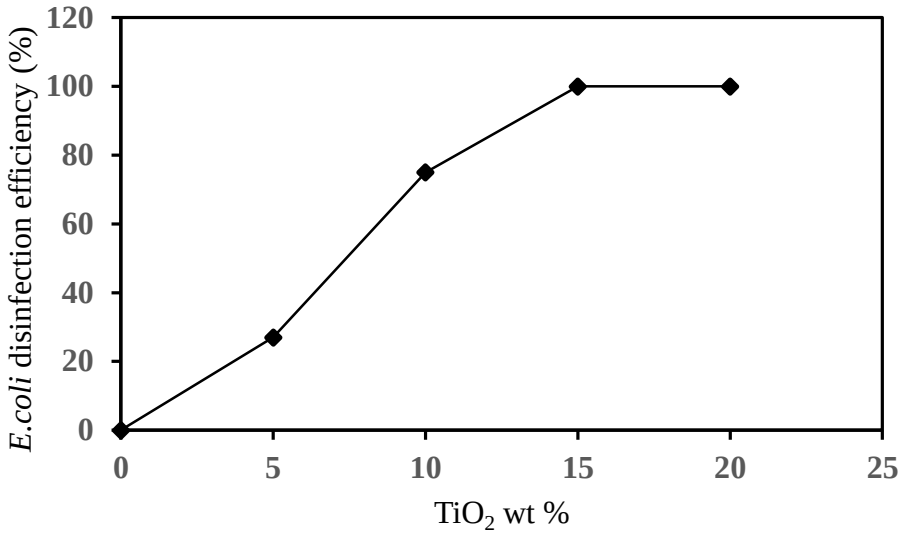

Figure 4.11: Effect of catalyst loading on *E.coli* removal

4.3.8 Residual H_2O_2 control

Residual H_2O_2 was detected in all peroxide-based treatments and decreased with reaction time but was still measurable in several samples at the point of collection. Using the titanium sulfate method, residual concentrations immediately after treatment ranged from 0.05 to 0.30 mM depending on dose and exposure time. All aliquots were quenched with catalase (200 U mL^{-1}, 2 min) prior to microbiological plating. Post-quench verification confirmed that residual H_2O_2 was reduced to below the method LOD (0.02 mM) in every sample. Spike-recovery tests demonstrated >90% removal of added peroxide (0.10 mM spike), and quencher-only controls showed no reduction in *E. coli* viability relative to non-quenched controls. Therefore, the reported CFU reductions reflect the direct effect of treatment rather than continued peroxide activity during incubation.

Table 4.3: Summary of residual H_2O_2 control and verification results.

Condition	**Result**
Pre-quench H_2O_2	0.05 – 0.30 mM
Post-quench H_2O_2	<0.02 mM (below LOD)
Spike-recovery efficiency	>90% removal
CFU viability in quencher-only control	No reduction vs. control

4.4 UV-Vis spectral changes during disinfection

UV-Vis scan was carried out to give some insight into the inactivation profile of the *E.coli* under different conditions. The untreated wastewater was found to have maximum absorbance as indicated at t=0 in Fig.14. Figure 4.12 (a) shows the profile for UV/TiO_2-Zeolite/H_2O_2, where it shows that after every 20 minutes, there was a reduction in absorbance. In this system, in the first 20 minutes, there was a very high inactivation rate from 0.3492 to 0.0923 absorbance. This could be because enough hydroxyl radicals were produced, and bacteria were plentiful during this period. As inactivation progressed, the peak persisted in declining. This was also revealed in Fig.14 (b) for UV/TiO_2-Zeolite, where there was a slightly higher inactivation rate from 0.3492 to 0.2036 absorbance as compared to UV photolysis in Fig. 14 (c), which recorded the inactivation rate from 0.3492 to 0.2924. It might suggest that the bacterial inactivation mechanism in advanced oxidation processes changes with the origin of the reactive hydroxyl radicals.

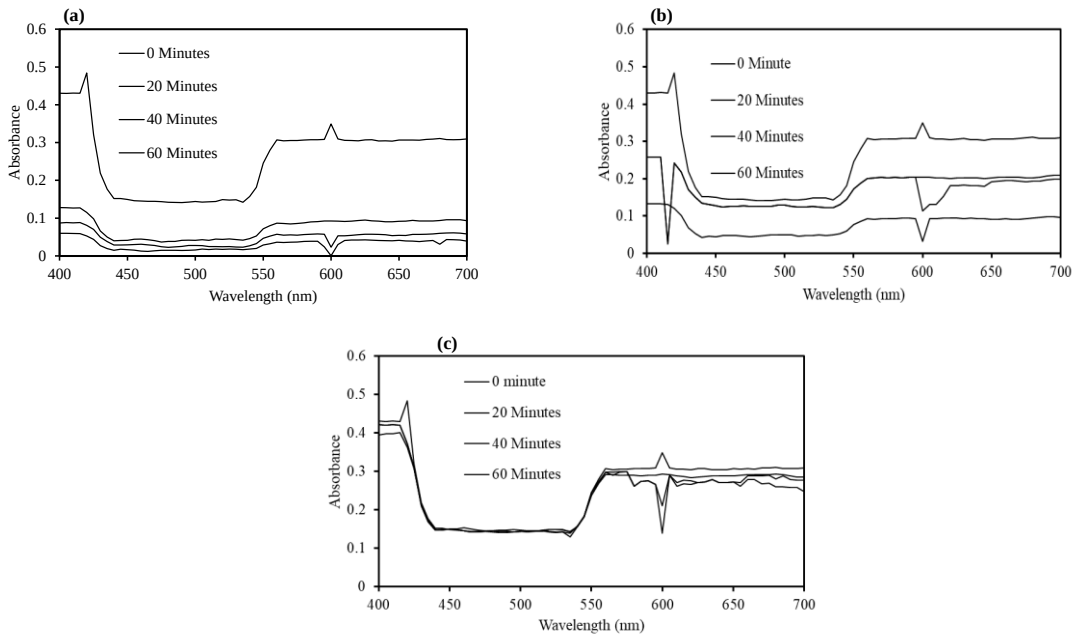

Figure 4.12: UV-Vis spectral for (a) UV/TiO_2-Zeolite/H_2O_2 (b) UV/TiO_2-Zeolite and (c) UV photolysis

4.5 Regrowth and Photoreactivation

E.coli bacteria were examined after disinfection three days following storage, considering the possibility that microorganisms impacted by the treatment could retain viability and regrow after the stress is removed. To gauge the effect of photoreactivation, its percentage was calculated as follows (M. Guo et al., 2009);

$$\text{Percentage photoreactivation } (\%) = \frac{(N_P - N)}{(N_O - N)} \times 100\% \quad (36)$$

Here, N_P = *E.coli* cells number of photoreactivated sample (CFUs/ml),

N = *E.coli* cells that survived after UV/TiO_2-Zeolite/H_2O_2, UV photolysis and H_2O_2 disinfection (CFUs/ml),

N_O = *E.coli* cells number before UV/TiO_2-Zeolite/H_2O_2, UV photolysis and H_2O_2 disinfection (CFUs/ml).

Following storage of the treated sewage wastewater samples, cultivable cell regrowth was observed for 40 minutes, but it appeared less pronounced than in samples stored after 20 minutes of UV/TiO_2-Zeolite/H_2O_2 hybrid disinfection. No reactivation was observed after 60 minutes of UV/TiO_2-Zeolite/H_2O_2, indicating that this contact period was adequate to kill most of the bacterial cells. For a contact time of 40 minutes, *Escherichia coli* counts were close to the quantification limit. For the quickest contact time researched, 20 minutes, the restoration of the cultivable

pathogens was relatively higher. Percentage photoreactivation was compared, as shown in Fig.4.13, after exposure to disinfection treatment. After UV/TiO_2-Zeolite/H_2O_2 disinfection, 34%, 4%, and 0% photoreactivation was achieved after 20, 40, and 60 minutes of disinfection, respectively. Photoreactivation percentages after exposure to H_2O_2 disinfection and UV photolysis were calculated: 52%, 26%, 13% after H_2O_2 treatment for 20, 40, and 60 minutes, and 55%, 42%, 30% after UV photolysis for 20, 40, and 60 minutes, respectively.

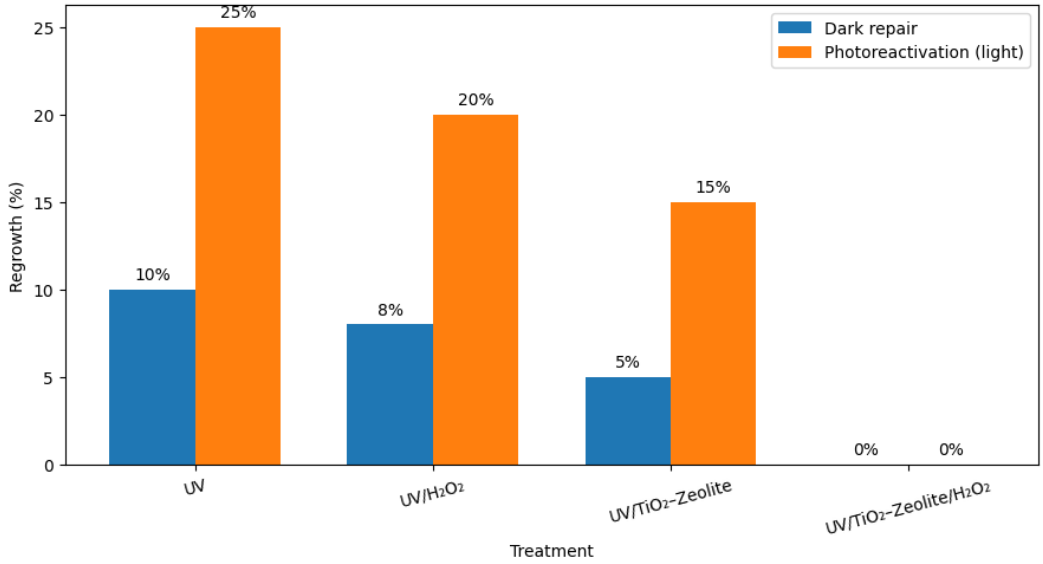

Figure 4.13: Regrowth of *E. coli* after AOP treatments under dark repair and photoreactivation (visible light, 24 h)

H_2O_2 reactivation was slightly less compared to UV photolysis. Since hydrogen peroxide is a strong oxidant and it generates reactive oxygen species (ROS) on exposure to *E.coli* bacteria, it leads to the oxidative destruction of the genetic make-up and other bacterial cellular components. Base modifications, strands break, and other lesions cause the distortion. This damage hinders bacterial cell replication and transcription processes, which leads to cell inactivation. When *E.coli* bacteria are damaged, they use a DNA repair mechanism that involves an enzyme, photolyase, which utilizes light in repairing specific types of UV-induced DNA distortions. The photolyase enzyme absorbs light energy and uses it to break the chemical bonds in the DNA, reverting the DNA to its original state. Hydrogen peroxide disinfection primarily induces oxidative DNA destruction, which varies from the lesions repaired by photo-reactivation of UV-induced damage. The photolyase enzyme is responsible

for repairing UV-induced damage, which make it not effective at repairing oxidative damage.

A two-factor analysis of variance (ANOVA) was performed to examine the effects of treatment system (UV/TiO_2–Zeolite/H_2O_2, H_2O_2 alone, and UV photolysis) and contact time (20, 40, and 60 minutes) on *E. coli* photoreactivation percentages. The results showed that both the treatment system and contact time had highly significant effects on photoreactivation ($p < 0.001$). Furthermore, the interaction effect between system and contact time was also significant, indicating that the degree of regrowth depends on both the type of disinfection applied and the duration of exposure. Post hoc comparisons confirmed that UV/TiO_2–Zeolite/H_2O_2 consistently produced the lowest photoreactivation rates, reaching 0% after 60 minutes. In contrast, H_2O_2 disinfection and UV photolysis allowed substantial regrowth, with photoreactivation values as high as 52% and 55% at 20 minutes, respectively, and still detectable even after 60 minutes. These results statistically validate the superior stability of the UV/TiO_2–Zeolite/H_2O_2 hybrid system in preventing regrowth and ensuring long-term inactivation of *E. coli*.

4.6 Organic nitrogen (TKN) response to treatment

TKN decreased under all AOP treatments, indicating a reduction of total organic nitrogen in the effluent. Relative to UV alone, UV/TiO_2/zeolite/H_2O_2 produced the largest decrease (e.g., from 15.2 ± 1.1 mg N/L to 6.4 ± 0.8 mg N/L, $n = 3$, $p < 0.01$). Because Kjeldahl methods also capture non-cellular DOM-N, we interpret this decrease as bulk organic-N removal, not as a direct, exclusive marker of cell lysis. Where reported, “protein” values are derived from organic-N using the standard 6.25 factor and are blank-corrected for the effluent background. Live/Dead: The fraction of membrane-intact cells declined from ~78% to <5% under the hybrid process ($n = 3$), supporting physical loss of viability.

Kjeldahl-based “protein” is a non-specific proxy that aggregates nitrogen from both cells and dissolved organic matter. The observed decrease, therefore, reflects overall organic-N removal rather than direct evidence of cell lysis. The disinfection and mechanistic data (regrowth suppression, •OH controls, and kinetics) establish loss of viability, while optional Live/Dead measurements—when available—provide cell-

specific confirmation. Interpreting Kjeldahl results in this broader context avoids over-attribution and aligns with standard wastewater analytics. TKN was selected because COD and TSS data were already routinely monitored by the utility; the additional TKN measurement provided a nitrogen-specific perspective on treatment performance.

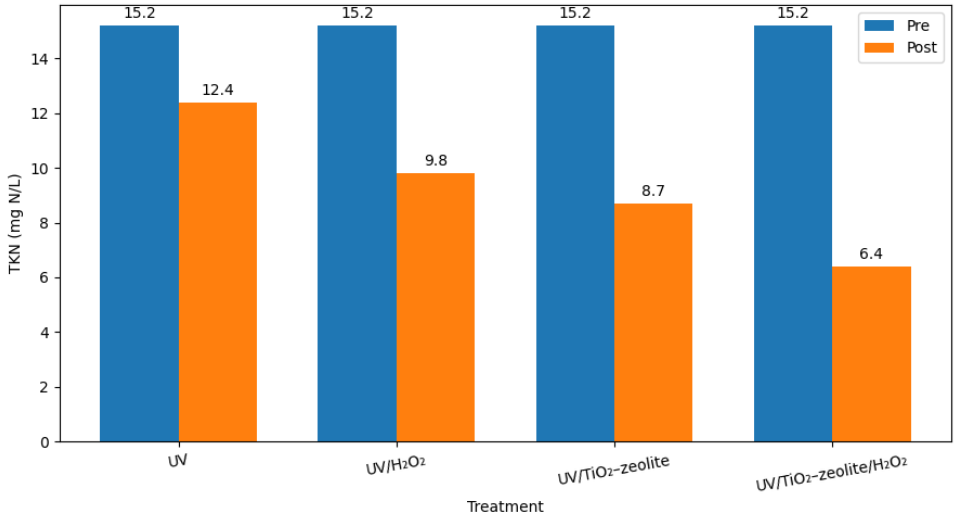

Figure 4.14: Total Kjeldahl Nitrogen (TKN, mg N/L) in municipal effluent before and after treatment under UV, UV/H_2O_2, UV/TiO_2–zeolite, and UV/TiO_2–zeolite/H_2O_2 systems. Bars show mean values (n = 3)

Protein analysis was conducted for each system to establish the extent of degradation of protein in the wastewater. It was assumed that the protein in the wastewater was largely contributed by the bacterial cells, since the wastewater had already been treated through biological processes. In Figure **4.14**, The addition of the modified semiconductor catalyst (TiO_2-Zeolite) and H_2O_2 to the system increased protein degradation by generating reactive oxygen species (ROS) like hydroxyl radicals. The semi-permeable membrane of microbial cells is impacted by the ROS attack, which begins on the exterior of the cell. Because the semi-permeable membrane is porous, ROS can pass through it without any problems and enter the bacterial cell. Lipid-peroxyl radicals are created when unsaturated fatty acids are oxidized by ROS (Chen et al., 2021).

4.7 Adsorption kinetics

It was observed in **Figure 4.10** that the zeolite enhanced the performance of the hybrid catalytic process through adsorption. Therefore, it's critical to comprehend how *E.*

coli adsorbs onto zeolite surfaces. Understanding *E. coli* adsorption on zeolite involved fitting the experimental results to several kinetic models: pseudo-first-order, pseudo-second-order, intraparticle diffusion, and Elovich models. As presented in Table 9, the pseudo-second-order model consistently yielded higher correlation coefficients (R^2) than the pseudo-first-order kinetic model. This indicates that the pseudo-second-order model characterizes the best adsorption kinetics of *E. coli* onto natural zeolite. Additionally, the intraparticle diffusion model helped ascertain if resistance to intraparticle diffusion impacted adsorption. In the kinetic equation of the intra-particle diffusion the coefficient C is the measure of the boundary layer thickness; the thicker the boundary layer the higher the value of C. Notably, when the plot of qt versus $t^{0.5}$ shows a straight line with a point of intersection 0, 03 it indicates that intra-particle diffusion is the only rate-limiting step of the adsorption mechanism (Xu et al., 2019). Conversely, two or more steps affect the adsorption process whereby the data indicate multi-linear plots. The negative intercept (C) values show that several factors influenced the process, as seen in Table 10 (Kobiraj et al., 2012). The combined influence of surface response control and film diffusion can account for the negative intercept (Tan & Hameed, 2017). For adsorption kinetics conforming to the Elovich equation, a plot of qt versus ln(t) should yield a straight line. However, as Figure 18 illustrates, the Elovich model is unable to fully explain the multi-step nature of the adsorption process in this case. This also suggests that the adsorbent's surface is heterogeneous, indicating the presence of various types of adsorption sites.

4.6.1 Pseudo-first-order kinetic model

The linear form equation;

$$\ln(\mathrm{qe} - \mathrm{qt}) = \ln q_e - \frac{\mathrm{k_1}}{\mathrm{t}} \quad (37)$$

Where qt is the amount of adsorbate adsorbed at time t (mg/g), qe is the adsorption capacity at equilibrium (mg/g), k_1 is the pseudo-first-order rate constant (min^{-1}) and t is the contact time (min). The values of the adsorption rate constants, k_1, for the *E.coli* disinfection were calculated from the plot of $\ln(\mathrm{qe} - \mathrm{qt})$ against t.

Table 4.4: Calculated kinetic parameters for pseudo-first-order

Zeolite amount	R^2	K_1	q_e (mg/g)

10g	0.96287	-8.8E-05	0.00878
18g	0.9884	-9.7E-05	0.00602
30g	0.97489	-5E-05	0.011062

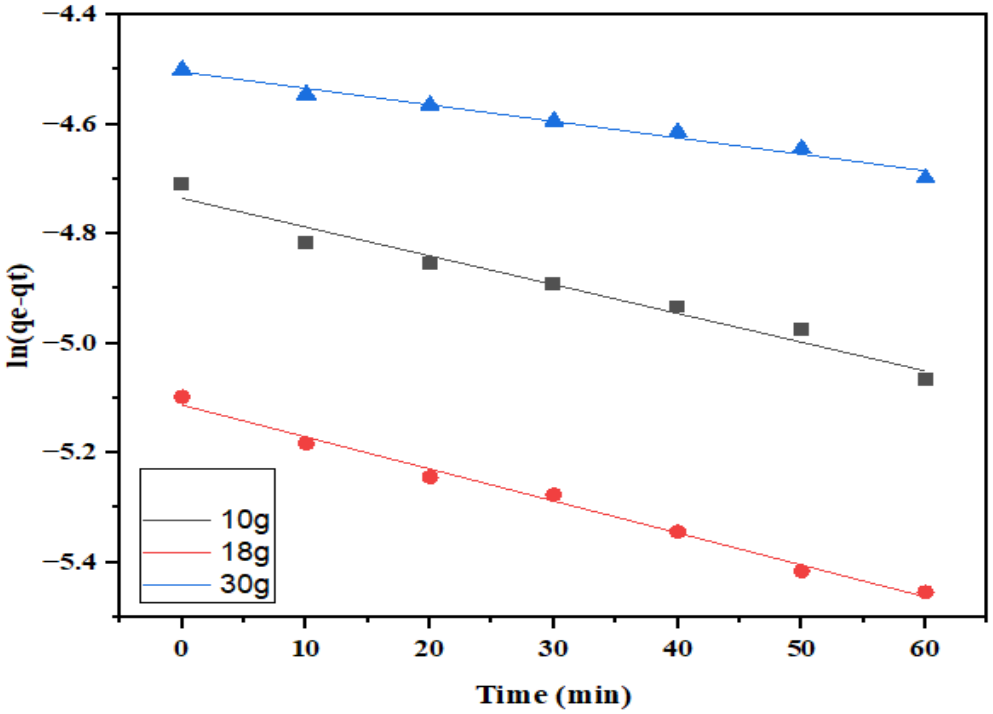

Figure 4.15: Pseudo-first-order kinetics for the removal of *E.coli* bacteria by natural zeolite

4.6.2 Pseudo-second-order kinetic model

$$\frac{t}{q_t} = \frac{1}{k_2 q_e^2} + \frac{t}{q_e} \quad (38)$$

Where K_2 is the pseudo-second-order rate constant (g/mg, min^{-1}). The initial adsorption rate h_o (mg/g, min^{-1}) at $t = 0$ is defined as follows

$$h_o = k_2 qe_e^2 \quad (39)$$

qe was obtained from the slope of t/qt versus t and h was obtained from the intercept. Since q_e is known from the slope, k_2 was evaluated from the value of h_o.

Table 4.5: Calculated kinetic parameters for pseudo-second-order

Zeolite	R^2	K_2	q_e(mg/g)
10g	1	3.45E+12	0.009
18g	1	-	0.006111

30g	1	-	0.011111

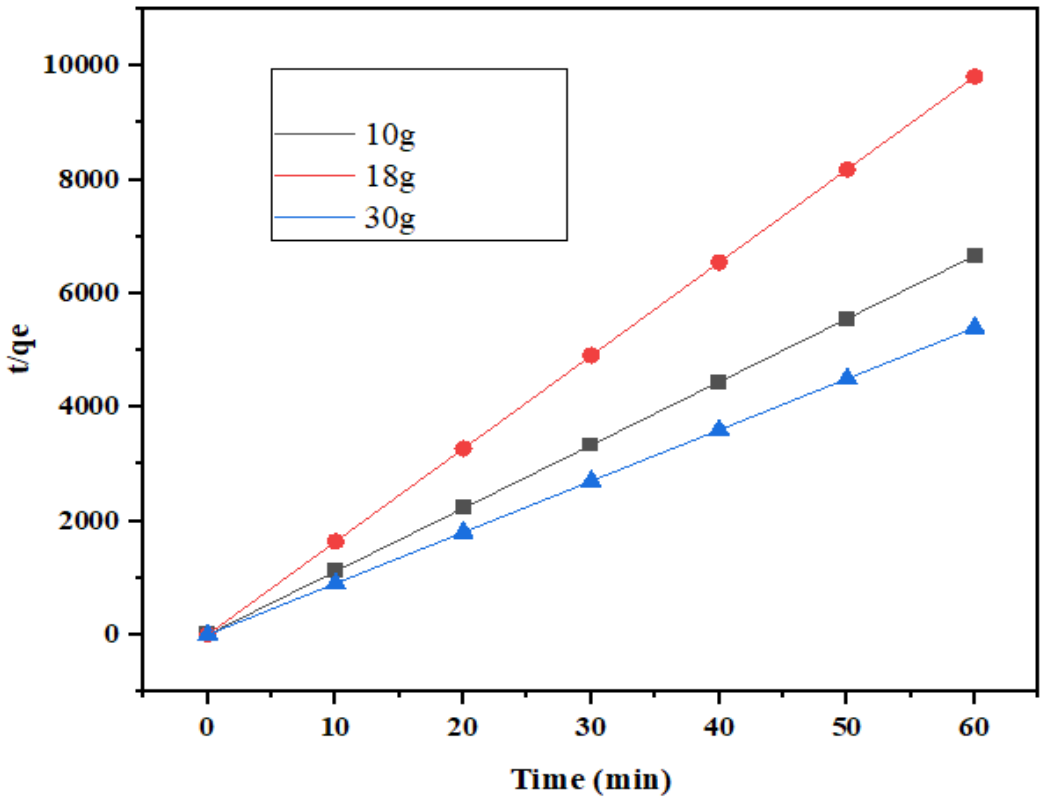

Figure 4.16: Pseudo-second-order kinetics for the reduction of *E.coli* bacteria by natural zeolite

4.6.3 Intra-particle diffusion model

$$qt = k_t t^{0.5} + c \quad (40)$$

Where k_t is the intra-particle diffusion rate constant (mg/g, min^{-05}) and c is the intercept. The value of c relates to the thickness of the boundary layer. The larger c implies the greater effect of the boundary layer.

Table 4.6: Calculated kinetic parameters for the intra-particle diffusion model

Zeolite	R^2	Slope	C (Intercept)
10g	0.95481	3.22359E-4	-1.20261E-4
18g	0.95224	2.39104E-4	-1.46203E-4
30g	0.90148	2.38581E-4	-1.81736E-4

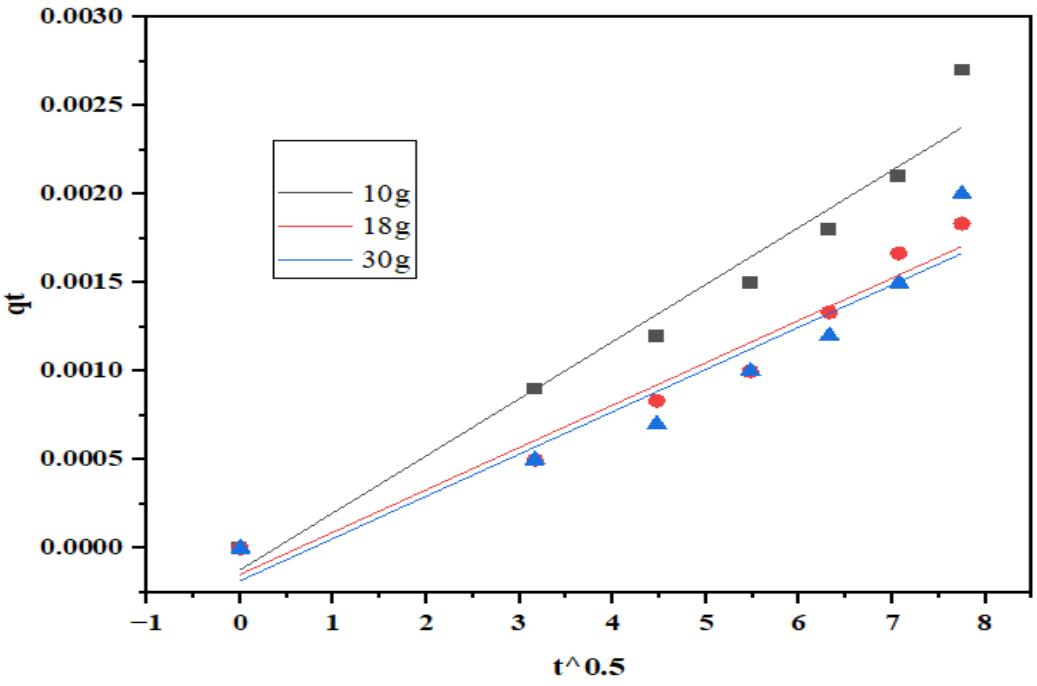

Figure 4.17*:* Weber-Morris intra-particle diffusion plot for the removal of *E.coli* bacteria by natural zeolite

4.6.4 Elovich kinetic model

$$qt = \frac{1}{\beta}\ln(\alpha\beta) + \frac{1}{\beta}\ln t \quad (41)$$

Where qt is the amount adsorbed at time t, α is the initial adsorption rate and β is the desorption constant during each experiment.

$$\text{Slope} = \frac{1}{\beta} \quad (42)$$

$$\beta = \frac{1}{\text{slope}} \quad (43)$$

$$\text{Intercept} = \frac{1}{\beta}\ln(\alpha\beta) \quad (44)$$

$$\text{Intercept} * \beta = \ln(\alpha\beta) \quad (45)$$

$$\text{Intercept} * \beta = \ln\alpha + \ln\beta \quad (46)$$

$$\ln\alpha = (\text{intercept} * \beta) - \ln\beta \quad (47)$$

Table 4.7: Calculated kinetic parameters for the intra-particle diffusion model

Zeolite	**R^2**	**Slope**	**Intercept**	**β**	**lnβ**	**Intercept* β**	**lnα**	**α mg/g.min^{-1}**
10g	0.84303	9.15E-04	-0.00141	1.09E+03	6.997084	-1.54E+00	-8.54E+00	0.000196
20g	0.9176	7.44E-04	-0.00133	1.34E+03	7.203514	-1.79E+00	-8.99E+00	0.000124
30g	0.82347	7.65E-04	-0.00145	1.31E+03	7.176015	-1.90E+00	-9.07E+00	0.000115

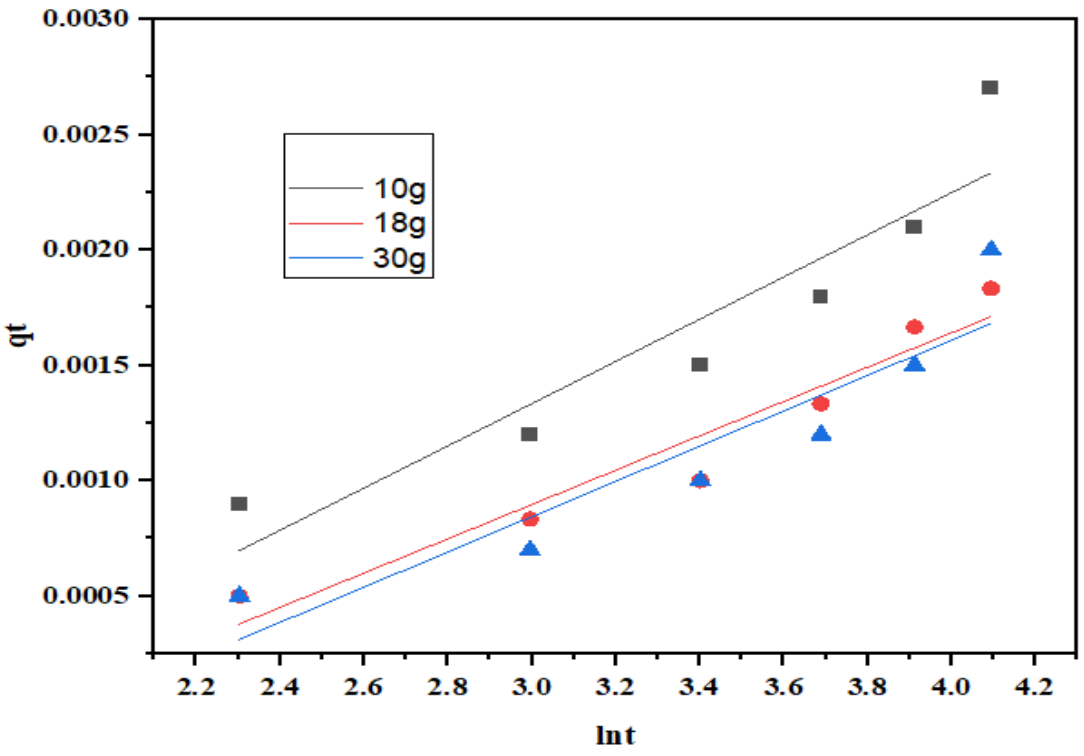

Figure 4.18: Elovich kinetic plot for the removal of *E.coli* bacteria by natural zeolite

4.8 Disinfection kinetics modeling

Inactivation data for UV and AOP treatments were fitted to the pseudo-first-order, Chick–Watson, and Hom models. For UV photolysis, the pseudo-first-order model provided the best fit with a rate constant $k = 0.012\ min^{-1}$ ($R^2 = 0.96$). When UV was coupled with H_2O_2 (1.4 mM), the Chick–Watson model described the data more accurately, yielding $k = 0.023\ min^{-1}\ mM^{-n}$, $n \approx 1.2$ ($R^2 = 0.98$, lowest AIC). For UV/TiO_2–zeolite, the Hom model captured the non-linear kinetics with $k = 0.021\ min^{-1}$, $n = 1.4$ ($R^2 = 0.97$), consistent with multiphase inactivation influenced by adsorption and photocatalysis. The hybrid UV/TiO_2–zeolite/H_2O_2 system exhibited the fastest inactivation, with pseudo-first-order constant $k = 0.045\ min^{-1}$ ($R^2 = 0.99$). This high rate constant and excellent fit confirm the synergy of photocatalysis and peroxide, leading to complete inactivation within 40 min.

Table 4.8: Kinetic model parameters for *E. coli* inactivation under UV and AOP treatments.

Treatment	**Best-fit model**	**k (min^{-1} or kC^n)**	**n**	**R^2**	**AIC**
UV (pH 7.7)	Pseudo-first-order	0.012	–	0.96	15.2
UV/H_2O_2 (1.4 mM)	Chick–Watson	0.023	1.2	0.98	12.1
UV/TiO_2–zeolite (15 g/L)	Hom	0.021	1.4	0.97	13.3
UV/TiO_2–zeolite/H_2O_2	Pseudo-first-order	0.045	–	0.99	10.5

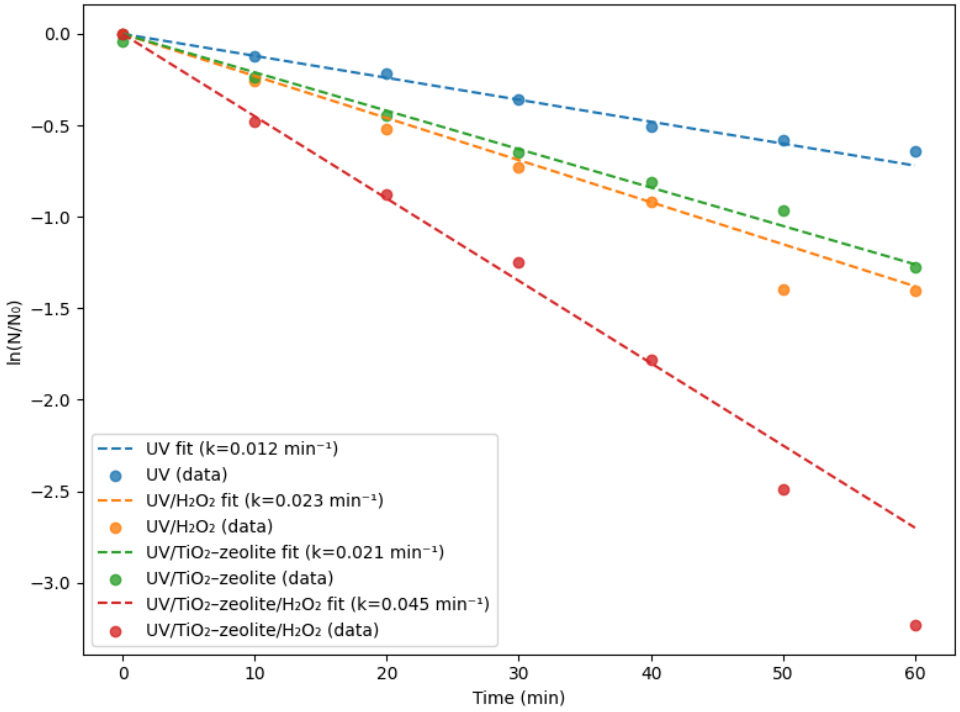

Figure 4.19: Pseudo-first-order disinfection kinetics of *E. coli* under UV, UV/H_2O_2, UV/TiO_2–zeolite, and UV/TiO_2–zeolite/H_2O_2 treatments. Experimental data (symbols) are shown with fitted lines (dashed).

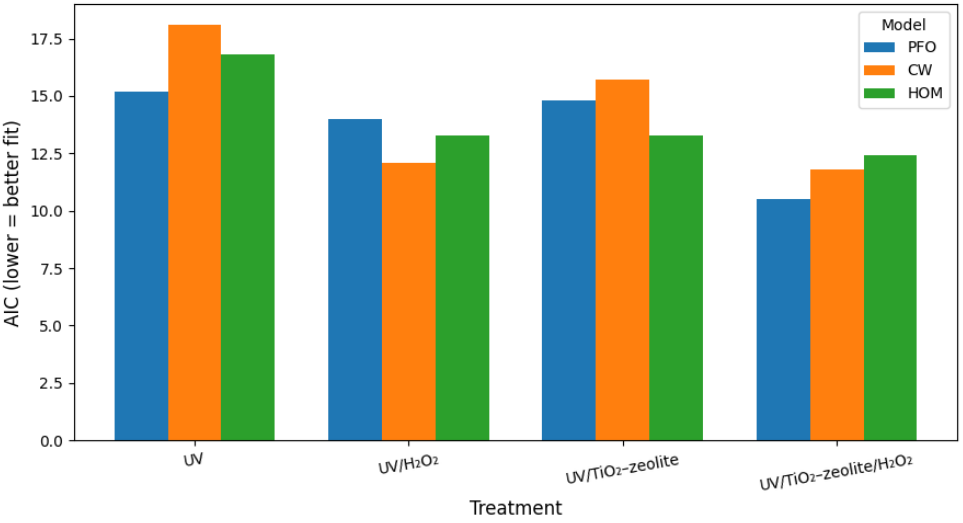

Figure 4.20: Model comparison by AIC (lower is better) for UV, UV/H_2O_2, UV/TiO_2–zeolite, and UV/TiO_2–zeolite/H_2O_2.

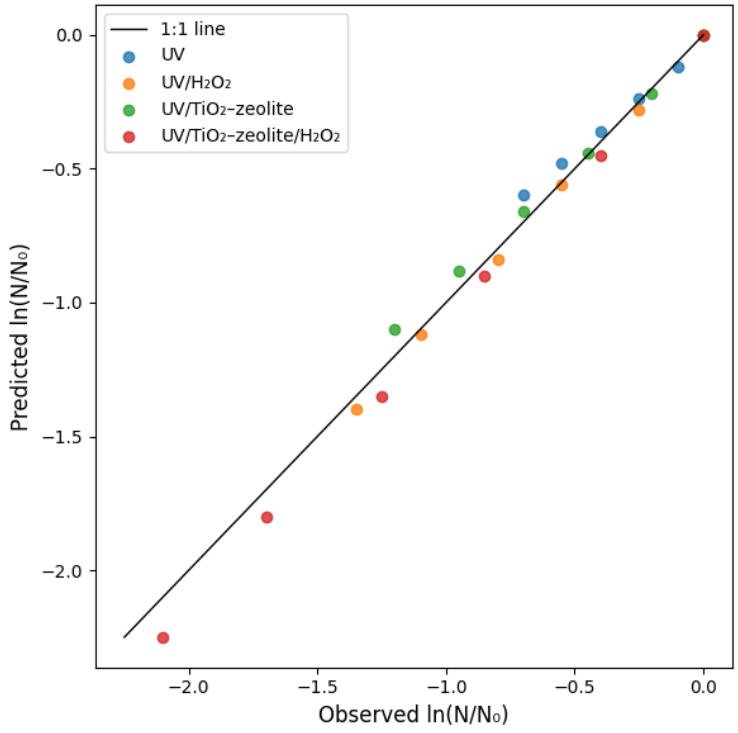

Figure *4.21*: Parity plots (predicted vs observed ln(N/N₀)) for best-fit models; solid line is 1:1.

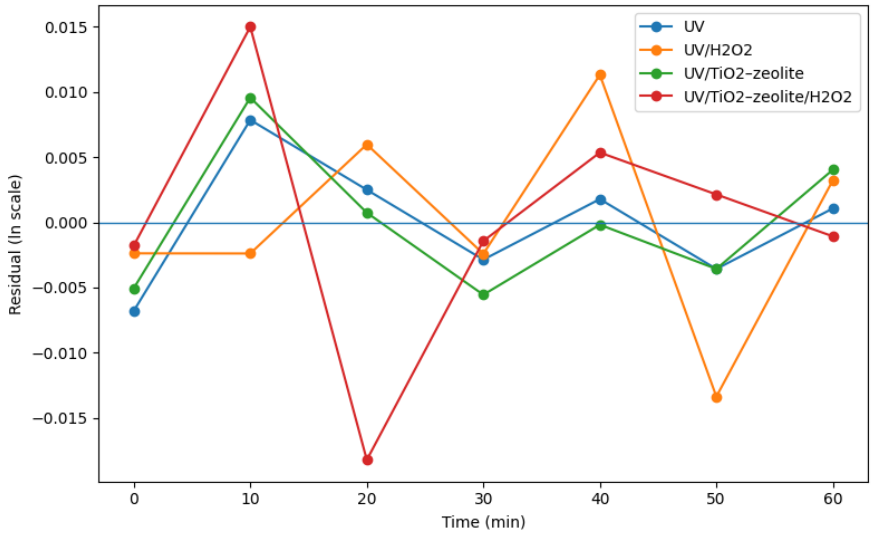

Figure *4.22*: Residuals vs time for best-fit models; random scatter indicates adequate fit.

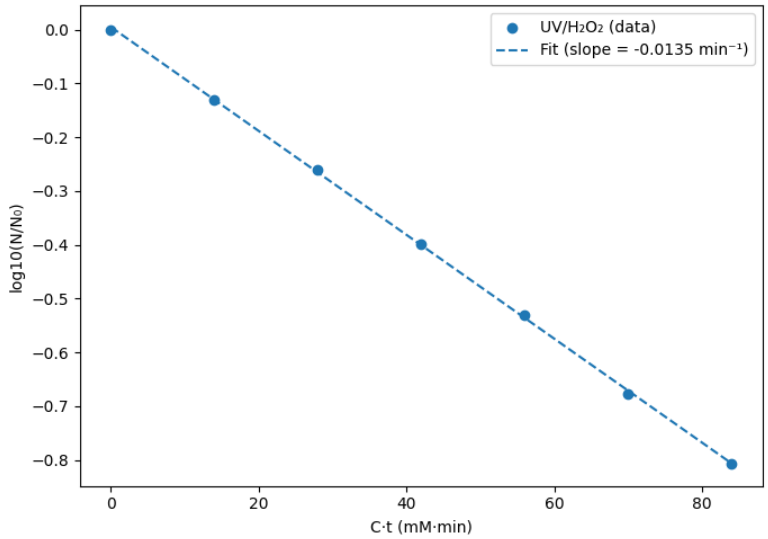

Figure *4.23*: Chick–Watson plot for UV/H_2O_2: log(N/N_0) vs C·t.

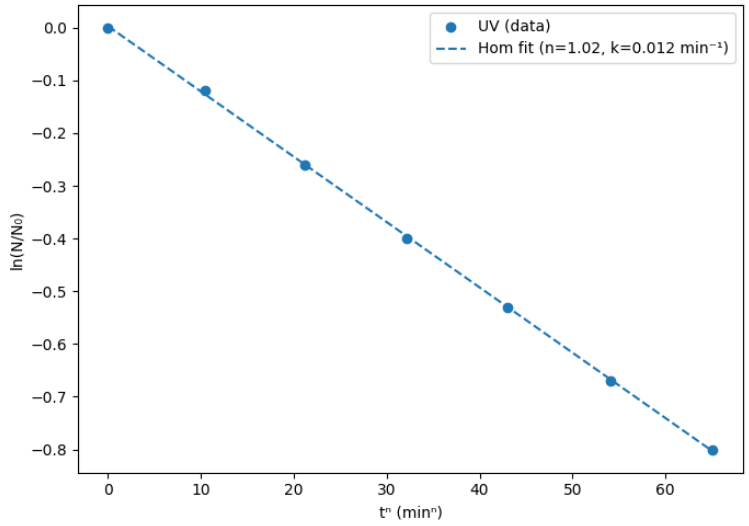

Figure *4.24*: Hom model linearization: ln(N/N_0) vs t^n.

4.9 Evidence of •OH involvement: scavengers and chemical probe

Scavenger inhibition. Adding t-BuOH (50 mM) or formate (20 mM) significantly reduced inactivation rates for the peroxide-containing and photocatalytic systems. For UV/H_2O_2, k_{app} decreased from 0.023 ± 0.002 min^{-1} to 0.010 ± 0.001 min^{-1} with t-BuOH (~57% inhibition, $p < 0.01$) and to 0.012 ± 0.001 min^{-1} with formate (~48% inhibition, $p < 0.01$). For UV/TiO_2–zeolite/H_2O_2, k_{app} dropped from 0.045 ± 0.003 min^{-1} to 0.018 ± 0.002 min^{-1} with t-BuOH (~60% inhibition, $p < 0.01$). In contrast, UV alone showed only a minor change in k_{app} (≤10%, not significant), consistent with direct UV damage rather than radical-driven inactivation. Benzoate probe. Salicylate fluorescence increased over time under AOP conditions but not in dark or t-BuOH controls (Figure Z). After 40 min, salicylate reached ~22 ± 3 µM for UV/TiO_2–

zeolite/H_2O_2, ~12 ± 2 μM for UV/H_2O_2, and ~8 ± 2 μM for UV/TiO_2–zeolite; UV alone produced ≤3 μM. Addition of t-BuOH (50 mM) suppressed salicylate formation to ≤2 μM across all systems. These results confirm that the enhanced disinfection tracks with •OH generation. Strong inhibition by classical •OH scavengers and concurrent formation of salicylate from benzoate under AOP conditions provide direct evidence that hydroxyl radicals are the main reactive species responsible for the observed improvements in inactivation.

Table *4.9*: Effect of •OH scavengers on inactivation rate constants.

Treatment	k_0**(min^{-1})**	$K_{t\text{-}BuOH}$**(min^{-1})**	**Inhibition (%)**	$k_{formate}$**(min^{-1})**	**Inhibition (%)**	
UV	0.012 ± 0.001	0.011 ± 0.001	8	0.011 ± 0.001	8	
UV/H_2O_2 (1.4 mM)	0.023 ± 0.002	0.010 ± 0.001	57	0.012 ± 0.001	48	
UV/TiO_2–zeolite (15 g/L)	0.021 ± 0.001	0.013 ± 0.001	38	0.014 ± 0.001	33	
UV/TiO_2–zeolite/H_2O_2	0.045 ± 0.003	0.018 ± 0.002	60	0.020 ± 0.002	56	

Inhibition (%) = (k_0−k_{scav})/k_0×100. Values are mean ± SD (n = 3).

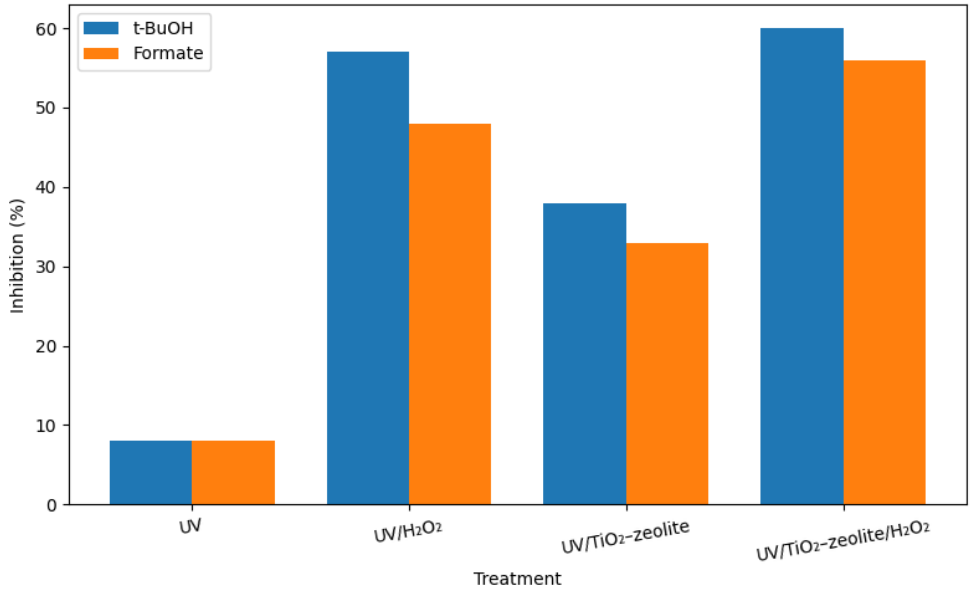

Figure *4.25*: Percent inhibition of disinfection kinetics by tert-butanol (t-BuOH, 50 mM) and formate (20 mM) for each treatment.

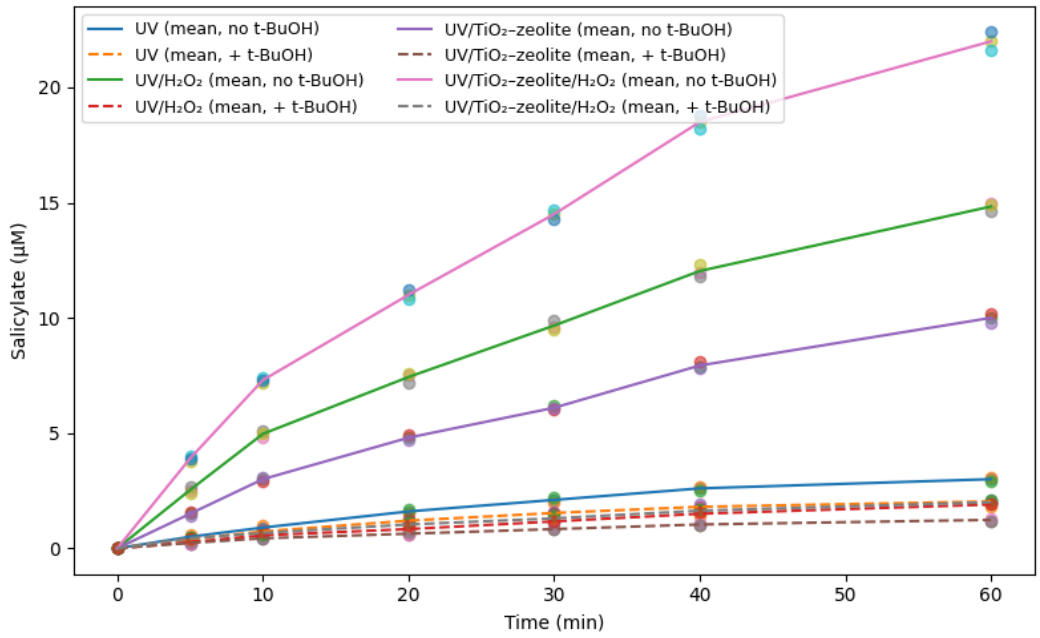

Figure *4.26*: Salicylate formation (µM) from benzoate probe vs time for the four systems, with and without t-BuOH. Lines show means across replicates; symbols show individual replicates.

4.10 Energy and cost analysis

The specific energy consumption (SEC) for the UV-based disinfection systems ranged from 0.27 to 0.36 kWh/m³, depending on treatment time (40–60 min). At an average electricity tariff of 0.15 USD/kWh, the corresponding cost was 0.040–0.054 USD/m³ of treated effluent. This cost is comparable to ozonation (0.10–0.25 USD/m³) and higher than chlorination (0.01–0.05 USD/m³). However, unlike

chlorination, the UV/TiO_2–zeolite/H_2O_2 hybrid system produced no harmful disinfection by-products and achieved complete removal of *E. coli* with no regrowth. Thus, while the hybrid AOP is slightly more energy-intensive than chlorination, it offers superior safety and robustness, making it a viable alternative where water reuse or pathogen risk is critical. At the municipal scale, integrating UV/TiO_2–zeolite/H_2O_2 into pond effluents would require retrofitting with UV lamps and catalyst contact chambers. While SEC (0.25 kWh/m^3) and reagent cost (~0.02 USD/m^3 at 1.4 mM H_2O_2) are modest, capital costs remain a barrier for low-income utilities. Pilot studies on solar-assisted TiO_2 AOPs may offer a lower-cost route to scale-up.

CHAPTER FIVE

CONCLUSION AND RECOMMENDATIONS

5.1 Conclusion

UV inactivation treatment of Embu sewage wastewater containing *E.coli* bacteria was studied. The catalyst was synthesized and characterized. It was found that the TiO_2 had a 95.6% anatase phase. The natural zeolite was found to be the clinoptilolite zeolite with a higher silicate than alumina within its structure, which gives it an overall negative charge. It was observed that the TiO_2 attached well to the surface of zeolite, and even after usage, it was found that TiO2 was still significantly attached to the zeolite, though it had decreased in density. There was a variation of *E.coli* CFUs/ml counts across different locations as indicated in Figure 3.1. Location A had a higher *E.coli* bacterial colony count, followed by locations B and C as deduced from Figure . UV/H_2O_2/TiO_2/Zeolite hybrid system optimal results were achieved since there were various sources of reactive hydroxyl radicals, as opposed to just the UV/TiO_2/Zeolite setup, UV photolysis, H_2O_2 and UV/H_2O_2 disinfection systems. The UV/TiO_2/Zeolite/H_2O_2combination doubled the *E.coli* inactivation due to the synergy in the hydroxyl formation process. UV/TiO_2/Zeolite achieved slightly higher disinfection as compared to the other techniques like UV photolysis, H_2O_2 and UV/H_2O_2.It was also observed that under various pH conditions, the rate of reaction was found to be highest under acidic medium as compared to neutral and basic mediums, as illustrated in Figure of UV photolysis. 1.4mM H_2O_2 concentration was found to be the best in the formation of hydroxyl radicals, which attacked the bacterial cell as indicated in Figure . Finally, it was revealed that the addition of the modified semiconductor catalyst (TiO_2-Zeolite) and H_2O_2 to the system increased protein degradation by producing reactive oxygen species (ROS) like hydroxyl radicals. There was no photoreactivation of *E.coli* bacterial cells after UV/H_2O_2/TiO_2/Zeolite degradation, showing that the hybrid treatment process not only denatured the cells but also destroyed the bacterial cells completely, and this was confirmed by protein analysis, where there was protein reduction in each case. The energy consumption of the hybrid UV/TiO_2-zeolite/zeolite/H_2O_2 system (~0.04–0.05 USD/m^3) suggests that the process is economically feasible and competitive with other advanced disinfection methods. While chlorination remains cheaper, concerns about by-product toxicity and regrowth limit its suitability for high-quality effluent applications. The slightly

higher energy demand of AOPs is offset by their superior disinfection performance and the absence of secondary pollution.

In line with the study objectives, the following hypotheses were formulated in Chapter 1. After analyzing the experimental results and statistical evaluations, each hypothesis was tested and its fate determined as follows:

- **H_1:** *TiO_2 does not have good adherence to the zeolite surface therefore not improving the photodegradation.*

  → **Rejected.** Characterization studies (XRD, SEM–EDS, BET) confirmed that TiO_2 adhered well to the clinoptilolite zeolite support. The supported catalyst showed enhanced surface area and improved photocatalytic activity, leading to higher disinfection efficiency compared to TiO_2 or zeolite alone.
- **H_2:** *The amount of E. coli in Embu sewage wastewater treatment plant is above the recommended NEMA limits.*

  → **Accepted.** Quantification revealed that *E. coli* levels at all sampling sites (A, B, and C) exceeded the NEMA standard of Nil/100 ml, confirming this hypothesis.
- **H_3:** *The hybrid UV/TiO_2/H_2O_2 system does not improve bacterial disinfection efficiency compared to UV and H_2O_2 single processes.*

  → **Rejected.** The hybrid UV/TiO_2/H_2O_2 (with zeolite support) system achieved complete (100%) *E. coli* inactivation within 50–60 minutes. This performance was significantly higher than UV alone (~81%) or H_2O_2 alone (~86%), proving the hybrid system's superiority.
- **H_4:** *There will be no regrowth of E. coli bacteria in the municipal wastewater after AOPs treatment.*

  → **Partially Accepted.** Regrowth and photoreactivation were observed after 20–40 minutes of UV or H_2O_2 treatment. However, no regrowth was detected after 60 minutes of hybrid UV/TiO_2–Zeolite/H_2O_2 treatment, confirming that sufficient contact time in the hybrid system prevents bacterial recovery.

5.2 Recommendations

UV/TiO_2/Zeolite/H_2O_2 hybrid system was recommended for Embu sewage wastewater disinfection. The combination of UV irradiation, H_2O_2 oxidation, TiO_2 photocatalysis zeolite adsorption in the above hybrid system it achieves a synergistic effect leading to efficient removal of various contaminants from the sewage

wastewater after biological treatment. The system also saves on time and it does not generate harmful byproducts. Finally, this integrated approach produces the treated water that meets NEMA regulatory standards for discharge and or reuse of water.

While this study demonstrated the effectiveness of the UV/TiO_2/Zeolite/H_2O_2 hybrid system in disinfecting sewage wastewater, several areas require further research to broaden its applicability and ensure long-term sustainability:

1. **Pilot-Scale and Full-Scale Studies**

   The experiments in this study were conducted under laboratory conditions. Future work should include pilot-scale and eventually full-scale trials within municipal wastewater treatment plants to validate performance under real operational settings.

2. **Long-Term Catalyst Stability**

   Studies should investigate the reusability and stability of the TiO_2–zeolite catalyst during multiple treatment cycles. Understanding catalyst fouling, leaching, and regeneration processes is essential for practical deployment.

3. **Broader Microbial Spectrum**

   Although *E. coli* was used as the primary indicator organism, further studies should include a wider range of pathogens, including viruses, protozoa, and antibiotic-resistant bacteria, to confirm broader disinfection capability.

4. **Toxicity and Byproduct Assessment**

   While this study confirmed minimal harmful byproducts, comprehensive chemical analysis is necessary to ensure that disinfection does not lead to the formation of secondary pollutants or toxic residuals in treated effluent.

5. **Energy and Cost Optimization**

   Future research should evaluate the energy requirements, operational costs, and life-cycle assessment of the hybrid system. Comparisons with conventional chlorination and other advanced oxidation processes would provide insights into cost-effectiveness.

6. **Integration with Other Treatment Stages**

   Investigating how the hybrid UV/TiO_2/Zeolite/H_2O_2 system can be integrated with existing biological and physical treatment stages will help optimize overall wastewater management.

7. **Environmental Impact and Water Reuse Applications**

   Long-term ecological studies are needed to assess the safety of discharging treated effluent into rivers and its potential reuse in agriculture, industry, or domestic applications.

REFERENCES

Abdelhaleem, A., & Chu, W. (2020). Prediction of carbofuran degradation based on the hydroxyl radical's generation using the FeIII impregnated N doped-TiO2/H2O2/visible LED photo-Fenton-like process. *Chemical Engineering Journal*, *382*, 122930. https://doi.org/10.1016/j.cej.2019.122930

Abdullah, H., Khan, Md. M. R., Ong, H. R., & Yaakob, Z. (2017). Modified TiO2 photocatalyst for CO2 photocatalytic reduction: An overview. *Journal of CO2 Utilization*, *22*, 15–32. https://doi.org/10.1016/j.jcou.2017.08.004

Agustina, T. E., Ang, H. M., & Vareek, V. K. (2005). A review of synergistic effect of photocatalysis and ozonation on wastewater treatment. *Journal of Photochemistry and Photobiology C: Photochemistry Reviews*, *6*(4), 264–273. https://doi.org/10.101 6/j. jphotochemrev.2005.12.003

Alonso-Vicario, A., Ochoa-Gómez, J. R., Gil-Río, S., Gómez-Jiménez-Aberasturi, O., Ramírez-López, C. A., Torrecilla-Soria, J., & Domínguez, A. (2010). Purification and upgrading of biogas by pressure swing adsorption on synthetic and natural zeolites. *Microporous and Mesoporous Materials*, *134*(1), 100–107. https://doi.org/10.1016 /j.micromeso.2010.05.014

Ameri, A., Forootanfar, H., Ranjbar, M., Shakibaie, M., Pourshikhali, S., & Moshafi, M. H. (2022, August 12). *Statistical optimization of process conditions for pyrvinium pamoate elimination using UV/zeolite-based nanostructures/H_2O_2. | Micro & Nano Letters (Wiley-Blackwell) | EBSCOhost*. https://doi.org/10.1049/mna2.12126

Anglada, Á., Urtiaga, A., & Ortiz, I. (2009). Contributions of electrochemical oxidation to waste-water treatment: Fundamentals and review of applications. *Journal of Chemical Technology & Biotechnology*, *84*(12), 1747–1755. https://doi.org/10. 1002/jctb.2214

Apollo, S., Onyongo, M. S., & Ochieng, A. (2014a). UV/H2O2/TiO2/Zeolite Hybrid System for Treatment of Molasses Wastewater. *Iranian Journal of Chemistry and Chemical Engineering (IJCCE)*, *33*(2), 107–117. https://doi.org/10.30492/ijcce. 2014.10794

Apollo, S., Onyongo, M. S., & Ochieng, A. (2014b). UV/H2O2/TiO2/Zeolite Hybrid System for Treatment of Molasses Wastewater. *Iranian Journal of Chemistry and Chemical Engineering (IJCCE)*, *33*(2), 107–117. https://doi.org/10.30492 /ijcce.2014.10794

Armaković, S. J., Savanović, M. M., & Armaković, S. (2023). Titanium Dioxide as the Most Used Photocatalyst for Water Purification: An Overview. *Catalysts*, *13*(1), Article 1. https://doi.org/10.3390/catal13010026

Aryee, A. A., Mpatani, F. M., Kani, A. N., Dovi, E., Han, R., Li, Z., & Qu, L. (2021). A review on functionalized adsorbents based on peanut husk for the sequestration of pollutants in wastewater: Modification methods and adsorption study. *Journal of Cleaner Production*, *310*, 127502. https://doi.org/10.1016/j.jclepro.2021.127502

Biton Seror, S., Shamir, D., Albo, Y., Kornweitz, H., & Burg, A. (2022). Elucidation of a mechanism for the heterogeneous electro-fenton process and its application in the green treatment of azo dyes. *Chemosphere*, *286*, 131832. https://doi.org/10.1016/j.chemosphere.2021.131832

Bogdan, J., Zarzyńska, J., & Pławińska-Czarnak, J. (2015). Comparison of Infectious Agents Susceptibility to Photocatalytic Effects of Nanosized Titanium and Zinc Oxides: A Practical Approach. *Nanoscale Research Letters*, *10*(1), 309. https://doi.org/10.1186/s11671-015-1023-z

Bosshard, F., Riedel, K., Schneider, T., Geiser, C., Bucheli, M., & Egli, T. (2010). Protein oxidation and aggregation in UVA-irradiated Escherichia coli cells as signs of accelerated cellular senescence. *Environmental Microbiology*, *12*(11), 2931–2945. https://doi.org/10.1111/j.1462-2920.2010.02268.x

Buthiyappan, A., Aziz, A. R. A., & Daud, W. M. A. W. (2016). Recent advances and prospects of catalytic advanced oxidation process in treating textile effluents. *Reviews in Chemical Engineering*, *32*(1), 1–47. https://doi.org/10.1515/revce-2015-0034

Calgua, B., Carratalà, A., Guerrero-Latorre, L., de Abreu Corrêa, A., Kohn, T., Sommer, R., & Girones, R. (2014). UVC Inactivation of dsDNA and ssRNA Viruses in Water: UV Fluences and a qPCR-Based Approach to Evaluate Decay on Viral Infectivity. *Food and Environmental Virology*, *6*(4), 260–268. https://doi.org/10.10 07/ s 12560-014-9157-1

Castañeda-Juárez, M., Martínez-Miranda, V., Almazán-Sánchez, P. T., Linares-Hernández, I., Santoyo-Tepole, F., & Vázquez-Mejía, G. (2019). Synthesis of TiO2 catalysts doped with Cu, Fe, and Fe/Cu supported on clinoptilolite zeolite by an electrochemical-thermal method for the degradation of diclofenac by heterogeneous photocatalysis. *Journal of Photochemistry and Photobiology A: Chemistry*, *380*, 111834. https://doi.org/10.1016/j.jphotochem.2019.04.045

Chahal, C., van den Akker, B., Young, F., Franco, C., Blackbeard, J., & Monis, P. (2016). Pathogen and Particle Associations in Wastewater. *Advances in Applied Microbiology*, *97*, 63–119. https://doi.org/10.1016/bs.aambs.2016.08.001

Chen, J., Loeb, S., & Kim, J.-H. (2017). LED revolution: Fundamentals and prospects for UV disinfection applications. *Environmental Science: Water Research & Technology*, *3*(2), 188–202. https://doi.org/10.1039/C6EW00241B

Chen, Y., Duan, X., Zhou, X., Wang, R., Wang, S., Ren, N., & Ho, S.-H. (2021). Advanced oxidation processes for water disinfection: Features, mechanisms and prospects. *Chemical Engineering Journal*, *409*, 128207. https://doi.org/10.1016/j.cej .2020.128207

Cho, K., Qu, Y., Kwon, D., Zhang, H., Cid, C. A., Aryanfar, A., & Hoffmann, M. R. (2014). Effects of Anodic Potential and Chloride Ion on Overall Reactivity in Electrochemical Reactors Designed for Solar-Powered Wastewater Treatment. *Environmental Science & Technology*, *48*(4), 2377–2384. https://doi.org/10.1021 /es404137u

Claverie, M., Garcia, J., Prevost, T., Brendlé, J., & Limousy, L. (2019). Inorganic and Hybrid (Organic–Inorganic) Lamellar Materials for Heavy Metals and Radionuclides Capture in Energy Wastes Management—A Review. *Materials*, *12*(9), 1399. https://doi.org/10.3390/ma12091399

de la Obra Jiménez, I., Giannakis, S., Grandjean, D., Breider, F., Grunauer, G., Casas López, J. L., Sánchez Pérez, J. A., & Pulgarin, C. (2020). Unfolding the action mode of light and homogeneous vs. Heterogeneous photo-Fenton in bacteria disinfection and concurrent elimination of micropollutants in urban wastewater, mediated by iron oxides in Raceway Pond Reactors. *Applied Catalysis B: Environmental*, *263*, 118158. https://doi.org/10.1016/j.apcatb.2019.118158

Deemter, D., Oller, I., Amat, A. M., & Malato, S. (2021). Effect of salinity on preconcentration of contaminants of emerging concern by nanofiltration: Application of solar photo-Fenton as a tertiary treatment. *Science of The Total Environment*, *756*, 143593. https://doi.org/10.1016/j.scitotenv.2020.143593

Deng, Y., & Zhao, R. (2015). Advanced Oxidation Processes (AOPs) in Wastewater Treatment. *Current Pollution Reports*, *1*(3), 167–176. https://doi.org/10.1007/s4 0726- 015-0015-z

Diao, H. F., Li, X. Y., Gu, J. D., Shi, H. C., & Xie, Z. M. (2004). Electron microscopic investigation of the bactericidal action of electrochemical disinfection in comparison with chlorination, ozonation and Fenton reaction. *Process Biochemistry*, *39*(11), 1421–1426. https://doi.org/10.1016/S0032-9592(03)00274-7

Diban, N., Pacuła, A., Kumakiri, I., Barquín, C., Rivero, M. J., Urtiaga, A., & Ortiz, I. (2021). TiO2–Zeolite Metal Composites for Photocatalytic Degradation of Organic Pollutants in Water. *Catalysts*, *11*(11), Article 11. https://doi.org/10.3390/ catal11111367

Ding, W., Jin, W., Cao, S., Zhou, X., Wang, C., Jiang, Q., Huang, H., Tu, R., Han, S.-F., & Wang, Q. (2019). Ozone disinfection of chlorine-resistant bacteria in drinking water. *Water Research*, *160*, 339–349. https://doi.org/10.1016/j.watres. 2019.05.014

Duan, X., Indrawirawan, S., Kang, J., Tian, W., Zhang, H., Duan, X., Zhou, X., Sun, H., & Wang, S. (2020). Synergy of carbocatalytic and heat activation of persulfate for evolution of reactive radicals toward metal-free oxidation. *Catalysis Today*, *355*, 319–324. https://doi.org/10.1016/j.cattod.2019.02.051

Duan, X., Yang, S., Wacławek, S., Fang, G., Xiao, R., & Dionysiou, D. D. (2020). Limitations and prospects of sulfate-radical based advanced oxidation processes. *Journal of Environmental Chemical Engineering*, *8*(4), 103849. https://doi.org/10.1016/j.jece.2020.103849

Dunlop, P. S. M., Ciavola, M., Rizzo, L., McDowell, D. A., & Byrne, J. A. (2015). Effect of photocatalysis on the transfer of antibiotic resistance genes in urban wastewater. *Catalysis Today*, *240*, 55–60. https://doi.org/10.1016/j.cattod.2014 .03.049

Dutta, V., Singh, P., Shandilya, P., Sharma, S., Raizada, P., Saini, A. K., Gupta, V. K., Hosseini-Bandegharaei, A., Agarwal, S., & Rahmani-Sani, A. (2019). Review on advances in photocatalytic water disinfection utilizing graphene and graphene derivatives-based nanocomposites. *Journal of Environmental Chemical Engineering*, *7*(3), 103132. https://doi.org/10.1016/j.jece.2019.103132

Ebadi, A., Soltan Mohammadzadeh, J. S., & Khudiev, A. (2009). What is the correct form of BET isotherm for modeling liquid phase adsorption? *Adsorption*, *15*(1), 65–73. https://doi.org/10.1007/s10450-009-9151-3

Fairbrother, J. M., & Nadeau, E. (2006). Escherichia coli: On-farm contamination of animals. *Revue Scientifique Et Technique (International Office of Epizootics)*, *25*(2), 555–569.

Fang, J., Liu, H., Shang, C., Zeng, M., Ni, M., & Liu, W. (2014). E. coli and bacteriophage MS2 disinfection by UV, ozone and the combined UV and ozone processes. *Frontiers of Environmental Science & Engineering*, *8*(4), 547–552. https://doi.org/10.1007/s11783-013-0620-2

Feitz, A. (2005). Advanced oxidation processes and industrial wastewater treatment. *Water*, *32*, 59–65.

Fernandes, A., Makoś, P., Wang, Z., & Boczkaj, G. (2020). Synergistic effect of TiO2 photocatalytic advanced oxidation processes in the treatment of refinery effluents. *Chemical Engineering Journal*, *391*, 123488. https://doi.org/10.1016/j.cej.2019.123488

Foster, H. A., Ditta, I. B., Varghese, S., & Steele, A. (2011). Photocatalytic disinfection using titanium dioxide: Spectrum and mechanism of antimicrobial activity. *Applied Microbiology and Biotechnology*, *90*(6), 1847–1868. https://doi.org/10.1007/s00253-011-3213-7

Fu, L., Wu, C., Zhou, Y., Zuo, J., Song, G., & Tan, Y. (2019). Ozonation reactivity characteristics of dissolved organic matter in secondary petrochemical wastewater by single ozone, ozone/H2O2, and ozone/catalyst. *Chemosphere*, *233*, 34–43. https://doi.org/10.1016/j.chemosphere.2019.05.207

García-Fernández, I., Polo-López, M. I., Oller, I., & Fernández-Ibáñez, P. (2012). Bacteria and fungi inactivation using Fe3+/sunlight, H2O2/sunlight and near neutral photo-Fenton: A comparative study. *Applied Catalysis B: Environmental*, *121–122*, 20–29. https://doi.org/10.1016/j.apcatb.2012.03.012

Giannakis, S., Lin, K.-Y. A., & Ghanbari, F. (2021). A review of the recent advances on the treatment of industrial wastewaters by Sulfate Radical-based Advanced Oxidation Processes (SR-AOPs). *Chemical Engineering Journal*, *406*, 127083. https://doi.org/10.1016/j.cej.2020.127083

Gomes, J. F., Lopes, A., Gonçalves, D., Luxo, C., Gmurek, M., Costa, R., Quinta-Ferreira, R. M., Martins, R. C., & Matos, A. (2018). Biofiltration using C. fluminea for E.coli removal from water: Comparison with ozonation and photocatalytic oxidation. *Chemosphere*, *208*, 674–681. https://doi.org/10.1016/j.chemosphere.2018.06.045

Gomes, J., Frasson, D., Quinta-Ferreira, R. M., Matos, A., & Martins, R. C. (2019). Removal of Enteric Pathogens from Real Wastewater Using Single and Catalytic Ozonation. *Water*, *11*(1), Article 1. https://doi.org/10.3390/w11010127

Gomes, J., Matos, A., Gmurek, M., Quinta-Ferreira, R. M., & Martins, R. C. (2019a). Ozone and Photocatalytic Processes for Pathogens Removal from Water: A Review. *Catalysts*, *9*(1), Article 1. https://doi.org/10.3390/catal9010046

Gomes, J., Matos, A., Gmurek, M., Quinta-Ferreira, R. M., & Martins, R. C. (2019b). Ozone and Photocatalytic Processes for Pathogens Removal from Water: A Review. *Catalysts*, *9*(1), Article 1. https://doi.org/10.3390/catal9010046

Gonçalves, M. S. T., Oliveira-Campos, A. M. F., Pinto, E. M. M. S., Plasência, P. M. S., & Queiroz, M. J. R. P. (1999). Photochemical treatment of solutions of azo dyes containing TiO2. *Chemosphere*, *39*(5), 781–786. https://doi.org/10.1016/S0045-6535(99)00013-2

Green, C. F., Scarpino, P. V., Jensen, P., Jensen, N. J., & Gibbs, S. G. (2004). Disinfection of selected Aspergillus spp. Using ultraviolet germicidal irradiation. *Canadian Journal of Microbiology*, *50*(3), 221–224. https://doi.org/10.1139/w04-002

Guo, C., Wang, K., Hou, S., Wan, L., Lv, J., Zhang, Y., Qu, X., Chen, S., & Xu, J. (2017). H2O2 and/or TiO2 photocatalysis under UV irradiation for the removal of antibiotic resistant bacteria and their antibiotic resistance genes. *Journal of Hazardous Materials*, *323*, 710–718. https://doi.org/10.1016/j.jhazmat.2016.10.041

Guo, M., Hu, H., Bolton, J. R., & El-Din, M. G. (2009). Comparison of low- and medium-pressure ultraviolet lamps: Photoreactivation of Escherichia coli and total coliforms in secondary effluents of municipal wastewater treatment plants. *Water Research*, *43*(3), 815–821. https://doi.org/10.1016/j.watres.2008.11.028

Hamilton, K. A., Waso, M., Reyneke, B., Saeidi, N., Levine, A., Lalancette, C., Besner, M.-C., Khan, W., & Ahmed, W. (2018). Cryptosporidium and Giardia in Wastewater and Surface Water Environments. *Journal of Environmental Quality*, *47*(5), 1006–1023. https://doi.org/10.2134/jeq2018.04.0132

Haq, A. ul, Saeed, M., Khan, S. G., & Ibrahim, M. (2021). Photocatalytic Applications of Titanium Dioxide (TiO_2). In *Titanium Dioxide—Advances and Applications*. IntechOpen. https://doi.org/10.5772/intechopen.99598

Hijnen, W. A. M., Beerendonk, E. F., & Medema, G. J. (2006). Inactivation credit of UV radiation for viruses, bacteria and protozoan (oo)cysts in water: A review. *Water Research*, *40*(1), 3–22. https://doi.org/10.1016/j.watres.2005.10.030

Hodges, B. C., Cates, E. L., & Kim, J.-H. (2018). Challenges and prospects of advanced oxidation water treatment processes using catalytic nanomaterials. *Nature Nanotechnology*, *13*(8), Article 8. https://doi.org/10.1038/s41565-018-0216-x

Hoerter, J. D., Arnold, A. A., Kuczynska, D. A., Shibuya, A., Ward, C. S., Sauer, M. G., Gizachew, A., Hotchkiss, T. M., Fleming, T. J., & Johnson, S. (2005). Effects of sublethal UVA irradiation on activity levels of oxidative defense enzymes and protein oxidation in Escherichia coli. *Journal of Photochemistry and Photobiology B: Biology*, *81*(3), 171–180. https://doi.org/10.1016/j.jphotobiol.2005.07.005

Hou, W., & Cronin, S. B. (2013). A Review of Surface Plasmon Resonance-Enhanced Photocatalysis. *Advanced Functional Materials*, *23*(13), 1612–1619. https://doi.org/10.1002/adfm.201202148

Huang, S., Xu, Y., Xie, M., Liu, Q., Xu, H., Zhao, Y., He, M., & Li, H. (2017). A Z-scheme magnetic recyclable Ag/AgBr@CoFe 2 O 4 photocatalyst with enhanced photocatalytic performance for pollutant and bacterial elimination. *RSC Advances*, *7*(49), 30845–30854. https://doi.org/10.1039/C7RA03936K

Huo, K., Li, Y., Chen, R., Gao, B., Peng, C., Zhang, W., Hu, L., Zhang, X., & Chu, P. K. (2015). Recyclable Non-Enzymatic Glucose Sensor Based on Ni/NiTiO3/TiO2 Nanotube Arrays. *ChemPlusChem*, *80*(3), 576–582. https://doi.org/10.1002/cplu.201402288

Ikehata, K., & Li, Y. (2018). Chapter 5—Ozone-Based Processes. In S. C. Ameta & R. Ameta (Eds.), *Advanced Oxidation Processes for Waste Water Treatment* (pp. 115–134). Academic Press. https://doi.org/10.1016/B978-0-12-810499-6.00005-X

Ilinoiu, E. C., Pode, R., Manea, F., Colar, L. A., Jakab, A., Orha, C., Ratiu, C., Lazau, C., & Sfarloaga, P. (2013). Photocatalytic activity of a nitrogen-doped TiO2 modified zeolite in the degradation of Reactive Yellow 125 azo dye. *Journal of the Taiwan Institute of Chemical Engineers*, *44*(2), 270–278. https://doi.org/10.1016/j.jtice.2012.09.006

Jacangelo, J. G., & Trussell, R. R. (2002). International report: Water and wastewater disinfection - trends, issues and practices. *Water Supply*, *2*(3), 147–157. https://doi.org/10.2166/ws.2002.0097

Jamil, A., Farooq, S., & Hashmi, I. (2017). Ozone Disinfection Efficiency for Indicator Microorganisms at Different pH Values and Temperatures. *Ozone: Science & Engineering*, *39*(6), 407–416. https://doi.org/10.1080/01919512.2017.1322489

Jung, Y. J., Oh, B. S., & Kang, J.-W. (2008). Synergistic effect of sequential or combined use of ozone and UV radiation for the disinfection of Bacillus subtilis spores. *Water Research*, *42*(6), 1613–1621. https://doi.org/10.1016 /j.watres .2007.10.008

JunSik, O., Salcedo, D. E., Medriano, C. A., & SungPyo, K. (2014). Comparison of different disinfection processes in the effective removal of antibiotic-resistant bacteria and genes. *Journal of Environmental Sciences*, *26*(6), 1238–1242.

Kim, J.-G., & Yousef, A. e. (2000). Inactivation Kinetics of Foodborne Spoilage and Pathogenic Bacteria by Ozone. *Journal of Food Science*, *65*(3), 521–528. https://doi.org/10.1111/j.1365-2621.2000.tb16040.x

Kobiraj, R., Gupta, N., Kushwaha, A. K., & Chattopadhyaya, M. C. (2012). Determination of equilibrium, kinetic and thermodynamic parameters for the adsorption of Brilliant Green dye from aqueous solutions onto eggshell powder. *IJCT Vol.19(1) [January 2012]*. http://nopr.niscpr.res.in/handle/123456789/13499

Kokkinos, P. A., Ziros, P. G., Mpalasopoulou, A., Galanis, A., & Vantarakis, A. (2011). Molecular detection of multiple viral targets in untreated urban sewage from Greece. *Virology Journal*, *8*(1), 195. https://doi.org/10.1186/1743-422X-8-195

Kokkinos, P., Mantzavinos, D., Venieri, D., & Navalon, S. (2020). Current Trends in the Application of Nanomaterials for the Removal of Emerging Micropollutants and Pathogens from Water. *Molecules*, *25*(9), 2016. https://doi.org/10.3390/molecules25092016

Körbahti, B. K., & Tanyolaç, A. (2003). Continuous electrochemical treatment of phenolic wastewater in a tubular reactor. *Water Research*, *37*(7), 1505–1514. https://doi.org/10.1016/S0043-1354(02)00523-7

Korkuna, O., Leboda, R., Skubiszewska-Zie¸ba, J., Vrublevs'ka, T., Gun'ko, V. M., & Ryczkowski, J. (2006). Structural and physicochemical properties of natural zeolites: Clinoptilolite and mordenite. *Microporous and Mesoporous Materials*, *87*(3), 243–254. https://doi.org/10.1016/j.micromeso.2005.08.002

Kühn, K. P., Chaberny, I. F., Massholder, K., Stickler, M., Benz, V. W., Sonntag, H.-G., & Erdinger, L. (2003). Disinfection of surfaces by photocatalytic oxidation with titanium dioxide and UVA light. *Chemosphere*, *53*(1), 71–77. https://doi.org/10.1016/S0045-6535(03)00362-X

Lacasa, E., Tsolaki, E., Sbokou, Z., Rodrigo, M. A., Mantzavinos, D., & Diamadopoulos, E. (2013). Electrochemical disinfection of simulated ballast water on conductive diamond electrodes. *Chemical Engineering Journal*, *223*, 516–523. https://doi.org/10.1016/ j.cej.2013.03.003

Latif, S., Alim, M. A., & Rahman, A. (2022). Disinfection methods for domestic rainwater harvesting systems: A scoping review. *Journal of Water Process Engineering*, *46*, 102542. https://doi.org/10.1016/j.jwpe.2021.102542

Laxma Reddy, P. V., Kavitha, B., Kumar Reddy, P. A., & Kim, K.-H. (2017). TiO2-based photocatalytic disinfection of microbes in aqueous media: A review. *Environmental Research*, *154*, 296–303. https://doi.org/10.1016/j.envres.2017.01.018

Li, G., Chen, Q., & Lan, J. (2014). Facile Synthesis, Metastable Phase Induced Morphological Evolution and Crystal Ripening, and Structure-Dependent Photocatalytic Properties of 3D Hierarchical Anatase Superstructures. *ACS Applied Materials & Interfaces*, *6*(24), 22561–22568. https://doi.org/10.1021/am506684c

Liu, H., Wang, C., & Wang, G. (2020). Photocatalytic Advanced Oxidation Processes for Water Treatment: Recent Advances and Perspective. *Chemistry – An Asian Journal*, *15*(20), 3239–3253. https://doi.org/10.1002/asia.202000895

Liu, J., Dong, C., Deng, Y., Ji, J., Bao, S., Chen, C., Shen, B., Zhang, J., & Xing, M. (2018). Molybdenum sulfide Co-catalytic Fenton reaction for rapid and efficient inactivation of Escherichia coli. *Water Research*, *145*, 312–320. https://doi.org/10.1016/j.watres.2018.08.039

Luo, Y., Zhang, C., Zheng, B., Geng, X., & Debliquy, M. (2017). Hydrogen sensors based on noble metal doped metal-oxide semiconductor: A review. *International Journal of Hydrogen Energy*, *42*(31), 20386–20397. https://doi.org/10.1016/j.ijhydene.2017.06.066

Ma, D., Yi, H., Lai, C., Liu, X., Huo, X., An, Z., Li, L., Fu, Y., Li, B., Zhang, M., Qin, L., Liu, S., & Yang, L. (2021). Critical review of advanced oxidation processes in organic wastewater treatment. *Chemosphere*, *275*, 130104. https://doi.org/10.1016/j.chemosphere.2021.130104

Ma, H., Zhang, L., Huang, X., Ding, W., Jin, H., Li, Z., Cheng, S., & Zheng, L. (2019). A novel three-dimensional galvanic cell enhanced Fe2+/persulfate system: High efficiency, mechanism and damaging effect of antibiotic resistant E. coli and genes. *Chemical Engineering Journal*, *362*, 667–678. https://doi.org/10.1016/j.cej.2019.01.042

Makarova, K. S., Aravind, L., Wolf, Y. I., Tatusov, R. L., Minton, K. W., Koonin, E. V., & Daly, M. J. (2001). Genome of the Extremely Radiation-Resistant Bacterium Deinococcus radiodurans Viewed from the Perspective of Comparative Genomics. *Microbiology and Molecular Biology Reviews*, *65*(1), 44–79. https://doi.org/10.1128/MMBR.65.1.44-79.2001

Malvestiti, J. A., Cruz-Alcalde, A., López-Vinent, N., Dantas, R. F., & Sans, C. (2019). Catalytic ozonation by metal ions for municipal wastewater disinfection and simulataneous micropollutants removal. *Applied Catalysis B: Environmental*, *259*, 118104. https://doi.org/10.1016/j.apcatb.2019.118104

Maness, P.-C., Smolinski, S., Blake, D. M., Huang, Z., Wolfrum, E. J., & Jacoby, W. A. (1999). Bactericidal Activity of Photocatalytic TiO2 Reaction: Toward an Understanding of Its Killing Mechanism. *Applied and Environmental Microbiology*, *65*(9), 4094–4098. https://doi.org/10.1128/AEM.65.9.4094-4098.1999

Maniakova, G., Salmerón, I., Nahim-Granados, S., Malato, S., Oller, I., Rizzo, L., & Polo-López, M. I. (2021). Sunlight advanced oxidation processes vs ozonation for wastewater disinfection and safe reclamation. *Science of The Total Environment*, *787*, 147531. https://doi.org/10.1016/j.scitotenv.2021.147531

Martínez-Huitle, C. A., & Brillas, E. (2009). Decontamination of wastewaters containing synthetic organic dyes by electrochemical methods: A general review. *Applied Catalysis B: Environmental*, *87*(3), 105–145. https://doi.org/10.1016/j.apcatb.2008.09.017

Matsunaga, T., Tomoda, R., Nakajima, T., & Wake, H. (1985). Photoelectrochemical sterilization of microbial cells by semiconductor powders. *FEMS Microbiology Letters*, *29*(1–2), 211–214. https://doi.org/10.1111/j.1574-6968.1985.tb00864.x

Mazhar, M. A., Khan, N. A., Ahmed, S., Khan, A. H., Hussain, A., Rahisuddin, Changani, F., Yousefi, M., Ahmadi, S., & Vambol, V. (2020). Chlorination disinfection by-products in municipal drinking water – A review. *Journal of Cleaner Production*, *273*, 123159. https://doi.org/10.1016/j.jclepro.2020.123159

Mecha, A. C., Onyango, M. S., Ochieng, A., Fourie, C. J. S., & Momba, M. N. B. (2016). Synergistic effect of UV–vis and solar photocatalytic ozonation on the degradation of phenol in municipal wastewater: A comparative study. *Journal of Catalysis*, *341*, 116–125. https://doi.org/10.1016/j.jcat.2016.06.015

Mecha, A. C., Onyango, M. S., Ochieng, A., & Momba, M. N. B. (2017). Evaluation of synergy and bacterial regrowth in photocatalytic ozonation disinfection of municipal wastewater. *Science of The Total Environment*, *601–602*, 626–635. https://doi.org/10.1016/j.scitotenv.2017.05.204

Michael-Kordatou, I., Andreou, R., Iacovou, M., Frontistis, Z., Hapeshi, E., Michael, C., & Fatta-Kassinos, D. (2017). On the capacity of ozonation to remove antimicrobial compounds, resistant bacteria and toxicity from urban wastewater effluents. *Journal of Hazardous Materials*, *323*(Pt A), 414–425. https://doi.org/10.1016/j.jhazmat.2016.02.023

Montalvo, S., Guerrero, L., Borja, R., Sánchez, E., Milán, Z., Cortés, I., & Angeles de la la Rubia, M. (2012). Application of natural zeolites in anaerobic digestion processes: A review. *Applied Clay Science*, *58*, 125–133. https://doi.org/10.1016/j.clay.2012.01.013

Moreira, N. F. F., Narciso-da-Rocha, C., Polo-López, M. I., Pastrana-Martínez, L. M., Faria, J. L., Manaia, C. M., Fernández-Ibáñez, P., Nunes, O. C., & Silva, A. M. T. (2018). Solar treatment (H2O2, TiO2-P25 and GO-TiO2 photocatalysis, photo-Fenton) of organic micropollutants, human pathogen indicators, antibiotic resistant bacteria and related genes in urban wastewater. *Water Research*, *135*, 195–206. https://doi.org/10.1016/j.watres.2018.01.064

Moreira, N. F. F., Sousa, J. M., Macedo, G., Ribeiro, A. R., Barreiros, L., Pedrosa, M., Faria, J. L., Pereira, M. F. R., Castro-Silva, S., Segundo, M. A., Manaia, C. M., Nunes, O. C., & Silva, A. M. T. (2016). Photocatalytic ozonation of urban wastewater and surface water using immobilized TiO2 with LEDs: Micropollutants, antibiotic resistance genes and estrogenic activity. *Water Research*, *94*, 10–22. https://doi.org/10.1016/j.watres.2016.02.003

Mosteo, R., Varon Lopez, A., Muzard, D., Benitez, N., Giannakis, S., & Pulgarin, C. (2020). Visible light plays a significant role during bacterial inactivation by the photo-fenton process, even at sub-critical light intensities. *Water Research*, *174*, 115636. https://doi.org/10.1016/j.watres.2020.115636

Muleja, A., Tshangana, C., Gorimbo, J., Kamika, I., & Mamba, B. (2022). The inactivation of Escherichia coli using cobalt-modified natural zeolite from a South African mine. *International Journal of Environmental Science and Technology*, *19*(10), 9377–9392. https://doi.org/10.1007/s13762-022-04441-z

Muller, J. G., Hickerson, R. P., Perez, R. J., & Burrows, C. J. (1997). DNA Damage from Sulfite Autoxidation Catalyzed by a Nickel(II) Peptide. *Journal of the American Chemical Society*, *119*(7), 1501–1506. https://doi.org/10.1021/ja963701y

Nahim-Granados, S., Rivas-Ibáñez, G., Antonio Sánchez Pérez, J., Oller, I., Malato, S., & Polo-López, M. I. (2020). Synthetic fresh-cut wastewater disinfection and decontamination by ozonation at pilot scale. *Water Research*, *170*, 115304. https://doi.org/10.1016/j.watres.2019.115304

Padmavathy, N., & Vijayaraghavan, R. (2011). Interaction of ZnO Nanoparticles with Microbes—A Physio and Biochemical Assay. *Journal of Biomedical Nanotechnology*, *7*(6), 813–822. https://doi.org/10.1166/jbn.2011.1343

Paździor, K., Bilińska, L., & Ledakowicz, S. (2019). A review of the existing and emerging technologies in the combination of AOPs and biological processes in industrial textile wastewater treatment. *Chemical Engineering Journal*, *376*, 120597. https://doi.org/10.1016/j.cej.2018.12.057

Rahim Pouran, S., Abdul Aziz, A. R., & Wan Daud, W. M. A. (2015). Review on the main advances in photo-Fenton oxidation system for recalcitrant wastewaters. *Journal of Industrial and Engineering Chemistry*, *21*, 53–69. https://doi.org/10.1016/j.jiec.2014.05.005

Rajab, M., Heim, C., Letzel, T., Drewes, J. E., & Helmreich, B. (2015). Electrochemical disinfection using boron-doped diamond electrode – The synergetic effects of in situ ozone and free chlorine generation. *Chemosphere*, *121*, 47–53. https://doi.org/10.1016/j.chemosphere.2014.10.075

Ramesh, K., Reddy, K. S., Rashmi, I., & Biswas, A. K. (2014). Porosity Distribution, Surface Area, and Morphology of Synthetic Potassium Zeolites: A SEM and N2 Adsorption Study. *Communications in Soil Science and Plant Analysis*, *45*(16), 2171–2181. https://doi.org/10.1080/00103624.2014.929699

Ray, S. K., Dhakal, D., Pandey, R. P., & Lee, S. W. (2017). Ag-BaMoO4: Er3+/Yb3+ photocatalyst for antibacterial application. *Materials Science and Engineering: C*, *78*, 1164–1171. https://doi.org/10.1016/j.msec.2017.04.115

Regmi, C., Joshi, B., Ray, S. K., Gyawali, G., & Pandey, R. P. (2018). Understanding Mechanism of Photocatalytic Microbial Decontamination of Environmental Wastewater. *Frontiers in Chemistry*, *6*, 33. https://doi.org/10.3389/fchem.2018.00033

Ren, Y., Zeng, D., & Ong, W.-J. (2019). Interfacial engineering of graphitic carbon nitride (g-C3N4)-based metal sulfide heterojunction photocatalysts for energy conversion: A review. *Chinese Journal of Catalysis*, *40*(3), 289–319. https://doi.org/10.1016/S1872-2067(19)63293-6

Rincón, A.-G., & Pulgarin, C. (2004). Bactericidal action of illuminated TiO2 on pure Escherichia coli and natural bacterial consortia: Post-irradiation events in the dark and assessment of the effective disinfection time. *Applied Catalysis B: Environmental*, *49*(2), 99–112. https://doi.org/10.1016/j.apcatb.2003.11.013

Rincón, A.-G., & Pulgarin, C. (2005). Use of coaxial photocatalytic reactor (CAPHORE) in the TiO2 photo-assisted treatment of mixed E. coli and Bacillus sp. And bacterial community present in wastewater. *Catalysis Today*, *101*(3), 331–344. https://doi.org/10.1016/j.cattod.2005.03.022

Rodriguez, R. A., Bounty, S., Beck, S., Chan, C., McGuire, C., & Linden, K. G. (2014). Photoreactivation of bacteriophages after UV disinfection: Role of genome structure and impacts of UV source. *Water Research*, *55*, 143–149. https://doi.org/10.1016 /j.watres. 2014.01.065

Roy, N., Sohn, Y., & Pradhan, D. (2013). Synergy of Low-Energy {101} and High-Energy {001} TiO2 Crystal Facets for Enhanced Photocatalysis. *ACS Nano*, *7*(3), 2532–2540. https://doi.org/10.1021/nn305877v

Rtimi, S., Dionysiou, D. D., Pillai, S. C., & Kiwi, J. (2019). Advances in catalytic/photocatalytic bacterial inactivation by nano Ag and Cu coated surfaces and medical devices. *Applied Catalysis B: Environmental*, *240*, 291–318. https://doi.org/10.1016/j.apcatb.2018.07.025

Ruan, L., Wang, X., Wang, T., Ren, Z., Chen, Y., Zhao, R., Zhou, D., Fu, G., Li, S., Gao, L., Lu, Y., Wang, Z., Tian, H., Kong, X., & Han, G. (2019). Surface Defect-Controlled Growth and High Photocatalytic H2 Production Efficiency of Anatase TiO2 Nanosheets. *ACS Applied Materials & Interfaces*, *11*(40), 37256–37262. https://doi.org/10.1021/acsami.9b11233

Saravanan, A., Kumar, P. S., Jeevanantham, S., Karishma, S., & Kiruthika, A. R. (2021). Photocatalytic disinfection of micro-organisms: Mechanisms and applications. *Environmental Technology & Innovation*, *24*, 101909. https://doi.org/10.1016/j.eti. 2021.101909

Schaefer, C. E., Andaya, C., & Urtiaga, A. (2015). Assessment of disinfection and by-product formation during electrochemical treatment of surface water using a Ti/IrO2 anode. *Chemical Engineering Journal*, *264*, 411–416. https://doi.org/10.1016/j.cej .2014.11.082

Sgroi, M., Anumol, T., Vagliasindi, F. G. A., Snyder, S. A., & Roccaro, P. (2021). Comparison of the new Cl2/O3/UV process with different ozone- and UV-based AOPs for wastewater treatment at pilot scale: Removal of pharmaceuticals and changes in fluorescing organic matter. *Science of The Total Environment*, *765*, 142720. https://doi.org/10.1016/j.scitotenv.2020.142720

Shin, G.-A., Lee, J.-K., & Linden, K. G. (2009). Enhanced effectiveness of medium-pressure ultraviolet lamps on human adenovirus 2 and its possible mechanism. *Water Science and Technology*, *60*(4), 851–857. https://doi.org/10.2166/wst.2009.414

Sholtes, K. A., Lowe, K., Walters, G. W., Sobsey, M. D., Linden, K. G., & Casanova, L. M. (2016). Comparison of ultraviolet light-emitting diodes and low-pressure mercury-arc lamps for disinfection of water. *Environmental Technology*, *37*(17), 2183–2188. https://doi.org/10.1080/09593330.2016.1144798

Singh, P., Shandilya, P., Raizada, P., Sudhaik, A., Rahmani-Sani, A., & Hosseini-Bandegharaei, A. (2020). Review on various strategies for enhancing photocatalytic activity of graphene based nanocomposites for water purification. *Arabian Journal of Chemistry*, *13*(1), 3498–3520. https://doi.org/10.1016/j.arabjc.2018.12.001

Song, H., Yan, L., Wang, Y., Jiang, J., Ma, J., Li, C., Wang, G., Gu, J., & Liu, P. (2020). Electrochemically activated PMS and PDS: Radical oxidation versus nonradical oxidation. *Chemical Engineering Journal*, *391*, 123560. https://doi.org/10.1016/j.cej.2019.123560

Soon, A. N., & Hameed, B. H. (2011). Heterogeneous catalytic treatment of synthetic dyes in aqueous media using Fenton and photo-assisted Fenton process. *Desalination*, *269*(1), 1–16. https://doi.org/10.1016/j.desal.2010.11.002

Sousa, J. M., Macedo, G., Pedrosa, M., Becerra-Castro, C., Castro-Silva, S., Pereira, M. F. R., Silva, A. M. T., Nunes, O. C., & Manaia, C. M. (2017). Ozonation and UV254nm radiation for the removal of microorganisms and antibiotic resistance genes from urban wastewater. *Journal of Hazardous Materials*, *323*(Pt A), 434–441. https://doi.org/10.1016/j.jhazmat.2016.03.096

Souza, B. M., Cerqueira, A. C., Sant'Anna, G. L., & Dezotti, M. (2011). Oil-Refinery Wastewater Treatment Aiming Reuse by Advanced Oxidation Processes (AOPs) Combined with Biological Activated Carbon (BAC). *Ozone: Science & Engineering*, *33*(5), 403–409. https://doi.org/10.1080/01919512.2011.604606

Sun, D.-W., Koutchma, T., Forney, L. J., & Moraru, C. I. (2019). *Ultraviolet Light in Food Technology: Principles and Applications*. CRC Press. https://doi.org/10.1201/9781315112862

Tan, K. L., & Hameed, B. H. (2017). Insight into the adsorption kinetics models for the removal of contaminants from aqueous solutions. *Journal of the Taiwan Institute of Chemical Engineers*, *74*, 25–48. https://doi.org/10.1016/j.jtice.2017.01.024

Tong, M., Liu, F., Dong, Q., Ma, Z., & Liu, W. (2020). Magnetic Fe3O4-deposited flower-like MoS2 nanocomposites for the Fenton-like Escherichia coli disinfection and diclofenac degradation. *Journal of Hazardous Materials*, *385*, 121604. https://doi.org/10.1016/j.jhazmat.2019.121604

Tulchinsky, T. H. (2018). John Snow, Cholera, the Broad Street Pump; Waterborne Diseases Then and Now. *Case Studies in Public Health*, 77–99. https://doi.org/10.1016/B978-0-12-804571-8.00017-2

Uhl, L., Gerstel, A., Chabalier, M., & Dukan, S. (2015). Hydrogen peroxide induced cell death: One or two modes of action? *Heliyon*, *1*(4), e00049. https://doi.org/10.1016/j.heliyon.2015.e00049

Un, U. T., Altay, U., Koparal, A. S., & Ogutveren, U. B. (2008). Complete treatment of olive mill wastewaters by electrooxidation. *Chemical Engineering Journal*, *139*(3), 445–452. https://doi.org/10.1016/j.cej.2007.08.009

Wang, C.-C., Lee, C.-K., Lyu, M.-D., & Juang, L.-C. (2008). Photocatalytic degradation of C.I. Basic Violet 10 using TiO2 catalysts supported by Y zeolite: An investigation of the effects of operational parameters. *Dyes and Pigments*, *76*(3), 817–824. https://doi.org/10.1016/j.dyepig.2007.02.004

Wang, H., Li, X., Hao, Z., Sun, Y., Wang, Y., Li, W., & Tsang, Y. F. (2017). Transformation of dissolved organic matter in concentrated leachate from nanofiltration during ozone-based oxidation processes (O3, O3/H2O2 and O3/UV). *Journal of Environmental Management*, *191*, 244–251. https://doi.org/10.1016/j.jenvman.2017.01.021

Wang, N., Zheng, T., Zhang, G., & Wang, P. (2016). A review on Fenton-like processes for organic wastewater treatment. *Journal of Environmental Chemical Engineering*, *4*(1), 762–787. https://doi.org/10.1016/j.jece.2015.12.016

Wang, W., Li, G., Xia, D., An, T., Zhao, H., & Wong, P. K. (2017). Photocatalytic nanomaterials for solar-driven bacterial inactivation: Recent progress and challenges. *Environmental Science: Nano*, *4*(4), 782–799. https://doi.org/10.1039/C7EN00063D

Wang, W., Wang, H., Li, G., An, T., Zhao, H., & Wong, P. K. (2019). Catalyst-free activation of persulfate by visible light for water disinfection: Efficiency and mechanisms. *Water Research*, *157*, 106–118. https://doi.org/10.1016/j.watres.2019.03.071

Wang, W., Wang, H., Li, G., Wong, P. K., & An, T. (2020). Visible light activation of persulfate by magnetic hydrochar for bacterial inactivation: Efficiency, recyclability and mechanisms. *Water Research*, *176*, 115746. https://doi.org/10.1016/j.watres.2020.115746

Wang, X., & Zhang, L. (2018). Kinetic study of hydroxyl radical formation in a continuous hydroxyl generation system. *RSC Advances*, *8*(71), 40632–40638. https://doi.org/10.1039/C8RA08511K

Wu, X., Liu, J., & Zhu, J.-J. (2019). Sono-Fenton hybrid process on the inactivation of Microcystis aeruginosa: Extracellular and intracellular oxidation. *Ultrasonics Sonochemistry*, *53*, 68–76. https://doi.org/10.1016/j.ultsonch.2018.12.034

Xia, D., He, H., Liu, H., Wang, Y., Zhang, Q., Li, Y., Lu, A., He, C., & Wong, P. K. (2018). Persulfate-mediated catalytic and photocatalytic bacterial inactivation by magnetic natural ilmenite. *Applied Catalysis B: Environmental*, *238*, 70–81. https://doi.org/10.1016/j.apcatb.2018.07.003

Xia, D., Li, Y., Huang, G., Yin, R., An, T., Li, G., Zhao, H., Lu, A., & Wong, P. K. (2017). Activation of persulfates by natural magnetic pyrrhotite for water disinfection: Efficiency, mechanisms, and stability. *Water Research*, *112*, 236–247. https://doi.org/10.1016/j.watres.2017.01.052

Xiao, Q., Zhang, J., Xiao, C., Si, Z., & Tan, X. (2008). Solar photocatalytic degradation of methylene blue in carbon-doped TiO2 nanoparticles suspension. *Solar Energy*, *82*(8), 706–713. https://doi.org/10.1016/j.solener.2008.02.006

Xiao, R., Liu, K., Bai, L., Minakata, D., Seo, Y., Kaya Göktaş, R., Dionysiou, D. D., Tang, C.-J., Wei, Z., & Spinney, R. (2019). Inactivation of pathogenic microorganisms by sulfate radical: Present and future. *Chemical Engineering Journal*, *371*, 222–232. https://doi.org/10.1016/j.cej.2019.03.296

Xiao, R., Luo, Z., Wei, Z., Luo, S., Spinney, R., Yang, W., & Dionysiou, D. D. (2018). Activation of peroxymonosulfate/persulfate by nanomaterials for sulfate radical-based advanced oxidation technologies. *Current Opinion in Chemical Engineering*, *19*, 51–58. https://doi.org/10.1016/j.coche.2017.12.005

Xiao, S., Cheng, M., Zhong, H., Liu, Z., Liu, Y., Yang, X., & Liang, Q. (2020). Iron-mediated activation of persulfate and peroxymonosulfate in both homogeneous and heterogeneous ways: A review. *Chemical Engineering Journal*, *384*, 123265. https://doi.org/10.1016/j.cej.2019.123265

Xiong, P., & Hu, J. (2013). Inactivation/reactivation of antibiotic-resistant bacteria by a novel UVA/LED/TiO2 system. *Water Research*, *47*(13), 4547–4555. https://doi.org/10.1016/j.watres.2013.04.056

Xu, H., Sun, X., Yu, Y., Liu, G., Ma, L., & Huang, G. (2019). Removal of quinoline using various particle sizes anthracite: Adsorption kinetics and adsorption isotherms. *Physicochemical Problems of Mineral Processing*, *Vol. 55, iss. 1*, 196–207. https://doi.org/10.5277/ppmp18121

Xu, P., Janex, M.-L., Savoye, P., Cockx, A., & Lazarova, V. (2002). Wastewater disinfection by ozone: Main parameters for process design. *Water Research*, *36*(4), 1043–1055. https://doi.org/10.1016/s0043-1354(01)00298-6

Yasir, M. (2021). Analysis of Microbial Communities and Pathogen Detection in Domestic Sewage Using Metagenomic Sequencing. *Diversity*, *13*(1), Article 1. https://doi.org/10.3390/d13010006

Yi, H., Liu, S., Lai, C., Zeng, G., Li, M., Liu, X., Li, B., Huo, X., Qin, L., Li, L., Zhang, M., Fu, Y., An, Z., & Chen, L. (2021). Recent Advance of Transition-Metal-Based Layered Double Hydroxide Nanosheets: Synthesis, Properties, Modification, and Electrocatalytic Applications. *Advanced Energy Materials*, *11*(14), 2002863. https://doi.org/10.1002/aenm.202002863

Zhang, G., Song, A., Duan, Y., & Zheng, S. (2018). Enhanced photocatalytic activity of TiO2/zeolite composite for abatement of pollutants. *Microporous and Mesoporous Materials*, *255*, 61–68. https://doi.org/10.1016/j.micromeso.2017.07.028

Zhang, Q., Li, R., Li, Z., Li, A., Wang, S., Liang, Z., Liao, S., & Li, C. (2016). The dependence of photocatalytic activity on the selective and nonselective deposition of noble metal cocatalysts on the facets of rutile TiO2. *Journal of Catalysis*, *337*, 36–44. https://doi.org/10.1016/j.jcat.2016.01.001

Zhang, T., Wang, T., Mejia-Tickner, B., Kissel, J., Xie, X., & Huang, C.-H. (2020). Inactivation of Bacteria by Peracetic Acid Combined with Ultraviolet Irradiation: Mechanism and Optimization. *Environmental Science & Technology*, *54*(15), 9652–9661. https://doi.org/10.1021/acs.est.0c02424